

**Heat Transfer and Pressure Drop Characteristics of  
the Plate and Shell Heat Exchanger**

(플레이트 앤 셸 열교환기의 열전달 및 압력강하  
특성에 관한 연구)

Advisor : Young Soo Kim



A thesis submitted in partial fulfillment of requirements

**Doctor of Philosophy**

**in the Department of Refrigeration and Air Conditioning  
Engineering**

**The Graduate School  
Pukyong National University**

**February 2002**

# 서무교의 공학박사 학위논문을

## 인준함

2001년 12월 26일

주	심	공학박사	김	종	수
부	심	공학박사	오	후	규
위	원	공학박사	권	오	봉
위	원	공학박사	정	형	호
위	원	공학박사	김	영	수



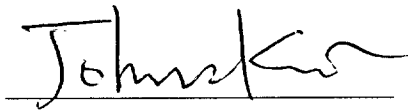
**Heat Transfer and Pressure Drop Characteristics of  
the Plate and Shell Heat Exchanger**

**A Dissertation**

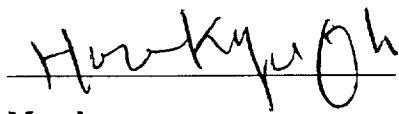
**by**

**Moo Gyo Seo**

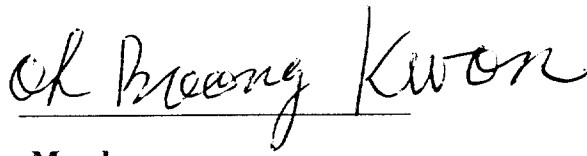
**Approved as to style and content by :**



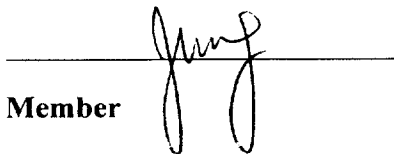
**Chairman**



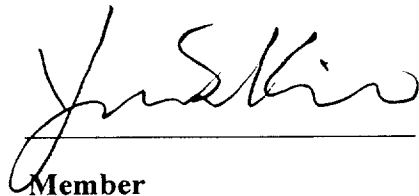
**Member**



**Member**



**Member**



**Member**

**26 December, 2001**

# **CONTENTS**

<b>CONTENTS</b> .....	i
<b>LIST OF FIGURES AND TABLES</b> .....	iv
<b>ABSTRACT</b> .....	x
<b>NOMENCLATURE</b> .....	xii

## **CHAPTER 1 INTRODUCTION**

1.1 BACKGROUNDS .....	1
1.2 REVIEW OF PREVIOUS STUDY .....	11
1.2.1 Preview of study on the plate heat exchangers .....	11
1.2.2 Preview of study on the two-phase flow heat transfer and pressure drop .....	15
1.3 OBJECTIVE OF THIS STUDY .....	18

## **CHAPTER 2 SINGLE-PHASE FLOW HEAT TRANSFER AND PRESSURE DROP**

2.1 EXPERIMENTAL APPARATUS AND METHOD .....	20
2.1.1 Experimental apparatus .....	20
2.1.2 Test section .....	22
2.1.3 Experimental procedures .....	22
2.1.4 Data reduction .....	26
2.2 RESULTS AND DISCUSSION .....	30

2.2.1 Single-phase flow heat transfer characteristics .....	30
2.2.2 Single-phase flow pressure drop characteristics .....	33
2.2.3 Comparison with conventional plate heat exchanger .....	38

## **CHAPTER 3 CFD ANALYSIS FOR SINGLE-PHASE FLOW**

3.1 MATHEMATICAL MODELS AND NUMERICAL ANALYSIS .....	42
3.1.1 Governing equation .....	42
3.1.2 Computational domain .....	44
3.1.3 Boundary conditions for the equations .....	45
3.1.4 Numerical analysis .....	48
3.2 RESULTS AND DISCUSSION .....	50
3.2.1 Selection of turbulence model .....	50
3.2.2 Influence of the partitioning rib .....	51
3.2.3 Influence of the Chevron angle on the performance .....	52
3.2.4 Influence of the height and pitch of the corrugate .....	52
3.2.5 Analysis of design parameters .....	61

## **CHAPTER 4 TWO-PHASE FLOW HEAT TRANSFER AND PRESSURE DROP**

4.1 EXPERIMENTAL APPARATUS AND PROCEDURES ..	65
4.1.1 Experimental apparatus .....	65
4.1.2 Experimental procedures .....	69
4.2 DATA REDUCTION .....	72
4.2.1 Two-phase heat transfer .....	72

4.2.2 Two-phase friction pressure drop .....	74
<b>4.3 CONDENSATION HEAT TRANSFER</b>	
<b>CHARACTERISTICS</b> .....	78
4.3.1 The effects of mass flux, heat flux, saturation temperature and feeding method .....	78
4.3.2 Comparison with plate heat exchanger .....	88
4.3.3 Correlation of condensation heat transfer .....	89
<b>4.4 EVAPORATION HEAT TRANSFER</b>	
<b>CHARACTERISTICS</b> .....	93
4.4.1 The effects of mass flux, heat flux, saturation temperature and feeding method .....	93
4.4.2 Comparison with plate heat exchanger .....	106
4.4.3 Correlation of evaporation heat transfer .....	106
<b>4.5 TWO-PHASE FLOW PRESSURE DROP</b>	
<b>CHARACTERISTICS</b> .....	111
4.5.1 The effects of mass flux, heat flux and saturation temperature .....	111
4.5.2 Comparison with plate heat exchanger .....	119
4.5.3 Correlation of pressure drop .....	119
 <b>CHAPTER 5 CONCLUSIONS</b> .....	 124
 <b>REFERENCE</b> .....	 127
<b>APPENDIX</b> .....	137
<b>ACKNOWLEDGEMENT</b> .....	146

## **LIST OF FIGURES AND TABLES**

### **Figures**

- Figure 1.1 Chevron plates
- Figure 1.2 Schematic diagram of plate and shell heat exchanger
- Figure 2.1 Schematic diagram of the single-phase heat transfer and pressure drop experimental system
- Figure 2.2 Schematic diagram of heat transfer plate in the plate and shell heat exchanger
- Figure 2.3 Details of flow pattern in plate and shell heat exchanger
- Figure 2.4 Modified Wilson plot results for the shell side and plate side used in this study
- Figure 2.5 Heat transfer coefficient for the shell side and plate side in this study
- Figure 2.6 Friction pressure drop variations with the Reynolds number in single-phase water-to-water test
- Figure 2.7 Friction factor variations with the Reynolds number for the plate and shell side in single-phase water-to-water test
- Figure 2.8 Schematic diagram of plate heat exchanger used in this study
- Figure 2.9 Experimental result of friction factor for the plate heat exchanger(PHE)
- Figure 2.10 Experimental result of heat transfer coefficient for the

plate heat exchanger(PHE)

Figure 2.11 Comparison of the P&SHE with conventional PHE in friction factor

Figure 2.12 Comparison of the P&SHE with conventional PHE in heat transfer

Figure 3.1 Schematic Modeling of plate and shell heat exchanger with partitioning rib

Figure 3.2 Geometric parameters of plate in the plate and shell heat exchanger

Figure 3.3 Comparison of CFD analysis results with experimental data for friction factor in partitioning rib type plate

Figure 3.4 Comparison of CFD analysis result with experimental data for heat transfer in partitioning rib type plate

Figure 3.5 Friction factor comparison of partitioning rib type with non-partitioning rib type plate

Figure 3.6 Heat transfer coefficient comparison of partitioning rib type with non-partitioning rib plate

Figure 3.7 Pressure distribution comparison of partitioning rib type with non-partitioning rib type plate in channel along y-direction

Figure 3.8 Temperature distribution comparison of partitioning rib type with non-partitioning rib type plate in channel along y-direction

Figure 3.9 Friction factor vs. Chevron angle for three different Reynolds number



- Figure 3.10 Heat transfer coefficient vs. Chevron angle for three different Reynolds number
- Figure 3.11 Temperature distribution of the non-partitioning rib type plate for  $Re=2000$  (Cross-section normal to the corrugated plate at  $x=0, y=0.09$  from bottom of plate)
- Figure 3.12 Velocity field of the non-partitioning rib type plate for  $Re=2000$  (Cross-section normal to the corrugated plate at  $x=0, y=0.09$  from bottom of plate)
- Figure 3.13 Friction factor vs. corrugate pitch for different height
- Figure 3.14 Colburn  $j$  factor vs. corrugate pitch for different height
- Figure 3.15 Comparison of the proposed correlation for friction factor with the CFD analysis data
- Figure 3.16 Comparison of the proposed correlation for heat transfer coefficient with the CFD analysis data
- Figure 3.17 Influence of the corrugation angle on construction, operation and total costs
- Figure 4.1 Schematic diagram of the two-phase flow experimental system
- Figure 4.2 Variations of condensation heat transfer coefficient with mean vapor quality for various mass fluxes, type A
- Figure 4.3 Variations of condensation heat transfer coefficient with mean vapor quality for various mass fluxes, type B
- Figure 4.4 Variations of condensation heat transfer coefficient with mean vapor quality for two heat fluxes, type A
- Figure 4.5 Variations of condensation heat transfer coefficient with

mean vapor quality for two heat fluxes, type B

Figure 4.6 Variations of condensation heat transfer coefficient with mean vapor quality for two saturation temperature, type A

Figure 4.7 Variations of condensation heat transfer coefficient with mean vapor quality for two saturation temperature, typeA

Figure 4.8 Effects of the refrigerant feeding method on the condensation heat transfer, type B

Figure 4.9 Comparison of the present heat transfer data with those for plate heat exchanger from Yan et. al.

Figure 4.10 Comparison of the proposed correlation for Nusselt number with the present data, Type A

Figure 4.11 Comparison of the proposed correlation for Nusselt number with the present data, Type B

Figure 4.12 Variations of evaporation heat transfer coefficient with mean vapor quality for various mass fluxes, type A

Figure 4.13 Variations of evaporation heat transfer coefficient with mean vapor quality for various mass fluxes, type B

Figure 4.14 Variations of evaporation heat transfer coefficient with mean vapor quality for two heat fluxes, type A

Figure 4.15 Variations of evaporation heat transfer coefficient with mean vapor quality for two heat fluxes, type B

Figure 4.16 Variations of evaporation heat transfer coefficient with mean vapor quality for two saturation temperature, type A

Figure 4.17 Variations of evaporation heat transfer coefficient with mean vapor quality for two saturation temperature, type B

- Figure 4.18 Effects of the refrigerant feeding method on the evaporation heat transfer, type B
- Figure 4.19 Effects of the refrigerant feeding method on the evaporation heat transfer, type B
- Figure 4.20 Comparison of the present heat transfer data with those for plate heat exchanger from Yan et. al.
- Figure 4.21 Comparison of the proposed correlation for Nusselt number with the present data, Type A
- Figure 4.22 Comparison of the proposed correlation for Nusselt number with the present data, Type B
- Figure 4.23 Variations of pressure drop with mean vapor quality for various mass fluxes, type A
- Figure 4.24 Variations of pressure drop with mean vapor quality for various mass fluxes, type B
- Figure 4.25 Variations of pressure drop with mean vapor quality for two heat fluxes, type A
- Figure 4.26 Variations of pressure drop with mean vapor quality for two heat fluxes, type B
- Figure 4.27 Variations of pressure drop with mean vapor quality for two heat fluxes, type A
- Figure 4.28 Variations of pressure drop with mean vapor quality for two heat fluxes, type B
- Figure 4.29 Comparison of the present friction factor with those for plate heat exchanger from Yan et. al.
- Figure 4.30 Comparison of the proposed correlation for friction factor

number with the present data, Type A

Figure 4.31 Comparison of the proposed correlation for friction factor  
number with the present data, Type B

## **Tables**

Table 1.1 Preview of study on the plate heat exchanger

Table 1.2 Preview of study on the two-phase flow heat transfer and  
pressure drop

Table 2.1 Specification of the plate and shell heat exchanger

Table 2.2 Single-phase flow test conditions

Table 3.1 Geometric parameters of plate in the analysis cases which  
were investigated numerically

Table 4.1 Summary of two-phase flow test conditions

Table 4.2 Parameters and estimated uncertainties

## **Photographs**

Photo. 1.1 Plate and shell heat exchanger

Photo. 2.1 Single-phase heat transfer and pressure drop experimental  
system

Photo. 2.2 Heat transfer plate in the plate and shell heat exchanger

Photo. 4.1 Two-phase flow heat transfer and pressure drop  
experimental system

Photo. 4.2 Test section

# **Study on the Heat Transfer and Pressure Drop Characteristic in the Plate and Shell Heat Exchanger**

**Moo Gyo Seo**

*Department of Refrigeration And Air Conditioning Engineering*

*The Graduate School,*

*Pukyong National University*

## **Abstract**

많은 산업적 용도를 갖는 에너지 변환기기로서의 열교환기는 현재까지 성능 개선을 위한 지속적인 연구와 개발이 이루어져 왔으나 아직도 그 성능과 효율개선의 여지가 많으며, 실질적으로도 많은 문제를 가지고 있다. 세계적으로도 고성능의 열교환기를 개발하기 위한 연구가 활발히 진행되고 있으며, 국내에서도 이에 대한 연구가 요구되고 있다. 또한 최근 들어 냉동·공조분야에서도 갈수록 심화되는 사용공간의 제약성으로 인해 단위부피당 전열면적을 극대화시킨 고밀도, 고효율 열교환기가 관심을 끌고 있다. 또 최적의 설계로 압력손실은 낮추고 열전달계수는 극대화시킨 경제적이고 효율적인 냉동·공조 시스템 설계에 노력을 기울이고 있다.

고밀도 열교환기의 하나인 플레이트 앤 셸 열교환기는 셸엔튜브열교환기와 판형열교환기의 장점을 동시에 가진 열교환기로서 판형열교환기의 장점인 높은 효율과 고밀도를 가지고 셸엔튜브열교환기의 장점인 고압 내구성으로 인해 냉동·공조 시스템에서의 이용 전망은 매우 높다. 그러나 판각형 열교환기는 판형 열교환기와 유사하나 그

에 대한 연구는 이루어지지 않은 상태이다. 따라서 본 연구에서는 단상유동 열전달 및 압력강하 특성에 관한 연구와 전산유체역학을 이용하여 플레이트 앤 셀 열교환기의 성능해석을 통해 유동최적화에 관한 연구 및 냉매 R-134a를 사용하여 판각형 열교환기의 이상유동 열전달 및 압력강하 특성에 관한 연구를 통해 다음과 같은 결론을 얻었다.

단상유동 열전달 및 압력강하 실험을 통해 단상유동 열전달 및 압력강하 상관식을 제안하였으며 또한 전산유체역학을 이용한 형상모델링 및 단상유동해석을 통해 단상유동해석결과를 실험결과와 비교, 그 타당성을 검증하였으며 판의 형상, 세브론 각, 코루게이트의 높이 및 피치에 따른 성능을 CFD해석을 통해 파악하였다.

이상유동 열전달 및 압력강하에 관한 연구에서는 실험 범위를 냉매 질량유속  $45 \sim 120 \text{ kg/m}^2\text{s}$ , 평균 부과된 열유속  $6 \sim 8 \text{ kW/m}^2$ , 냉매의 포화온도  $20 \sim 40 \text{ }^\circ\text{C}$ 로 실험하여 냉매의 질량유량, 열유속, 포화온도 및 냉매공급방법이 이상유동 열전달 및 압력강하에 미치는 영향에 대한 실험을 통해 응축, 증발 및 압력강하에 적용할 수 있는 상관식을 제안하였다.

이상과 같이 단상유동 열전달 및 압력강하 특성에 관한 연구와 전산유체역학을 이용한 해석 및 이상유동 열전달 및 압력강하 특성에 관한 연구를 통해 플레이트 앤 셀 열교환기의 설계에 필요한 기초설계자료를 제공하고자 한다.

## NOMENCLATURE

### SYMBOLS

$A$	: heat transfer area of the plate	[m <sup>2</sup> ]
$A_{fa}$	: free flow area between plates	[m <sup>2</sup> ]
$A_p$	: projected heat transfer area of the plate	[m <sup>2</sup> ]
$b$	: channel spacing	[m]
$C_p$	: specific heat	[J/kgK]
$d$	: pipe diameter	[m]
$D$	: plate diameter	[m]
$D_{eq}$	: equivalent diameter	[m]
$D_h$	: hydraulic diameter	[m]
$f$	: friction factor	
$g$	: gravity acceleration	[m/s <sup>2</sup> ]
$G$	: mass flux	[kg/m <sup>2</sup> s]
$h$	: heat transfer coefficient	[W/m <sup>2</sup> K]
$H$	: corrugate height	[m]
$i_{fg}$	: enthalpy of vaporization	[J/kg]
$k$	: thermal conductivity	[W/mK]
$L$	: channel length from center of inlet port to center of exit port	[m]
LMTD	: log mean temperature difference	[°C]
$\dot{m}$	: mass flow rate	[kg/s]
Nu	: nusselt number, dimensionless	
$p$	: pressure	[MPa]
$P$	: corrugate pitch	[m]

$Pr$	: prandtl number, dimensionless	
$Q$	: heat transfer rate	[W]
$q_w''$	: average imposed heat flux	[W/m <sup>2</sup> ]
$R_{wall}$	: heat transfer resistance of the wall	[K/W]
$Re$	: reynolds number, dimensionless	
$t$	: thickness of plate	[m]
$T$	: temperature	[°C]
$U$	: overall heat transfer coefficient	[W/m <sup>2</sup> K]
$u$	: velocity	[m/s]
$w$	: channel width of the plate	[m]
$x$	: vapor quality	

### GREEK SYMBOLS

$\Delta p$	: pressure drop	[Pa]
$\Delta T$	: temperature difference	[°C]
$\Delta x$	: total quality change in the exchanger	
$\varepsilon$	: dissipation rate	[m <sup>2</sup> /s <sup>3</sup> ]
$\theta$	: Chevron angle	[°]
$\kappa$	: kinetic energy	[m <sup>2</sup> /s <sup>2</sup> ]
$\mu$	: viscosity	[Ns/m <sup>2</sup> ]
$v$	: specific volume	[m <sup>3</sup> /kg]
$\rho$	: density	[kg/m <sup>3</sup> ]
$\Phi$	: surface area enlargement factor	



## **SUBSCRIPTS**

<i>ave</i>	: average
<i>c</i>	: cold side of the test section
<i>de</i>	: deceleration
<i>ele</i>	: elevation
<i>exp</i>	: experiment
<i>f</i>	: friction
<i>fg</i>	: difference between liquid phase and vapor phase
<i>g</i>	: vapor phase
<i>h</i>	: hot side of the test section
<i>i</i>	: inlet and exit of test section
<i>l</i>	: liquid phase
<i>lat</i>	: latent heat
<i>m</i>	: average value for the two phase mixture or between the inlet and exit
<i>man</i>	: test section inlet and exit manifolds and ports
<i>o</i>	: exit of test section
<i>p</i>	: pre-heater
<i>sat</i>	: saturate
<i>sens</i>	: sensible heat
<i>r</i>	: refrigerant
<i>t</i>	: test section
<i>w</i>	: water
<i>wall</i>	: wall

## **CHAPTER 1**

### **INTRODUCTION**

#### **1.1 BACKGROUND**

It is well recognized that the quick destruction of the ozone layer in the earth atmosphere noted recently has been primarily related to the wide use of the chlorofluorocarbon(CFC) refrigerants, which have been employed as the working fluids in many refrigeration, air conditioning and heat pump systems or as cleansing fluids for processing micro-electronic devices. Under the mandate of the Montreal Protocol, the use of CFCs had been phased out and the use of HCFCs will also be phased out in a short period of time. Therefore, we have to replace the CFCs by new alternative refrigerants. In order to use properly these new refrigerants, we need to know their thermodynamic, thermo-physical, flow and heat transfer properties. Specifically, we realize that a much more detailed understanding of the flow boiling and condensation heat transfer of new refrigerants(R-134a, R-125, R-152, etc.) is very important in the design of evaporators and condensers used in many current refrigeration and air conditioning systems.

Also, in the competitive commercial environment of the industrial world, there is always a pressure to reduce the capital and running costs for each and every operation: heat transfer is no exception to this. The pressure difference acts as a driving force for running cost of heat

exchangers, whether they are compact or not. In addition to this cost saving pressure, however, there is an overriding requirement from industry about the long term reliability of any equipments under operating conditions. This requirement sometimes manifests itself as an apparent reluctance of industry to adopt new forms of technologies and designs. Yet, another positive force, driving the new developments in heat exchangers, comes from innovative ideas, and designs. Innovative ideas come from better understanding of the underlying processes of heat transfer, and new designs from advances in manufacturing technology. All these forces, either driving the new developments positively or apparently holding them back, often interact with each other in a complex way.

A heat exchanger is defined as a compact heat exchanger if it has area density in excess of  $700 \text{ m}^2/\text{m}^3$ <sup>(1)</sup>.

### **Desirable Features of Heat Exchangers**

In order to obtain maximum heat exchanger performance at the lowest possible operating and capital costs without compromising the reliability, the following features are required of an exchanger.

1. Higher heat transfer coefficient and larger heat transfer area: These two factors increase the heat transfer rate for a given temperature difference and improve the heat exchanger effectiveness or temperature approach.

High heat transfer coefficient can be obtained by using heat transfer surfaces which promote local turbulence for single phase flow or have some special features for two-phase flow. Heat transfer area can be

increased by using larger exchangers, but the most economical way is to use a heat exchanger having a large area density per unit exchanger volume. For some duties, such as those involving a gaseous phase, secondary heat transfer area is also very useful. High area densities become economically even more attractive when an exchanger is built from expensive special materials such as titanium or nickel.

2. Low pressure drop : Pumping costs are dependent on pressure drop within an exchanger. Therefore low pressure drop means low operating costs. Normally the devices or surfaces that provide high heat transfer coefficients also give high pressure gradients i.e. the pressure drop per unit length of flow path. Exchangers designed to give enhanced performance, however, require shorter flow paths to achieve a given duty. It is therefore possible that these exchangers have a high pressure gradient but not so high a pressure drop.

3. Counter current flow arrangement : In order to obtain maximum mean temperature driving difference, a pure counter current flow arrangement is desirable. Any deviation from this arrangement reduces the mean temperature driving difference and a correction factor to the log mean temperature difference needs to be applied.<sup>(2)</sup> Most of the compact heat exchangers are configured to provide pure counter current flow arrangement.

### **Flow passage structure in plate heat exchangers**

The common feature of all plate heat exchangers is the use of corrugations in the plates, giving both support against internal pressures and heat transfer enhancement. The most common type of plate uses

crossed corrugations, that is, the corrugation patterns in adjacent plates are at an angle to each other, giving lattice of support points where they touch, and a complex flow channel shape between the plates. The corrugations are usually formed as chevrons. There may be a single chevron pattern or multiple chevrons across the plate width. Other variants have the chevron pattern running along the length of the plate. In all cases, however, the local flow geometry has the same cross corrugated structure.

For the cross corrugated plates formed from the chevron pattern, chevron angle is an important variable. The chevron angle referred to here is the angle, of the corrugations with respect to a horizontal line. A low chevron angle plate gives high heat transfer and high pressure drop whereas a high chevron angle plate gives lower heat transfer as well as lower pressure drop. The low and high chevron angle plates are also referred to as hard plates and soft plates respectively, reflecting the resistance that they present to a flowing fluid. For single phase duties, reliable information is generally available for the effect of chevron angle on heat transfer and pressure drop. Therefore selecting soft or hard plates or a combination of those to match the given requirements of pressure drop and heat transfer is relatively straightforward.

In addition to the main chevron pattern, the pattern on the distribution regions of the plates is also important and has a significant role to play in uniform distribution of a stream in a given plate channel.<sup>(3~5)</sup>

Of the many different types of plate corrugations available (Shah and Focke<sup>(6)</sup>), the more commonly used chevron plate pattern is illustrated in Fig. 1.1. Plates with  $\theta = 30^\circ$  or  $60^\circ$  are usually stacked together in

either a symmetric or mixed arrangement as shown in Fig. 1.1(a). The plate surface geometry is characterized by the corrugation inclination angle  $\theta$ , its wavelength  $\lambda$ , amplitude  $b$ , and profile (Fig. 1.1 (b)), and the surface enlargement factor  $\Phi$  (ratio of effective corrugated surface area to the projected area of the plate). The enhanced heat transfer is directly related to these features, which provide increased effective heat transfer area, disruption and reattachment of boundary layer, swirl or vortex flow generation, and small hydraulic diameter flow channels. Generally both heat transfer coefficients and flow friction losses increase with higher  $\theta$  and  $\Phi$  chevron plate (Manglik<sup>(7)</sup>)

#### **Advantages of a plate heat exchanger.**

Compared with the well-established shell-and-tube heat exchangers, the plate heat exchanger (PHE) shows a number of advantages within its capability range.

The PHE is increasingly becoming the standard for closed-circuit cooling applications aboard ships, on oil platforms, in power stations, where, for example, a titanium PHE may be used to transfer heat from closed-circuit cooling water to seawater. Wherever a close temperature approach is required, weight or space is at a premium, or corrosion-resistant materials such as stainless steel or titanium are needed, the PHE becomes the prime candidate for heat exchanger selection. It is also used widely as a steam heater, as an evaporator, as part of air-conditioning plants in large buildings, as a wet gas cooler, and more recently in refrigeration plants. The significant advantages are given below.

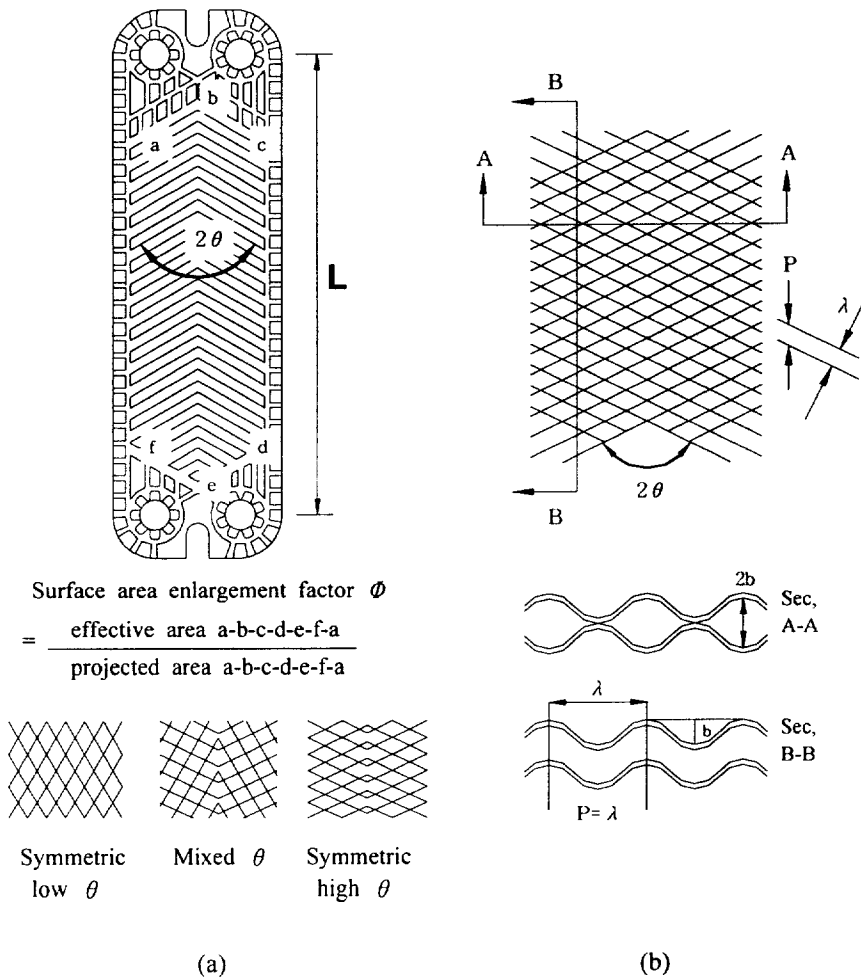


**Fig. 1.1** Chevron plates : (a) different chevron angle plates and their stack arrangements, and (b) geometrical features of plate corrugations

### 1. High NTU values

The general trend of increasing energy cost and the need to conserve energy resources imply a requirement for high heat recoveries in heat exchangers. The PHE attains high heat transfer coefficients and basically operates with full counter-current flow, enabling small end temperature differences. These features allow high recuperative efficiencies, and often a number of transfer units (NTU) of 6 can be achieved in a single pass. In a recuperative interchange this is equivalent to 86% heat recovery.

### 2. Compactness

In a tubular heat exchanger, liquid holdup compared with the surface area is large. In a PHE, use of essentially rectangular channels with narrow gaps leads to a compact construction and low liquid holdup. This feature is enhanced by the high heat transfer coefficients, which reduce the surface area requirements compared with a shell-and-tube exchanger. Another advantages of the low holdup are low weight and a short start-up time.

### 3. Low cost

Simple pressing combined with no welding means a low cost per unit surface area, particularly with more expensive corrosion-resistant materials. Even when the heat transfer surface in a PHE is constructed from stainless steel, it should not be assumed that a carbon steel shell and tube will be less expensive.

### 4. Multiple duties

Use of special connector plates that act as intermediate headers allows a number of separate heat exchanger duties to be housed in a single frame.



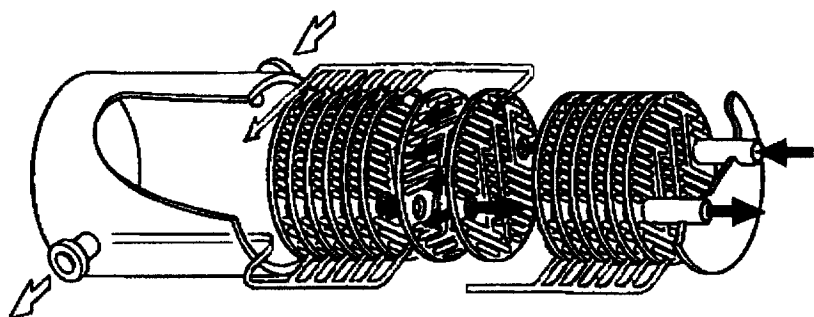
This feature has the attendant advantages of reduced cost, weight, and space requirement.

#### 5. Reduced fouling

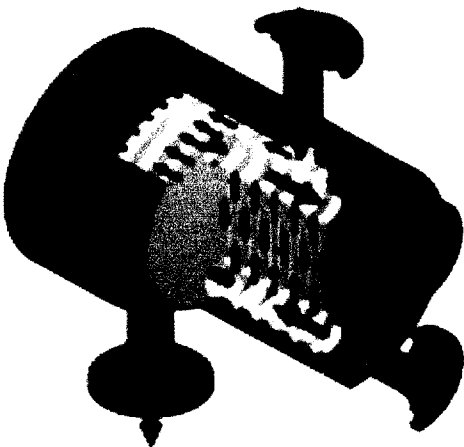
Because the high heat transfer coefficients in a PHE are generated by turbulence, the surface shear stresses are very high, allowing a high fouling removal rate. Comparing with the shell and tube, fouling resistances are very low for most types of fouling.

#### **Plate and shell heat exchanger**

The P&SHE is a variant on the conventional plate heat exchanger. The plates are circular, and welded into a stack, which fits into a cylindrical shell. Operating temperatures up to 350°C, and pressures up to 100 bar can be achieved. Although apparently very different from the conventional rectangular plate exchanger, the underlying flow passage structure through the exchanger is the same as in the conventional plate heat exchanger.



(a)



(b)

Fig. 1.2 Schematic diagram of plate and shell heat exchanger.

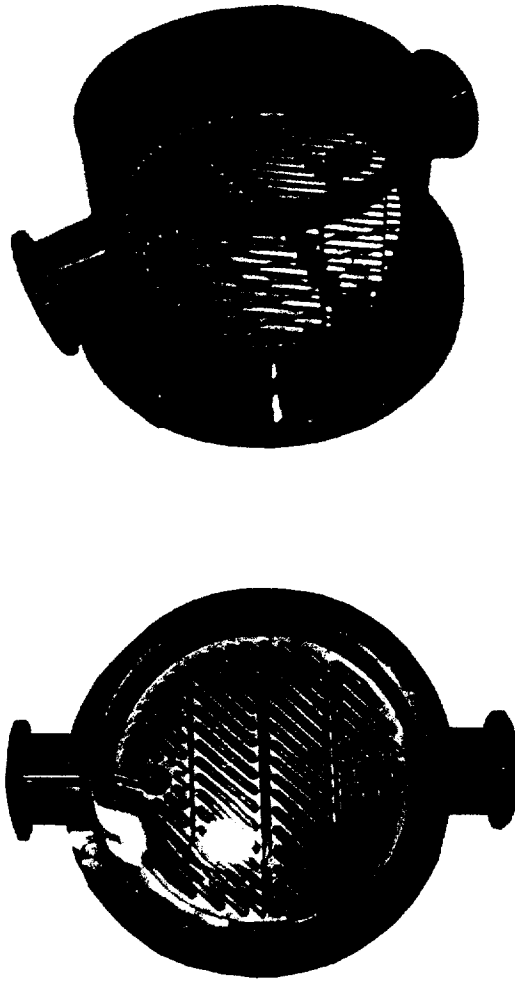


**Photo 1.1** Plate and shell heat exchanger.

## 1.2 REVIEW OF PREVIOUS STUDY

### 1.2.1 Preview of study on the plate heat exchangers

A brief review of literature relevant to the present study is given in the following.

Buonopane et al.<sup>(8)</sup> proposed design method of plate heat exchanger by using LMTD analysis method in single-phase flow, and Jackson et al. proposed heating and cooling overall heat transfer coefficient correlation and experimentally verified in case of  $Re < 400$ . Raju et al.<sup>(9)</sup> arranged for the heat transfer and pressure drop correlation, proposed outline of the PHE design method, and compared performance of PHE and shell and tube heat exchanger. Edwards<sup>(10)</sup> tried to obtain the correlation between pressure and heat transfer based on the average hydraulic diameter, and also investigated general characteristics of PHE. Cooper<sup>(11)</sup> compared the advantage, disadvantage and performance of PHE and tube type heat exchanger. He suggested equation of heat transfer coefficient and friction factor for the PHE. By using FDM, Kandlikar and Shah et al.<sup>(3)</sup> researched the end effect for the number and arrangement of various flow channels. In there research, LMTD correction factor and effectiveness were proposed with tables. In recent, Gaiser et al.<sup>(12)</sup> obtained the distribution of local heat transfer coefficient by the analogy of mass transfer and heat transfer, and proposed average heat transfer coefficient, average mass transfer and pressure drop etc. In the decade of 1990, research was activated for the brazed type PHE by developing fabrication teachings. Bogaert et al.<sup>(13)</sup> investigated thermal and hydraulic performances of the brazed type PHE. Heat transfer and fluid-flow of the

brazed type PHE were investigated experimentally and numerically and experimental results for the heat transfer and pressure drop were proposed by Stasiek et al.<sup>(14)</sup> On the other hand, 3-D FVM analysis was tried and compared with various numerical researches. The reviews by Shah and Focke<sup>(6)</sup>, Manglik and Muley<sup>(15)</sup>, and Manglik<sup>(7)</sup> addressed some aspects of the thermal-hydraulic performance, product development, and design applications of PHEs. Several investigators reported thermal-hydraulic characteristics of chevron plate PHEs (Okada et al.<sup>(16)</sup>; Marriott<sup>(17)</sup>; Focke et al.<sup>(18)</sup>; Talik et al.<sup>(19),(20)</sup>; Muley and Manglik<sup>(21~23)</sup>; Thonon et al.<sup>(24)</sup>). The recent survey by Manglik<sup>(7)</sup> provides a detailed summary of the available  $Nu$  and  $f$  correlations for Chevron plates. The predictions from most of these equations are observed to disagree considerably with each other and present a rather wide performance envelope(Manglik<sup>(7)</sup>). In virtually all studies, separate power-law type curve-fit equations are given for each plate surface with different  $\theta$  that cover a rather limited data set and range of flow conditions. Savostin and Tikhonov<sup>(25)</sup>, Tovazhnyanski et al.<sup>(26)</sup> and Wanniarachchi et al.<sup>(27)</sup> have attempted to incorporate  $\theta$  effects into single equations for  $Nu$  and  $f$ , respectively. However, their equations have different functional forms, with little agreement between their predictions for typical flow conditions and  $\theta$  (Manglik<sup>(7)</sup>). The effect of surface enlargement factor,  $\Phi$  has been largely ignored. This lack of generalized predictive tools inhibits effective usage of Chevron plates in many PHE applications.

**Table 1.1** Preview of study on the plate heat exchanger

<b>Investigator</b>	<b>Working Fluid</b>	<b>Description</b>
Buonopane et al. <sup>(8)</sup>		Design method of plate heat exchanger by using LMTD analysis
Raju et al. <sup>(9)</sup>		arranged for the heat transfer and pressure drop correlation, proposed outline of the PHE design method and compared performance of PHE and shell and tube heat exchanger
Edwards <sup>(10)</sup>	water, lubricating oil etc.	obtain the correlation between pressure and heat transfer based on the average hydraulic diameter
Cooper <sup>(11)</sup>		Compared the advantage, disadvantage and performance of PHE and tube type heat exchanger
Kandlikar and Shah <sup>(3)</sup>		By using FDM researched on the end effect for the number and arrangement of various flow channels
Gaiser et al. <sup>(12)</sup>	reactive gas, air	obtained the distribution of local heat transfer coefficient by the analogy of mass transfer and heat transfer
Bogaer et al. <sup>(13)</sup>	water, mineral oil	investigated the thermal and hydraulic performance of the brazed type PHE
Stasiek et al. <sup>(14)</sup>	air	heat transfer and fluid-flow of the brazed type PHE were investigated experimentally and numerically

Investigator	Working Fluid	Description
Shah and Focke <sup>(6)</sup> manglik and Muley <sup>(15)</sup>		addressed some aspects of the thermal-hydraulic performance, product development and design applications of PHEs
Okada et al. <sup>(16)</sup> etc <sup>(17~24)</sup>		thermal-hydraulic characteristics of Chevron plate PHEs
Savostin and Tikhonov <sup>(25)</sup>		separate power-law type curve-fit equation are given for each plate surface with different $\theta$
Tovazhnyanski et al. <sup>(26)</sup> and Wanniarachchi et al. <sup>(27)</sup>		attempt to incorporate $\theta$ effects into single equation for Nu and f

### **1.2.2 Preview of study on the two-phase flow heat transfer and pressure drop.**

For in-tube condensation, Schlager et al.<sup>(28)</sup> used R-22 as the working fluid and three micro-finned tubes with an outer diameter of 12.7 mm were tested. A smooth tube was also tested to establish a basis for comparison. The average condensation heat transfer coefficients of the micro-finned tubes were 1.5 to 2.0 times larger than those in the smooth tube. Micro-finned tubes having 9.5 mm OD and 8.9 mm maximum ID were also tested<sup>(29)</sup>. The condensation heat transfer enhancement factors were between 1.4 and 1.8 while the pressure drop penalty factors ranged from 1.0 to slightly higher than 1.2.

Later, Eckels and Pate<sup>(30)</sup> examined the in-tube flow evaporation and condensation heat transfer for refrigerants R-134a and R-12. The heat transfer coefficients were measured in a horizontal, smooth tube with an inner diameter of 8.0 mm. For similar mass fluxes, R-134a showed a 25 to 35% higher heat transfer coefficient when compared with R-12 for condensation. Torikoshi and Ebisu<sup>(31)</sup> experimentally investigated evaporation and condensation heat transfer and pressure drop for R-134a, R-32, and a mixture of R-134a/R32 in a horizontal smooth tube. The condensation heat transfer coefficients for R-32 and R-134a are respectively about 65% and 10% larger than those for R-22 at the same mass flux. For a mixture of R-32 and R-134a, the condensation heat transfer coefficients fall below those for R-22. In the study by Liu<sup>(32)</sup>, condensation and evaporation heat transfer and pressure drop of R-134a and R-22 in a tube were investigated. The condensation heat transfer coefficients for R-134a are 8 to 18% higher and the pressure drop is



50% higher than those for R-22.

Recently, Chamra and Webb<sup>(33)</sup> tested some advanced micro-finned tubes formed by applying a second set of grooves at the same helix angle but in an opposite angular direction to the first set. They found that the tubes provided 27% higher condensation heat transfer coefficient than the single-helix tube, while the pressure drop was only 6% higher.

Some correlations for estimating in-tube condensation heat transfer coefficient were proposed in the literature. Akers et al.<sup>(34)</sup> measured average condensation heat transfer coefficients for R-12 and propane inside horizontal tubes. The heat transfer coefficient was found to be increased with the vapor velocity. Their experimental data were correlated in terms of an equivalent Reynolds number. Moreover, Shah<sup>(35)</sup> proposed a correlation for film condensation inside pipes based on a wide variety of experimental data including water, R-11, R-12, R-22 and R-113 in horizontal, vertical and inclined pipes with diameter ranging from 7 to 40 mm. Yan et al.<sup>(36,37)</sup> investigated condensation and evaporation heat transfer and pressure drop of refrigerant R-134a in a plate heat exchanger. A close inspection of the literature reviewed above reveals that only some heat transfer characteristics and pressure drop for the in-tube condensation and evaporation of the new refrigerant R-134a have been investigated. Unfortunately, there are rather limited data available for the design of PHEs and P&SHEs.

**Table 1.2** Preview of study on the two-phase flow heat transfer and pressure drop

Investigator	Working Fluid	Test section	Description
Schlager et al. <sup>(28)</sup>	R-22	micro-finned tubes OD 12.7 mm	in-tube condensation
Eckels and Plate <sup>(30)</sup>	R-134a R-12	smooth tube ID 8.0 mm	in-tube flow evaporation
Torikoshi and Ebisu <sup>(31)</sup>	R-134a R-32 R-134a/R32	horizontal smooth tube	evaporation and condensation heat transfer and pressure drop
Liu <sup>(32)</sup>	R-134a R-22		condensation and evaporation heat transfer and pressure drop
Chamra and Webb <sup>(33)</sup>		micro-finned tubes formed by applying a second set of grooves at the same helix angle	condensation heat transfer
Akers et al. <sup>(34)</sup>	R-12	inside horizontal tube	condensation heat transfer coefficient
Shah <sup>(35)</sup>	R-11,R-12 R-22,R-113	7 ~ 40 mm	proposed a correlation for film condensation inside pipes
Yan et al. <sup>(36,37)</sup>	R-134a	plate heat exchanger	condensation and evaporation heat transfer and pressure drop

### **1.3 OBJECTIVES AND OUTLINE OF THE STUDY**

A close inspection of the literature reviewed above reveals that only some heat transfer characteristics and pressure drop for in-tube condensation and evaporation of the new refrigerant R-134a have been investigated. Some studies about PHE have been reported in the open literature focusing on the single phase liquid to liquid heat transfer. But there is little data available for the design of P&SHE used as evaporators and condensers.

Plate and shell heat exchanger (P&SHE) are widely applied to refrigeration and air conditioning systems such as evaporators or condensers for their higher efficiency and compactness. In order to set up the database for the design of the P&SHE, heat transfer and pressure drop characteristics for single phase flow of water were experimentally and numerically investigated in this study. Single phase heat transfer coefficients were measured for turbulent water flow in a plate and shell heat exchangers by Wilson plot method. Numerical work was conducted using the FLUENT code.

And, the characteristics of condensation and evaporation heat transfer and pressure drop for refrigerant R-134a flowing in a plate and shell heat exchanger were explored experimentally.

This paper includes five chapters and the respective summary is briefly mentioned below.

Chapter 1 shows background and object of study an investigation of the primary item including the previous study.

In chapter 2, heat transfer and pressure drop characteristics for single

phase flow of water in a plate & shell heat exchanger are experimentally investigated. Single phase heat transfer coefficients were measured for turbulent water flow in a plate and shell heat exchangers by the Wilson plot method.

In chapter 3, heat transfer and pressure drop characteristics for single phase flow of water were numerically investigated. Numerical work was conducted using the FLUENT code. The study includes the flow distribution, thermal distribution and the pressure distribution in the channel of plate and shell heat exchanger.

In chapter 4, the characteristics of condensation and evaporation heat transfer and pressure drop for refrigerant R-134a flowing in a plate and shell heat exchanger were explored experimentally.

Chapter 5 summarizes the previous chapters and shows the final conclusions.

## **CHAPTER 2**

# **SINGLE-PHASE FLOW HEAT TRANSFER AND PRESSURE DROP CHARACTERISTICS**

An experimental investigation of the single-phase flow heat transfer and pressure drop characteristics in a plate and shell heat exchanger was reported in this chapter. Single-phase turbulent flow of water is considered and two types of plate were used. Based on the experimental data, correlations for  $Nu$  and  $f$  are developed along with the  $Re$  dependence.

## **2.1 EXPERIMENTAL APPARATUS AND METHOD**

### **2.1.1 Experimental apparatus**

Figure 2.1 and photograph 2.1 show the schematic diagram and the photograph of the experimental apparatus used in this study. In the test section, hot water flows between plates and cold-water flows in the shell side. The hot and cold-water circuit includes a 200 ℓ water thermostat with a 5 kW heater and a water-cooled refrigeration system of 2 RT cooling capacity. To minimize the heat loss to the ambient, the whole test section is wrapped with 10 cm thick polyethylene. The average heat flux in the test section was calculated by the water temperature rise between the channel inlet and outlet and by the water flow rate. The

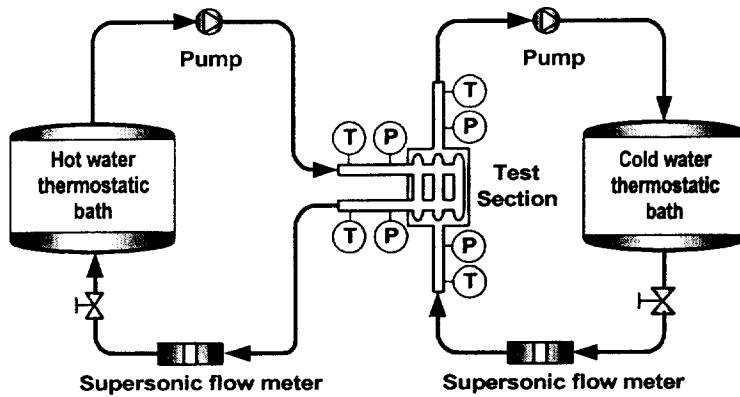


**Fig. 2.1** Schematic diagram of the single-phase heat transfer and pressure drop experimental system.

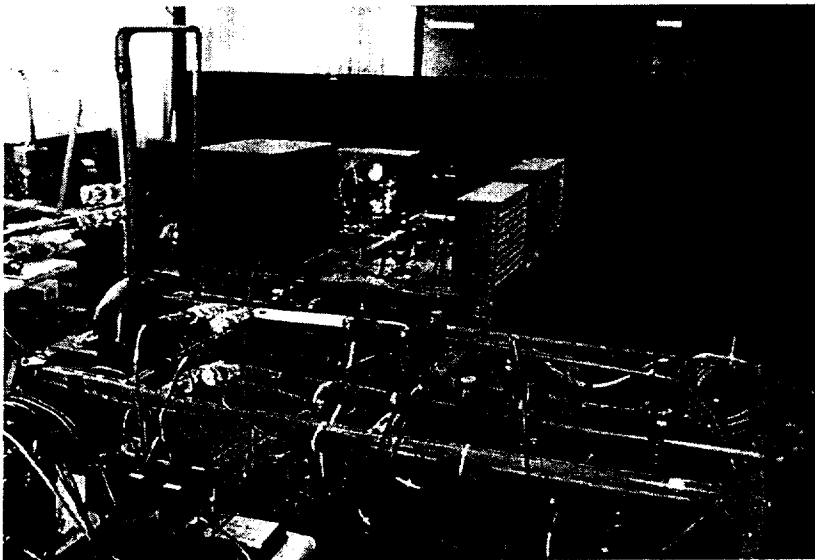


**Photo. 2.1** Single-phase heat transfer and pressure drop experimental system.

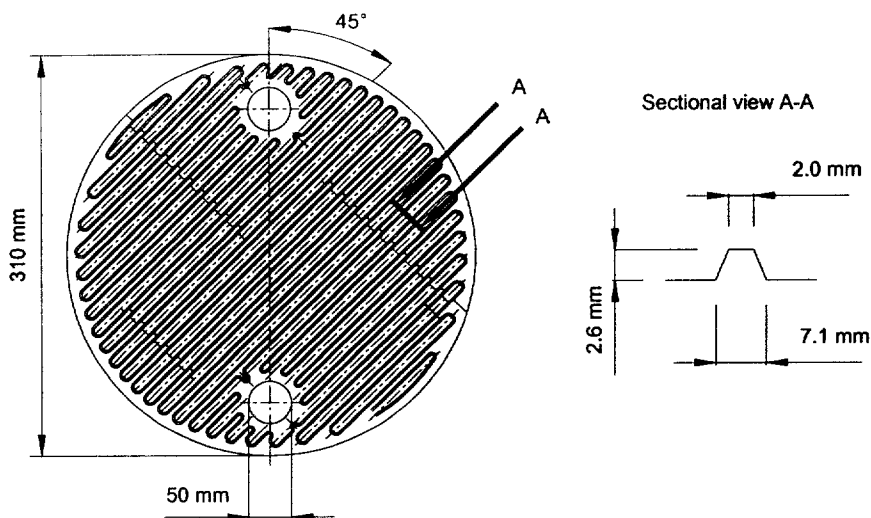
accuracy of temperature measurement of water by the sheath type thermo-couple is  $0.1^{\circ}\text{C}$ . The water flow meter(Controtron, Model 1010WDP1) has an accuracy of 1%. The pressure transducers(Keller, Model PR-23) having accuracy of 0.2% were also connected to the inlet and outlet of the test section.

### **2.1.2 The test section : Plate and shell heat exchanger**

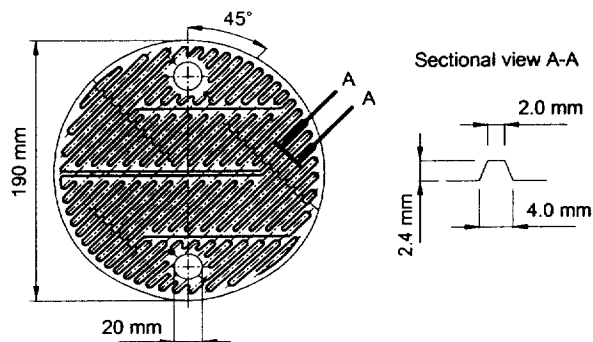
The two types of plate and shell heat exchanger used in this study, as schematically shown in Fig. 2.2 were formed by three commercialized SUS-304 plates. The plate surfaces were stamped to become grooved with a corrugated trapezoid shape and  $45^{\circ}$  of chevron angle. Photo. 2.2 show the photograph of the heat transfer plate. The corrugated grooves on the right and left outer plates have an oblique shape but the middle plate has a contrary oblique shape on both sides. Due to the contrary oblique shapes between two neighbor plates the flow streams near the two plates cross each other in each channel. This cross flow creates a significantly unsteady and random flow. In fact, the flow is highly turbulent even at low Reynolds number. Fig. 2.3 show the details of flow pattern in plate and shell exchanger and Table. 2.1 represents the specification of the two types of plate and shell heat exchangers used in this study.

### **2.1.3 Experimental Procedures**

The heat transfer rate between the counter flow channels in the test section is varied by changing the flow rates of hot and cold water. Any change of the system variables leads to fluctuation in the temperature and



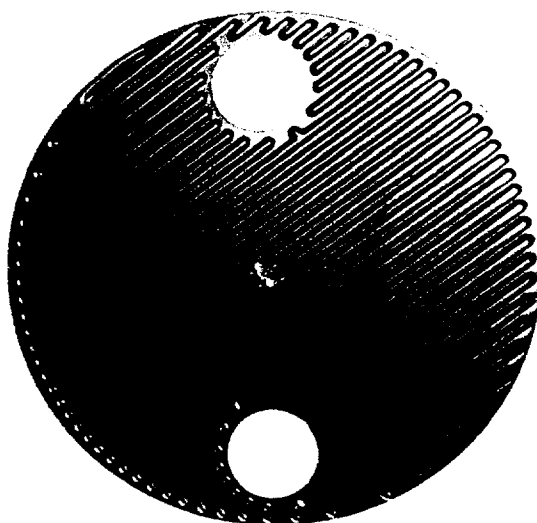
(a) P&SHE Type A



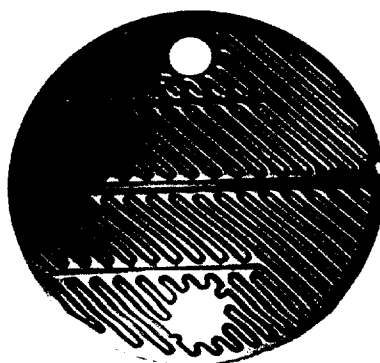
(b) P&SHE Type B

**Fig. 2.2** Schematic diagram of heat transfer plate in the plate and shell heat exchanger.





(a) P&SHE Type A



(b) P&SHE Type B

**Photo. 2.2** Heat transfer plate in the plate and shell heat exchanger.

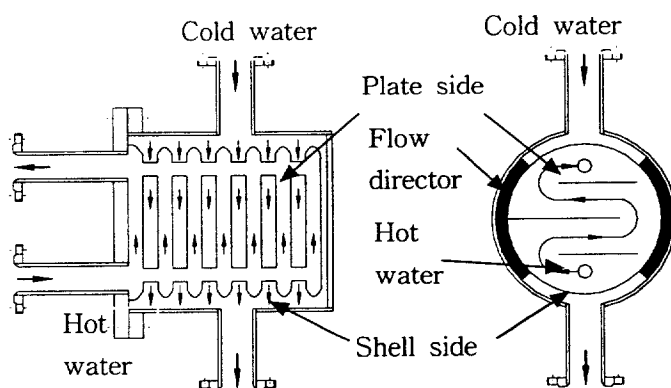


**Fig. 2.3** Details of flow pattern in plate and shell heat exchanger.

**Table 2.1** Specification of the plate and shell heat exchanger

	Type A	Type B
Plate material	SUS 304	
Shell material	Steel	
Number of plate	3	
Chevron angle [ ° ]	45	
Plate thickness [m]	0.007	
Plate diameter [m]	0.31	0.19
Port diameter [m]	0.05	0.02
Surface per plate [m <sup>2</sup> ]	0.078	0.0325
Corrugate pitch [m]	0.0071	0.004
Hydraulic diameter [m]	0.0052	0.0048

pressure of the flow. It takes about 20~100 minutes to reach a steady state at which variations of the time-average inlet and outlet temperatures are less than  $0.1^{\circ}\text{C}$  and the variations of the pressure is within 5%. Then the data acquisition unit(Fluke Model NetDAQ 2645A) scans all the data channels for 30 times in 3 min. The mean values of the data for each channel are obtained to calculate the heat transfer coefficient and pressure drop. Additionally, the flow rate of water in the test section should be high enough to have turbulent flow in the water side. In the present study, The Reynolds number of the water flow is maintained beyond 200 to make the turbulent flow. Table 2.2 show the single-phase flow test conditions.

#### 2.1.4 Data Reduction

From the definition of the hydraulic diameter, Shah and Wanniarachchi<sup>(38)</sup> suggested the use of two times the mean channel spacing as the hydraulic diameter for the plate heat exchangers when the channel width is much larger than the channel spacing, i.e.,

**Table 2.2** Single-phase flow test conditions

	Type A	Type B
Range of Reynolds Number	$800 < Re < 5000$	$1000 < Re < 8000$
Hot water inlet temperature [ $^{\circ}\text{C}$ ]	40 ( $\pm 0.5$ )	40 ( $\pm 0.5$ )
Cold water inlet temperature [ $^{\circ}\text{C}$ ]	25 ( $\pm 0.5$ )	25 ( $\pm 0.5$ )

$$D_h = \frac{4 \times A_c}{P} = \frac{4 \times b \times w}{(2b + 2w)} \approx 2b \quad \text{for} \quad w \gg b \quad (2.1)$$

The mass flux obtained from the measured mass flow rate such as

$$G = \frac{\dot{m}}{A_{fa}} \quad (2.2)$$

Since, shape of the plate in P&SHE is circular, plate width,  $w$  can be defined as the equivalent diameter,  $w = D_{eq} = \frac{2}{3} \cdot D$

$$A_{fa} = b \times D_{eq} \quad (2.3)$$

The Reynolds number is defined as,

$$Re = \frac{G \cdot D_h}{\mu} \quad (2.4)$$

The overall heat transfer coefficient between the two counter channel flows of water can be expressed as

$$U = \frac{Q_{ave}}{A \cdot LMTD} \quad (2.5)$$

Where the log mean temperature difference(LMTD) is determined from the inlet and exit temperatures of two flow channels:

$$LMTD = \frac{(\Delta T_1 - \Delta T_2)}{\ln(\Delta T_1 / \Delta T_2)} \quad (2.6)$$

with

$$\Delta T_1 = T_{h,i} - T_{c,o} \quad (2.7)$$

$$\Delta T_2 = T_{h,o} - T_{c,i} \quad (2.8)$$

$$Q_h = \dot{m}_h C_p (T_{h,i} - T_{h,o}) \quad (2.9)$$

$$Q_c = \dot{m}_c C_p (T_{c,i} - T_{c,o}) \quad (2.10)$$

energy balance between the hot and cold sides of water were within 5% for all cases, that is

$$\frac{|Q_h - Q_c|}{Q_{ave}} < 5\% \quad (2.11)$$

$$Q_{ave} = \frac{(Q_h + Q_c)}{2} \quad (2.12)$$

The relation between the overall heat transfer coefficient and the convective heat transfer coefficients on both sides can be expressed as

$$\left(\frac{1}{UA}\right) = \left(\frac{1}{h_h A}\right) + \left(\frac{1}{h_c A}\right) + \left(\frac{t}{kA}\right) \quad (2.13)$$

Where, fouling resistance and contact resistance is ignored. The heat transfer area was adopted from the real area in this study. Surface area

enlargement factor( $\phi$ ) was calculated from the CFD computational modeling.

$$A = \phi \times A_p = 1.13 \times A_p \quad (2.14)$$

The modified Wilson plot method as described by Farrell et al.<sup>(39)</sup> was used to calibrate the  $h_c$  and  $h_h$ .

## 2.2 RESULTS AND DISCUSSION

### 2.2.1 Single-phase flow heat transfer characteristics

In the present study, single-phase heat transfer correlation in plate side and shell side have been developed by the modified Wilson plot method. In order to determine the single-phase heat transfer coefficients in the plate side, the overall heat transfer coefficients were measured during heat exchange between the plate side and shell side passages. For a specified heat transfer resistance in shell side, the heat transfer resistance in the plate side was varied systematically.

Figure 2.4 shows the modified Wilson plot for the plate side and shell side used in the present study. The Wilson plot is graphical technique, which allowed the unknowns  $C_1$  and  $m$ . Here,  $X_1$  and  $Y_1$  are variables to obtain  $C_1$  and  $m$  from experimental data. Also, Figure 2.5 represents the heat transfer coefficient determined by this method. From the experimental result, a heat transfer correlation in the shell side and the plate side were developed as follows:

Type A (  $800 < Re < 5000$  ,  $4.16 < Pr < 5.83$  )

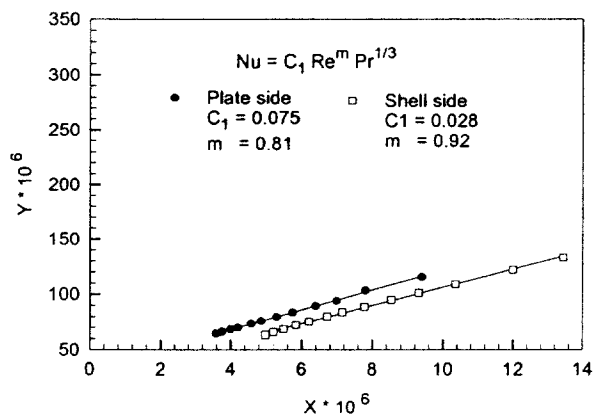
$$\text{Plate side : } Nu = 0.075 Re^{0.81} Pr^{1/3} \quad (2.15)$$

$$\text{Shell side : } Nu = 0.028 Re^{0.92} Pr^{1/3} \quad (2.16)$$

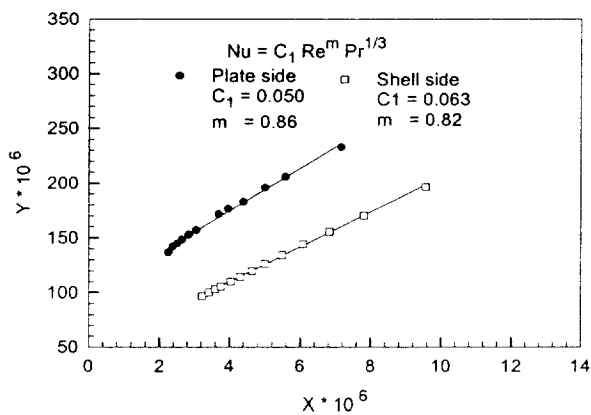
Type B (  $1000 < Re < 8000$ ,  $4.16 < Pr < 5.83$  )

$$\text{Plate side : } Nu = 0.05 Re^{0.86} Pr^{1/3} \quad (2.17)$$

$$\text{Shell side : } Nu = 0.063 Re^{0.82} Pr^{1/3} \quad (2.18)$$



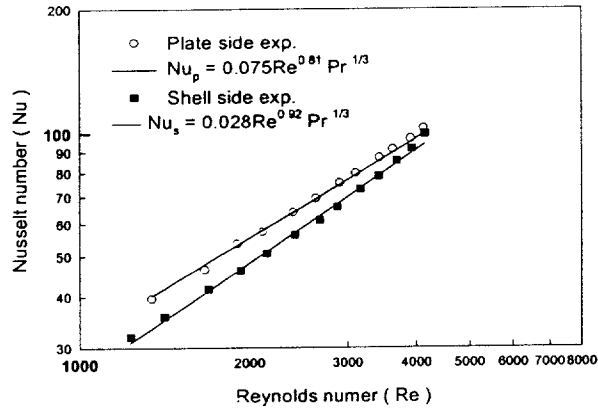
(b) P&SHE Type A



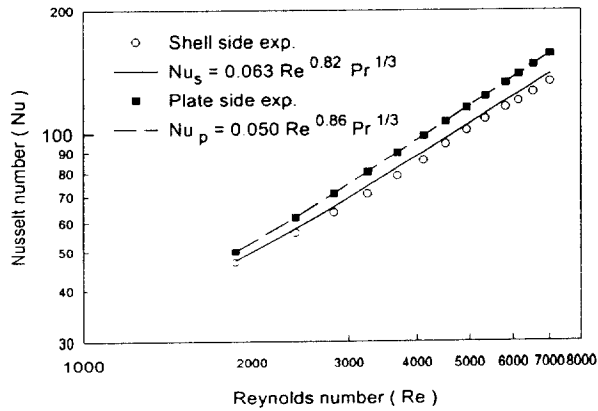
(a) P&SHE Type B

**Fig. 2.4** Modified Wilson plot results for the shell side and plate side used in this study.





(a) P&SHE Type A



(b) P&SHE Type B

**Fig. 2.5** Heat transfer coefficient for the shell side and plate side in this study.

### 2.2.2 Single-phase flow pressure drop characteristics

From the measured overall pressure drop across the plate side in the process stream, the frictional pressure drop can be obtained from

$$\Delta p_{core} = \Delta p_{measured} - \Delta p_{port} - \Delta p_{pipe} \quad (2.19)$$

Here, based on an empirical equation (Shah and Focke<sup>(6)</sup>; Kays and London<sup>(1)</sup>; Kays<sup>(40)</sup>) and the mean port velocity, port losses were estimated by

$$\Delta p_{port} = 1.5(\rho u_{port}^2/2) \quad (2.20)$$

The bulk velocity obtained from the measuring the mass flow rate of hot and cold water, are such as

$$u = \frac{\dot{m}}{\rho A_{fa}} \quad (2.21)$$

where  $\dot{m}$  is mass flow rate of hot and cold water,  $A_{fa}$  is free flow area between plates.

The pressure loss in small pipe sections at the inlet and outlet of the P&SHE was estimated on the basis of smooth tube friction factor and pipe flow velocity.

Friction pressure drop in shell side can be obtained from

$$\Delta p_{core} = \Delta p_{measured} - \Delta p_{SE} - \Delta p_{SC} - \Delta p_{pipe} \quad (2.22)$$

Here, sudden expansion and sudden contract loss is obtained from

$$\Delta p = K \frac{\rho u_{pipe}^2}{2} \quad (2.23)$$

$$K_{SE} = \left(1 - \frac{d^2}{D^2}\right)^2, \quad K_{SC} \approx 0.42 \left(1 - \frac{d^2}{D^2}\right) \quad (2.24)$$

Here,  $d$  is pipe diameter and  $D$  is plate diameter.

Thus, for the shear loss within the corrugated passages, the friction factor was calculated as

$$f = \frac{\Delta p_{friction}}{\frac{4L}{D_h} \frac{1}{2} \rho u^2} \quad (2.25)$$

To facilitate the use of the P&SHE correlating equations for the dimensionless friction factor based on the present data are provided. The results from this single-phase experiment were illustrated in Fig. 2.6 and 2.7. The measured friction pressure drop in the plate and shell side can be correlated by the least-square method as

Type A

$$\text{Plate side : } f = 1.02 Re^{-0.08} \quad (800 < Re < 5000) \quad (2.26)$$

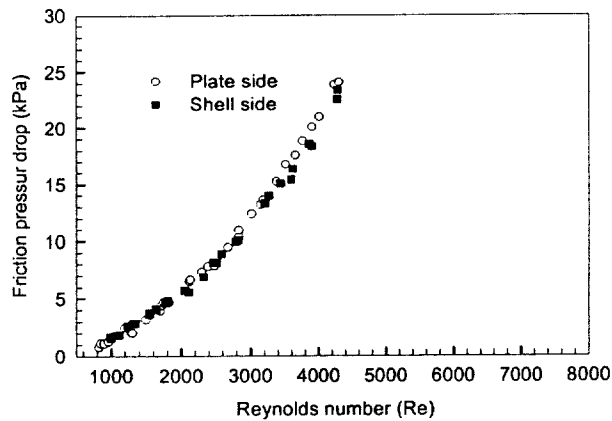
$$\text{Shell side : } f = 3.303 Re^{-0.227} \quad (800 < Re < 5000) \quad (2.27)$$

Type B

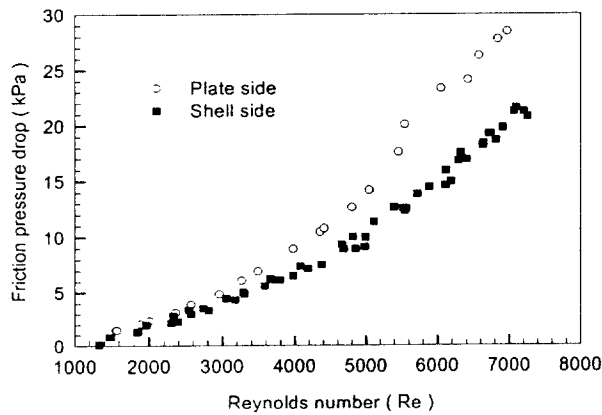
$$\text{Plate side : } f = 0.38 Re^{-0.032} \quad (1000 < Re < 8000) \quad (2.28)$$

$$\text{Shell side : } f = 0.92 Re^{-0.167} \quad (1000 < Re < 8000) \quad (2.29)$$

It is found that the average deviation is about 3.6% between the correlation and the experimental data.

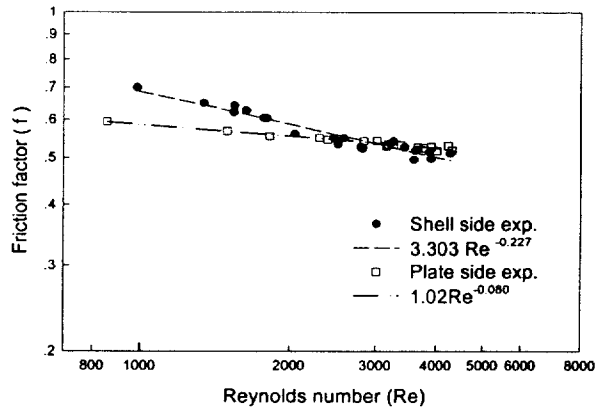


(a) P&SHE Type A

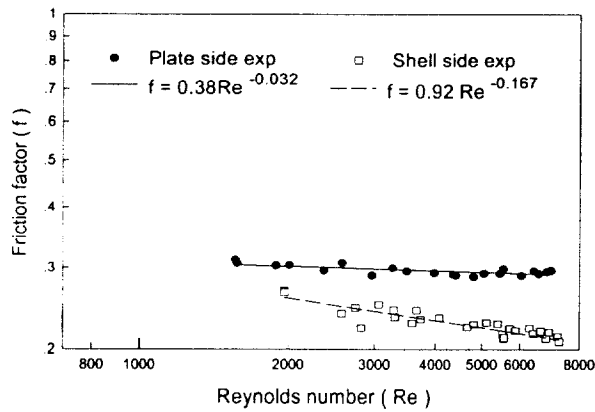


(b) P&SHE Type B

**Fig. 2.6** Friction pressure drop variations with the Reynolds number in single-phase water-to-water test.



(a) P&SHE Type A



(b) P&SHE Type B

**Fig. 2.7** Friction factor variations with the Reynolds number for the plate and shell side in single-phase water-to-water test.

### 2.2.3 Comparison with conventional plate heat exchangers

It is necessary to compare the present data for the single-phase heat transfer coefficient and friction factor in the P&SHE to those in conventional plate heat exchanger.

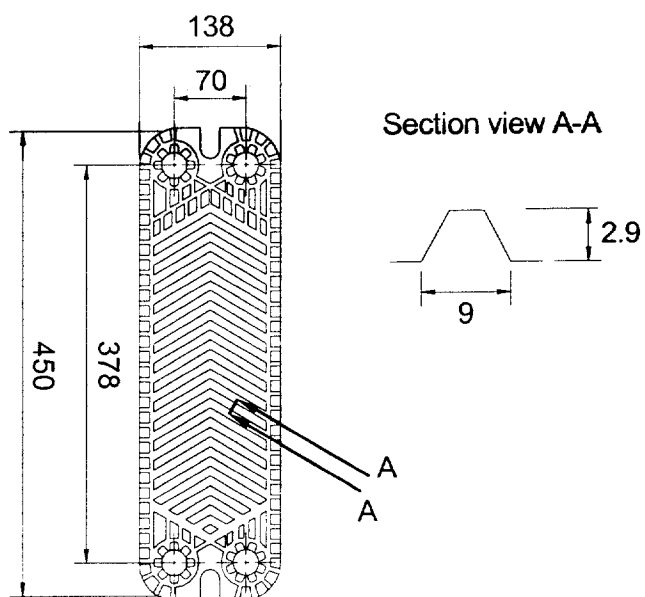
The plate heat exchanger used in this study, as schematically shown in Fig. 2.8. From the experimental result, a friction factor and heat transfer correlation in the plate heat exchanger were developed as follows.

$$f = 14.84 Re^{-0.3} \quad \text{for } Re < 3000 \quad (2.30)$$

$$f = 1.488 Re^{-0.011} \quad \text{for } Re > 3000 \quad (2.31)$$

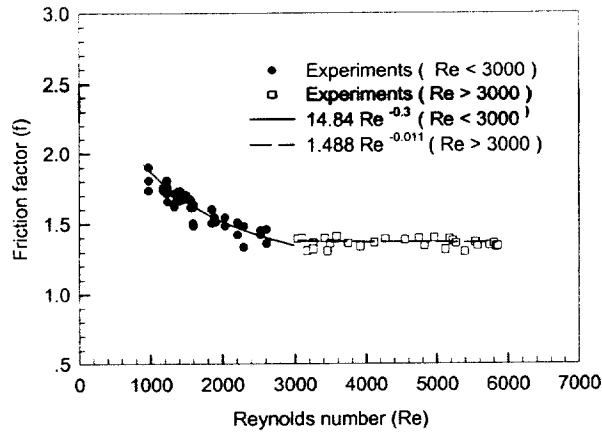
$$Nu = 0.657 Re^{0.55} Pr^{1/3} \quad (2.32)$$

Fig. 2.9 and 2.10 show friction factor and heat transfer for the conventional plate heat exchanger used in this study. Fig. 2.11 show the comparison of the P&SHE with conventional PHE in friction factor. The friction factor for P&SHE is much less than that for the PHE. It can be considered that flow distribution at port of the P&SHE much regular than that of PHE. Fig. 2.12 show the comparison of the P&SHE with conventional PHE in heat transfer. The comparison clearly shows that the heat transfer coefficient for P&SHE is less than that for the PHE in  $Re < 4000$ , but the increasement of heat transfer coefficient for P&SHE is higher than that for the PHE in  $Re > 4000$ . These result can be resumed that the heat transfer coefficient of the P&SHE highly increased due to the developed turbulent flow in the relatively high range of Reynolds number.



**Fig. 2.8** Schematic diagram of plate heat exchanger used in this study.





**Fig. 2.9** Experimental result of friction factor for the plate heat exchanger(PHE).

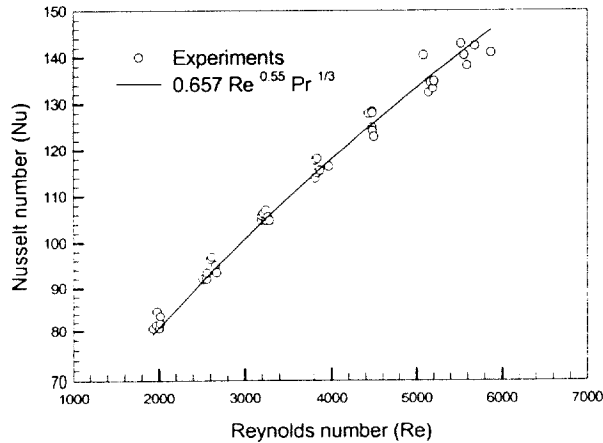


**Fig. 2.10** Experimental result of heat transfer coefficient for the plate heat exchanger(PHE).

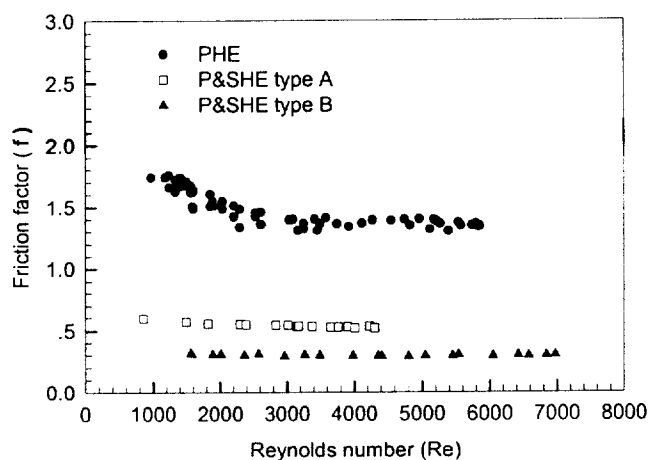


**Fig. 2.11** Comparison of the P&SHE with conventional PHE in friction factor.

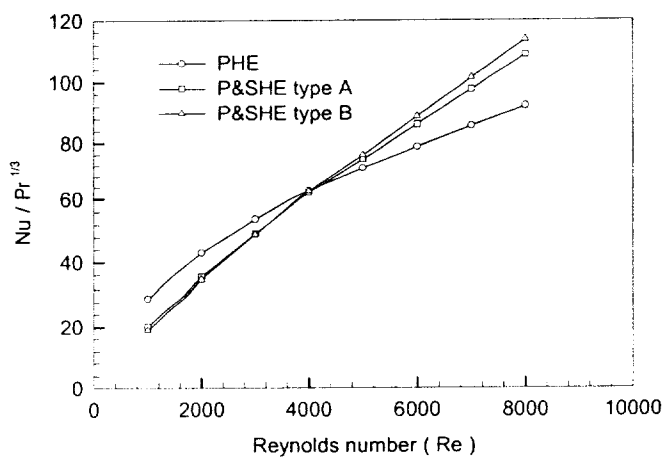


**Fig. 2.12** Comparison of the P&SHE with conventional PHE in heat transfer.

## **CHAPTER 3**

### **CFD ANALYSIS FOR SINGLE-PHASE FLOW**

This chapter focuses on the study of the heat transfer and pressure drop taking place within a plate and shell heat exchanger using computational fluid dynamics(CFD) techniques.

One major advantage of CFD modelling is that once the numerical solution has been shown to be correct, then the effects of altering any of the design parameters of the P&SHE can be studied and in a short space of time. The model is based on the numerical solution of the Reynolds averaged Navier-Stokes equations<sup>(41)</sup> and energy transport equations for a system of finite volumes using a commercial software package, FLUENT.

#### **3.1 MATHEMATICAL MODELS AND NUMERICAL ANALYSIS**

In this section the governing equations for the solution of fluid flow and heat transfer, and the boundary conditions will be presented.

##### **3.1.1 Governing Equations**

The Reynolds-averaged continuity, momentum, and energy equations<sup>(41)</sup> for incompressible Newtonian, turbulent, buoyant flow are: continuity equation:

$$\frac{\partial u_i}{\partial x_i} = 0 \quad (3.1)$$

**momentum equation:**

$$\rho \frac{\partial u_i}{\partial t} + u_j \frac{\partial u_i}{\partial x_j} = F_i - \frac{\partial p}{\partial x_i} + \frac{\partial}{\partial x_j} \left[ (\mu + \mu_t) \left( \frac{\partial u_i}{\partial x_j} + \frac{\partial u_j}{\partial x_i} \right) \right] \quad (3.2)$$

**energy equation:**

$$\rho C_p \frac{\partial T}{\partial t} + \rho C_p u_j \frac{\partial T}{\partial x_j} = \frac{\partial}{\partial x_j} \left[ (k_m + k_t) \frac{\partial T}{\partial x_j} \right] \quad (3.3)$$

where  $u_i$  is the turbulent mean velocity of the fluid;  $F_i$ ,  $\rho$  and  $\mu$  are the volume force acting on the fluid, the density, and the molecular viscosity of the fluid, respectively.  $\mu_t$  is the eddy viscosity, which depends on both the physical properties of the fluid and the properties of the flow. It generally changes from one position to another, and from one time to another time in time-dependent problems.  $C_p$  is the heat capacity of the fluid at constant pressure;  $k_m$  and  $k_t$  are the molecular and turbulent conductivities, respectively. A solution of these equations will produce the velocity, pressure, and temperature fields for the specified problem. It should be noted that these equations are not closed because the eddy viscosity and turbulent conductivity are not constants and are not known in advance. Turbulence models have been developed to close the system of equations. These models simulate

the effects of turbulence on the mean flow behaviour, leaving the details of the turbulence structure unresolved. A well established turbulence model is the k- $\epsilon$  model<sup>(42)</sup>.

$$\frac{\partial k}{\partial t} + \mu_j \frac{\partial k}{\partial x_j} = \frac{\partial}{\partial x_j} \left( \frac{\mu + \mu_t}{\rho \sigma_k} \frac{\partial k}{\partial x_j} \right) + G - \epsilon \quad (3.4)$$

$$\frac{\partial \epsilon}{\partial t} + \mu_j \frac{\partial \epsilon}{\partial x_j} = \frac{\partial}{\partial x_j} \left( \frac{\mu + \mu_t}{\rho \sigma_\epsilon} \frac{\partial \epsilon}{\partial x_j} \right) + \frac{C_1 \epsilon G - C_2 \epsilon^2}{k} \quad (3.5)$$

where k is the turbulent kinetic energy, i.e.

$$k = \frac{1}{2} ( \overline{(u'_1)^2} + \overline{(u'_2)^2} + \overline{(u'_3)^2} ) \quad (3.6)$$

and  $\epsilon$  is the turbulent energy dissipation rate; G is the turbulence generation term;  $C_1$ ,  $C_2$ ,  $\sigma_k$ ,  $\sigma_\epsilon$  are empirical constants. With k and  $\epsilon$  known the eddy viscosity and turbulent conductivity can be calculated as:

$$\mu_t = \rho C_\mu \frac{k^2}{\epsilon} \quad (3.7)$$

and

$$k_t = C_b \frac{\mu_t}{\sigma_T} \quad (3.8)$$

### 3.1.2 Computational domain

The partitioning rib type plate was modeled the true geometry of the

P&SHE(type B) used in the experimental investigations of the chapter 2. Figure 3.1 shows schematic modeling of plate side in the plate and shell heat exchanger. Figure 3.2 and Table 3.1 show the geometric parameters **of plate in the plate and shell heat exchanger used in this analysis**. Various non-partitioning rib type plate's geometries were investigated as specified in Table 3.1.

All simulations were performed using a 3-D, body-fitted grid with Cartesian coordinates. Using the laminar and  $k-\epsilon$  model, grid independence was checked under isothermal, incompressible and steady state conditions. To get accurate numerical results, 350,000 ~ 500,000 cells were taken accounted in these analyses.

### **3.1.3 Boundary conditions for the equations**

The solution of the Navier Stokes equations and energy transport equations requires a knowledge of the boundary conditions. Generally, inlet conditions such as flow velocity and temperature were specified together with pressure at the outlet.

Uniform wall temperature condition was adopted in this study, which was one of the closest thermal boundary condition to simulate the real heat exchanger normally. The reason is that the conductive thermal resistance of the plates is usually negligible as compared with the film(wall-to-fluid) thermal resistance.

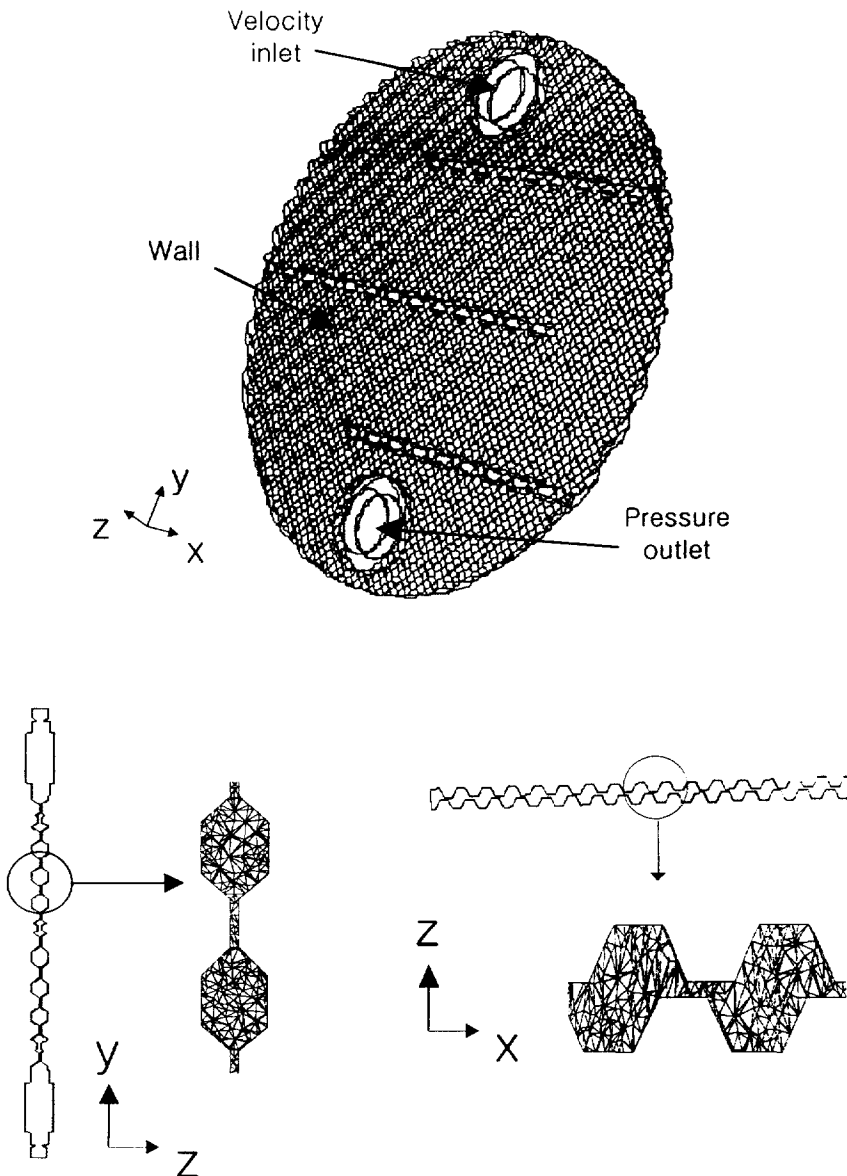


**Fig. 3.1** Schematic Modeling of plate side in the Plate and Shell heat exchanger with partitioning rib.

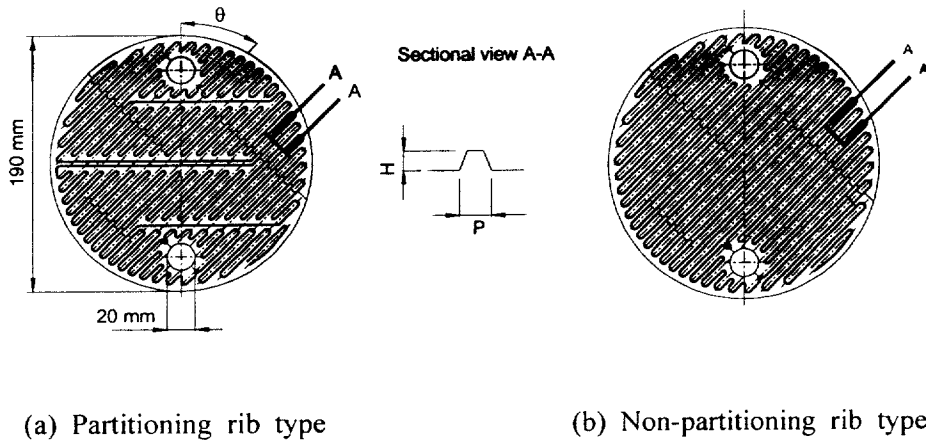


**Fig. 3.2** Geometric parameters of plate in the plate and shell heat exchanger.

**Table 3.1** Geometric parameters of plate in the analysis cases which were investigated numerically

	Partitioning rib type	Non-partitioning rib type
Chevron angle, $\theta$ [°]	45	15, 30, 45, 60 75
corrugate pitch, $P$ [mm]	4	4, 5.2, 6
corrugate height, $H$ [mm]	2.4	2.2, 2.4, 2.6



### 3.1.4 Numerical analysis

Computational fluid dynamics is a discretization method of the mathematical formulation of the flow and transport processes, and it involves two components. One is the space discretization, that is to divide the system under investigation into cells. The other component is the equation discretization, which leads to the transformation of the

governing differential equations to a set of linear algebraic equations involving the values of the unknowns at the mesh points. They are then solved with various iterative methods to establish numerical values for the unknown flow and heat transfer parameters.

The resulting numerical values can be processed with a graphics program to give a detailed picture of the fluid flow and heat transfer. The CFD package, FLUENT, uses the finite volume method (FVM). With FVM a non-orthogonal body-body-fitted curvilinear grid system is used to discretise the geometry space, which can map an arbitrary physical boundary very precisely, to generate the computational domain. The governing differential equations, except the continuity equations, are then integrated and solved for this computational domain. One major feature of the finite volume method is that the resulting solution implies the integral conservation of mass, momentum, and energy over any group of cells and, in addition, the whole domain.

CFD modeling of fluid flow was performed using a commercial package, FLUENT5, on a pentium PC linked by eXceed. The fluid under investigation was water, and its properties were obtained from the FLUENT5 data base.

In the double precision calculations performed, a maximum mass

tolerance of  $1 \times 10^{-6} \text{ kg/s}$  was attained for the sum of the absolute residual of all the cells in the grid and each computation took about 5~6 hours CPU time on a pentium PC.

## 3.2 RESULTS AND DISCUSSION

In compact heat exchangers the hydraulic diameter usually ranges from **a few mm to ten mm, and the velocity of the fluid from 1 to 10 m/s**; this makes for Reynolds numbers between 1000 ~ 10000. Therefore the flow (considering the twisted shape of the flow passages) cannot be completely laminar, but neither is it fully turbulent; it is a transitional flow in most cases.

### 3.2.1 Selection of turbulence model

Figure 3.3 shows behavior of the friction factor  $f$  as a function of the Reynolds number for fully developed flow in partitioning rib type plate. A series of predictable results were obtained by using laminar flow assumptions, the standard  $k-\epsilon$  method with "wall functions" and the RNG  $k-\epsilon$  model<sup>(43)</sup>, and they were compared with the authors' own experimental results. Laminar and RNG  $k-\epsilon$  computations are unsatisfactory, as they under-predict  $f$  over most of the Reynolds number range of applications. The best agreement with the experimental data was obtained by using standard  $k-\epsilon$  model.

For the same geometry, the average Nusselt number in fully developed flow is shown as a function of the Reynolds number in Fig. 3.4. Although the actual temperature distribution of the actual P&SHE is not uniform, parts of the channel walls were specified at constant temperature in order to simplify the heat transfer simulations.

To investigate the effect of wall temperature for heat transfer, several analyses were executed for various wall temperature. But, the effect of

the wall temperature was neglectable in the heat transfer analysis. Therefore for the Fig. 3.4 a wall temperature of 30°C was imposed. Fig. 3.4 includes results from laminar flow assumptions, standard and RNG  $k-\epsilon$  simulations. The authors' own experimental data, obtained by modified Wilson plot method, are also shown. As in the case of the friction factor laminar and RNG  $k-\epsilon$  results are not satisfactory, because they under-predict Nusselt number over most of the range considered. The best agreement with the experiments is obtained by using the standard  $k-\epsilon$  model. Therefore, the standard  $k-\epsilon$  model was adopted for the further CFD analysis.

### **3.2.2 Influence of the partitioning rib**

Investigating the effect of partitioning rib for the pressure drop and heat transfer, CFD analysis was performed for the partitioning rib type and non-partitioning rib type plate according to the Reynolds number.

A comparison of the friction factor and Nusselt number for the partitioning rib type and non-partitioning rib type plate was given in Fig.3.5 and Fig. 3.6. Note that the friction factor  $f$  of the partitioning rib type is about 40% higher than that of the non-partitioning rib type. But the Nusselt number of the partitioning rib type is about 3% higher than that of the non-partitioning rib type. Fig. 3.7 and Fig. 3.8 show the pressure and temperature distribution comparison of partitioning rib type with non-partitioning rib type plate in channel along y-direction. The pressure distribution of the partitioning rib type plate was revealed as jumping down in partitioning rib. Therefore, it can be considered that partitioning rib has large effect on the pressure drop but small effect on

the heat transfer.

### 3.2.3 Influence of the Chevron angle on the performance

The predicted dependence of  $f$  and  $Nu$  on the Chevron angle  $\theta$  of the non-partitioning rib type plate for  $H=2.4$  mm,  $P=4$  mm,  $Re=2000 \sim 8000$  and the Chevron angle  $\theta$  varying between  $15$  and  $75^\circ$  was reported in Fig. 3.9 and Fig. 3.10.

Fig. 3.11 and Fig. 3.12 show the distribution of temperature and velocity field predicted in non-partitioning rib type plate for  $Re=2000$  in a cross-section normal to the corrugated plate (at  $x=0$ ,  $y=0.09$  from bottom of plate). While the chevron plate surface corrugations promote higher heat transfer coefficients, there is a higher pressure drop penalty as well. Higher Nusselt numbers are obtained with increasing  $\theta$ , which reflects the increased intensity of swirl flows generated by the larger  $\theta$  Chevron plates. The Nusselt numbers increased about 1.4 times but friction factor increased more than 4.4 times when  $\theta$  increased from  $15^\circ$  to  $75^\circ$ . As would be expected, the swirling fluid motion in the inter-plate channel results in larger flow friction, which increases with  $\theta$ .

### 3.2.4 Influence of the height and pitch of the corrugate

The influence of the height and pitch for the pressure drop and heat transfer can be appreciated by comparing various cases of height and pitch combination as  $H=2.2, 2.4, 2.6$  and  $P=4, 5.2, 6$  mm. In these analyses, non-partitioning rib type plate was adapted and the Chevron angle and reynolds number was prescribed as  $\theta=45^\circ$ ,  $Re=2000$ .

Figure 3.13 and Fig. 3.14 show the friction factor and Colburn  $j$  factor

according to the corrugate pitch for the different height.

As regards the influence of  $H$  and  $P$  on the heat transfer and friction factor, computational results indicate a increase of  $j$  and  $f$  as  $H$  varies from 2.2 mm to 2.6 mm and decrease of  $j$  and  $f$  as  $P$  varies from 4.0 mm to 6.0 mm. As shown in fig. 3.14, the heat transfer coefficient was increased according to the decreased pitch. but, fabrication limit was considered as 4 mm. The deeper furrows in the plate would tend to induce greater swirl mixing, and hence have higher  $j$  and  $f$ , but it causes increasement of heat exchanger's volume.

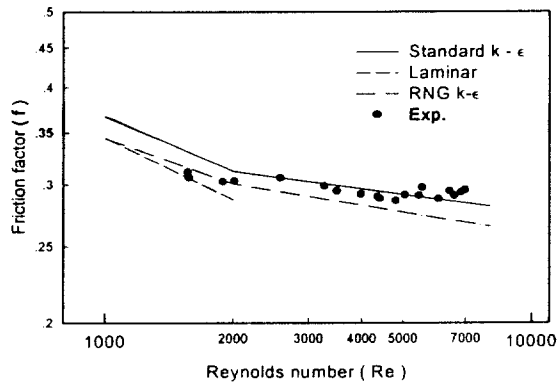


**Fig. 3.3** Comparison of CFD analysis results with experimental data for friction factor in partitioning rib type plate.

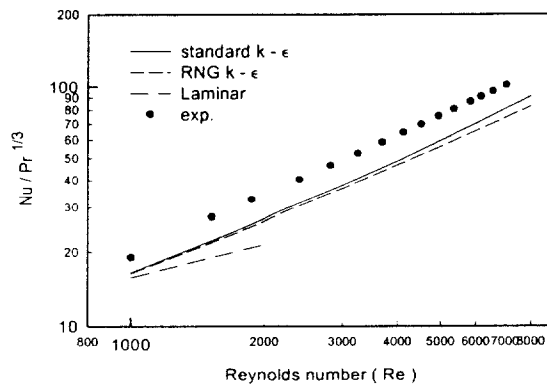


**Fig. 3.4** Comparison of CFD analysis result with experimental data for heat transfer in partitioning rib type plate.

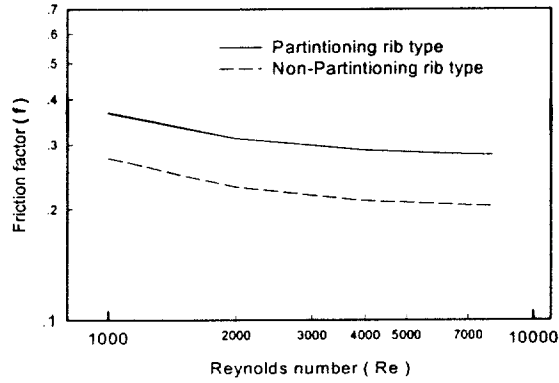


Fig. 3.5 Friction factor comparison of partitioning rib type with non-partitioning rib type plate.

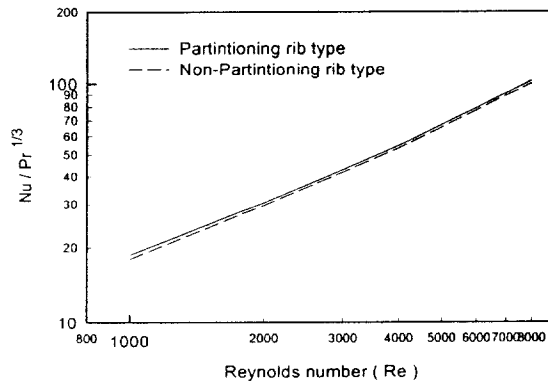
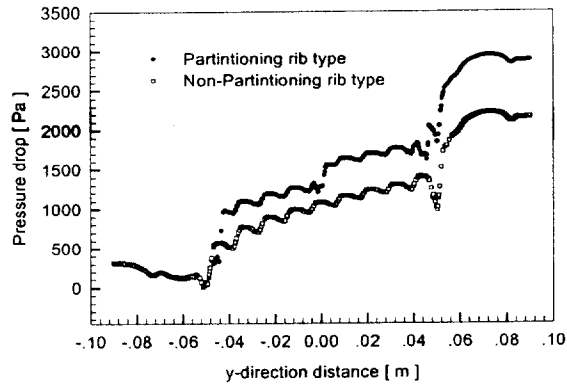
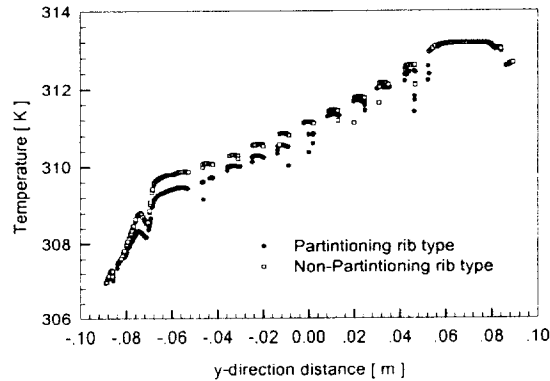


Fig. 3.6 Heat transfer coefficient comparison of partitioning rib type with non-partitioning rib type plate.





**Fig. 3.7** Pressure distribution comparison of partitioning rib type with non-partitioning rib type plate in channel along  $y$ -direction



**Fig. 3.8** Temperature distribution comparison of partitioning rib type with non-partitioning rib type plate in channel along  $y$ -direction

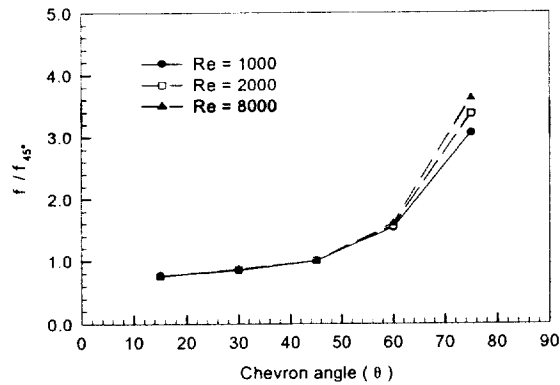


**Fig. 3.9** Friction factor vs. Chevron angle for three different Reynolds number.

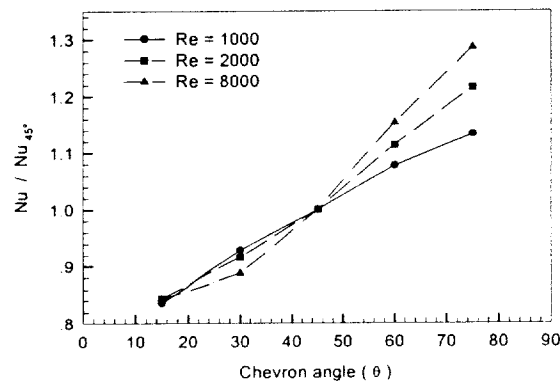


**Fig. 3.10** Heat transfer coefficient vs. Chevron angle for three different Reynolds number.

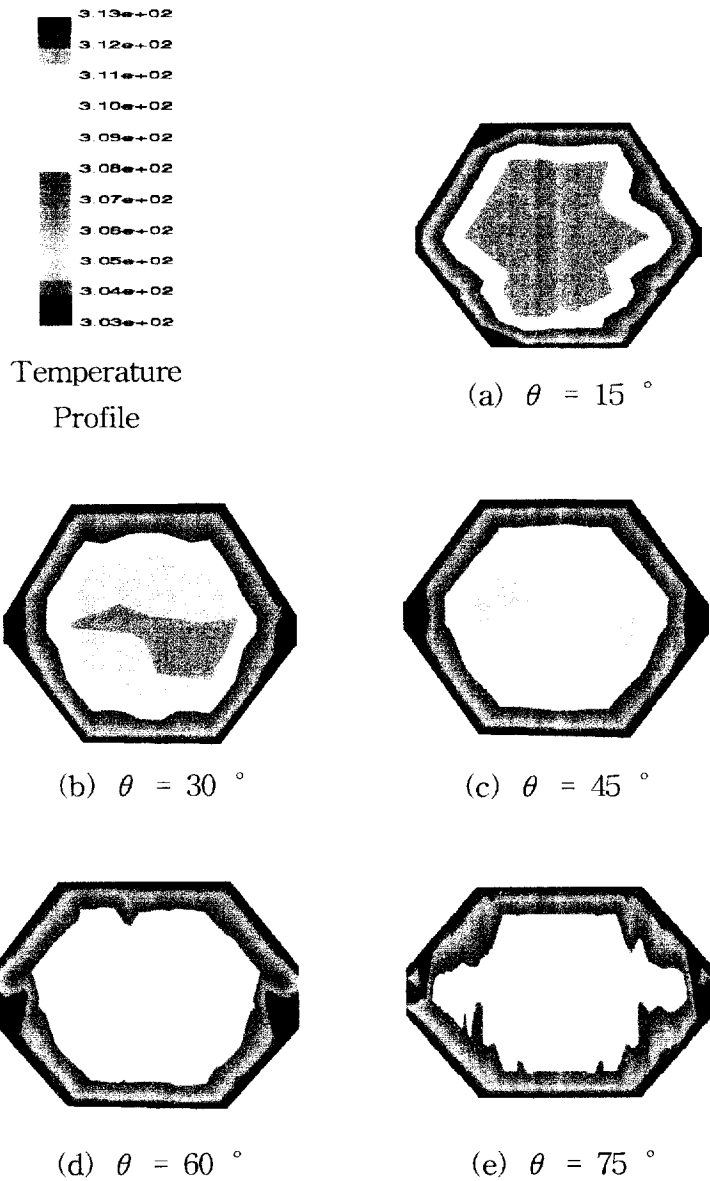


**Fig. 3.11** Temperature distribution of the non-partitioning rib type plate for  $Re=2000$  (Cross-section normal to the corrugated plate at  $x=0$ ,  $y=0.09$  from bottom of plate)



(a)  $\theta = 15^\circ$

(b)  $\theta = 30^\circ$

(c)  $\theta = 45^\circ$

(d)  $\theta = 60^\circ$

(e)  $\theta = 75^\circ$

**Fig. 3.12** Velocity field of the non-partitioning rib type plate for  $Re=2000$  (Cross-section normal to the corrugated plate at  $x=0$ ,  $y=0.09$  from bottom of plate)

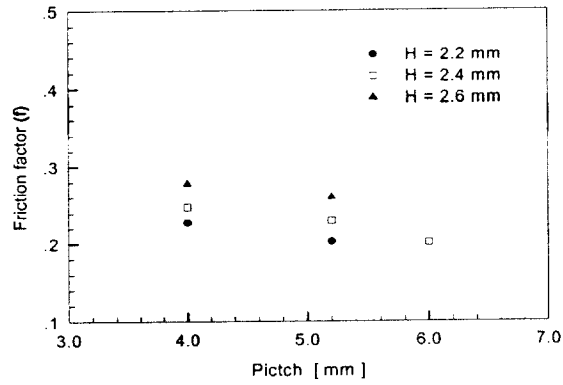


Fig. 3.13 Friction factor vs. corrugate pitch for different height

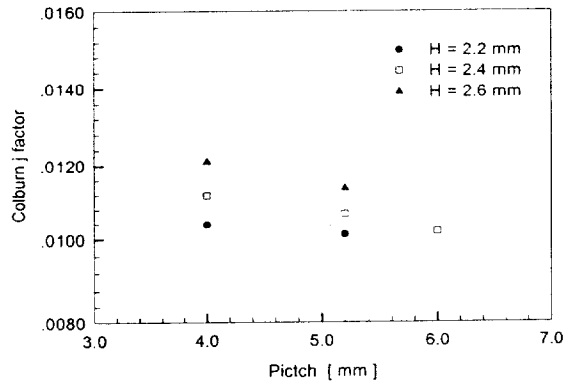


Fig. 3.14 Colburn  $j$  factor vs. corrugate pitch for different height

### 3.2.5 Analysis of design parameters

The ultimate goal of either experimental or computational investigations is the efficient design of the flow passages. Given a specific application, **an optimization problem can usually be formulated, in that the most economically convenient compromise between heat transfer and pressure drop is sought under a number of design constraints.** An example will be described in this section in order to clarify the issue.

Consider a 100 kW heat exchanger designed (cold water, initially at 20°C is fed into the heat exchanger at a rate of 50 m<sup>3</sup>/h and flows through the passages in counter-current flow to hot water, initially at 80°C, flowing at a same rate.) A crucial step now is to express the average Nusselt number and the friction factor  $f$  as functions of Re and  $\theta$ . For the geometry under consideration, Nu and  $f$  correlation proposed by CFD analysis results:

$$f = f_{45^\circ} \{0.757 + 0.0073 \exp(0.0784 \theta)\} \quad (3.9)$$

$$\text{Nu} = \text{Nu}_{45^\circ} \{0.764 \exp(0.0062 \theta)\} \quad (3.10)$$

Fig. 3.15 and Fig. 3.16 show comparison of the proposed correlation for friction factor and heat transfer coefficient with the CFD analysis data. Once Nu is computed from Eq. (3.10), the convection coefficient,  $h = \text{Nu} \cdot k/D_h$ , and the overall heat transfer coefficient,  $U = h/2$ . Since the product  $UA/2$  is known, the surface area  $A$  of the plates can be obtained. The Pressure drop can be computed as  $\Delta p = f \cdot (4L/D_h) \cdot \rho u^2/2$ ,  $f$  being obtained from Eq. (3.9). It should be

observed that changing the corrugation angle  $\theta$  affects the pressure drop both directly via changes in the friction factor  $f$ , and indirectly via changes in the total surface area  $A$  and thus in the length of the passages; the two effects are opposite in sign but the former usually prevails.

Now, the surface area  $A$  is directly related to the mass of the exchanger and thus, roughly, to its construction cost; as a crude approximation, assuming that the corrugated plates have a thickness  $s$  and a density  $\rho_p$ , the mass will be  $\rho_p \cdot A \cdot s$  and the associated cost will be  $C_1 \cdot \rho_p \cdot A \cdot s$ ,  $C_1$  being the unitary cost of the plates (e. g., in \$/kg). On the other hand, the pressure drop  $\Delta p$  is directly related to the required pumping power and thus to the operation costs of the exchanger. In fact, the required pumping power will roughly be  $\Delta p \cdot (2\dot{m}/\rho)$  (inclusive of the cold and the hot fluids), and as a crude approximation again, the associated cost over an effective period  $t$  will be  $C_2(2\Delta p\dot{m}/\rho)t/\eta$ ,  $C_2$  being the cost of electrical energy ( inclusive of the construction and maintenance cost of the fan units) and  $\eta$  the efficiency of the pumps. For the case of  $H = 2.4$  mm and different included angles  $\theta$ , the results of the above analysis are shown in Fig. 3.17 for  $C_1 = 7.5$  \$/kg,  $C_2 = 0.125$  \$/kWh<sup>(44)</sup>,  $\eta = 0.75$  and  $t = 1.5768 \times 10^8$  s ( corresponding to about 5 years of continuous operation). It can be seen that the overall cost has a minimum for a specific value of  $\theta$ ; in the present example,  $\theta \cong 50^\circ$ . Thus, the flow passages should be chosen to be as small as possible compatible with other considerations, e.g. those related to fouling.

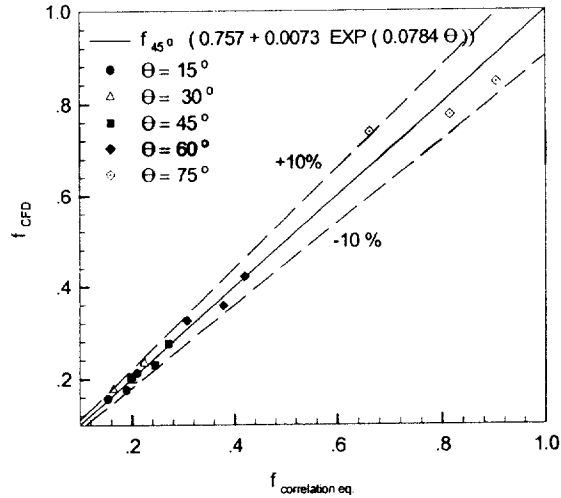


**Fig. 3.15** Comparison of the proposed correlation for friction factor with the CFD analysis data

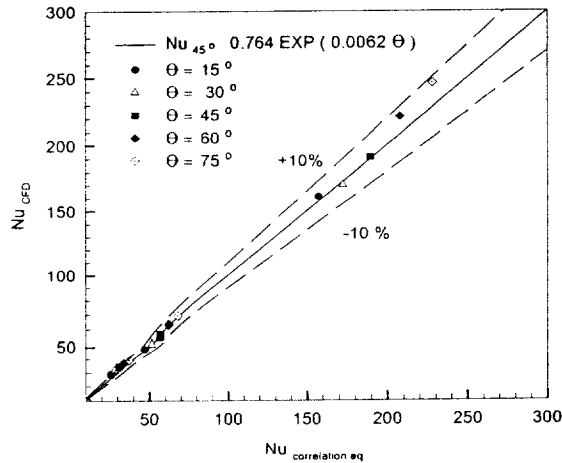


**Fig. 3.16** Comparison of the proposed correlation for heat transfer coefficient with the CFD analysis data



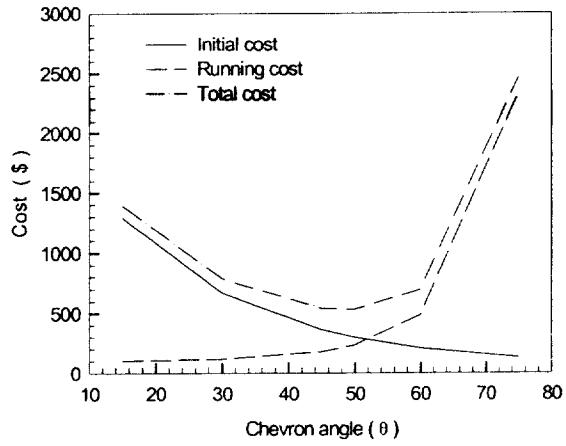


**Fig. 3.17** Influence of the Chevron angle on construction, operation and total costs

## **CHAPTER 4**

# **TWO-PHASE FLOW HEAT TRANSFER AND PRESSURE DROP**

## **4.1 EXPERIMENTAL APPARATUS AND PROCEDURES**

### **4.1.1 Experimental apparatus**

The experimental system established here to study the condensation and evaporation of R-134a, as schematically and photograph shown in Fig. 4.1 and Photo. 4.1, has three main loops and a data acquisition unit. Specifically, the system includes a refrigerant loop, two water loop (one for the test section and the other for the sub-cooler). Refrigerant R-134a is circulated in the refrigerant loop. In order to obtain different test conditions of R-134a (including mass flux, imposed heat flux and saturation temperature) in the test section, we need to control the temperatures and flow rates of the working fluids in the water loop.

The refrigerant loop contains a refrigerant pump, a pre-heater, a test section (the plate and shell heat exchanger), a sub-cooler, a strainer, a refrigerant mass flow meter, a dryer&filter, and three sight glasses. The refrigerant pump used a magnetic pump(TUTHILL-DDS 1.2) to circulate the refrigerant so that testing could be performed in an oil-free environment. It was driven by a DC motor that is, in turn, controlled by a variable DC output motor controller. The variation of the liquid R-134a flow rate was controlled by a rotational DC motor through the change of the DC current. The refrigerant flow rate was measured by a mass flow

meter(Micro motion, Oval D040S-SS-200) installed between the receiver and refrigerant pump with an accuracy of  $\pm 0.2 \%$ . The pre-heater is used to evaporate the refrigerant to a specified vapor quality at the test section inlet by transferring heat from the electrical heater to R-134a. The power input was measured with a watt meter(YOKOGAWA WT110) with a factory-specified uncertainty of 2%.

The dryer&filter intends to filter the solid particles possibly present in the loop. Meanwhile, a sub-cooler were used to condense the refrigerant vapor from the test section by a cold water system to avoid cavitation at the pump inlet. The saturation temperature of the refrigerant loop can be controlled by varying the temperature and flow rate of the water loop in the sub-cooler and test section. After condensed, the liquid refrigerant flows back to the receiver. In the condensation test the top feeding of the refrigerant R-134a in one channel was cooled by the up-flow of the cold water in the other channel. In the evaporation test bottom feeding of refrigerant R-134a in one channel is heated by the downflow of hot water in the other channel. To reduce the heat loss to the ambient, the whole test section is wrapped with polyethylene as shown in Photo. 4.2. The average heat flux in the test section was calculated by measuring the water temperature rise between the channel inlet and outlet and by measuring the water flow rate. The temperatures throughout the loop were measured with T-type thermocouple and the water flow rates were measured with mass flow meter(Micro motion, Oval DO40S-SS-200) that was calibrated with an accuracy of  $\pm 0.12\%$ .

Inlet pressure to the test section was measured with a 0 to 35 MPa strain-gauge-type pressure transducer(DRUK, Model : PMP1400) that was

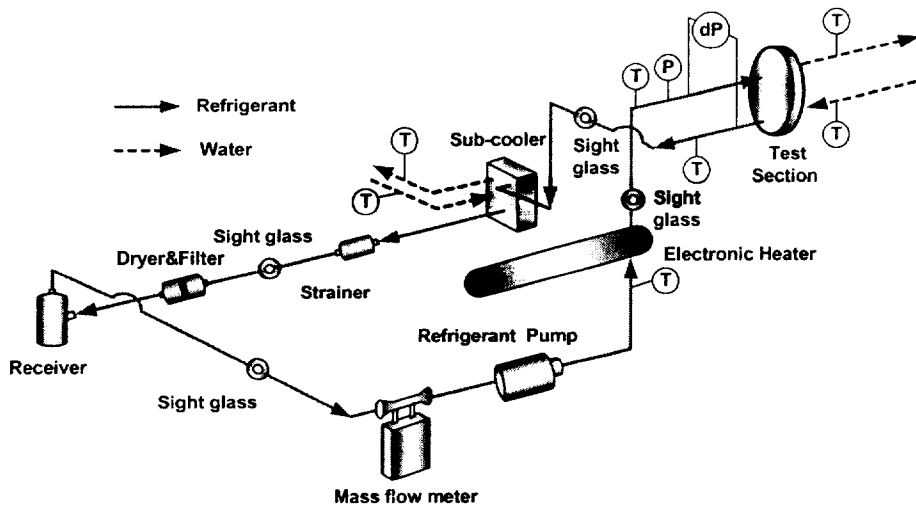
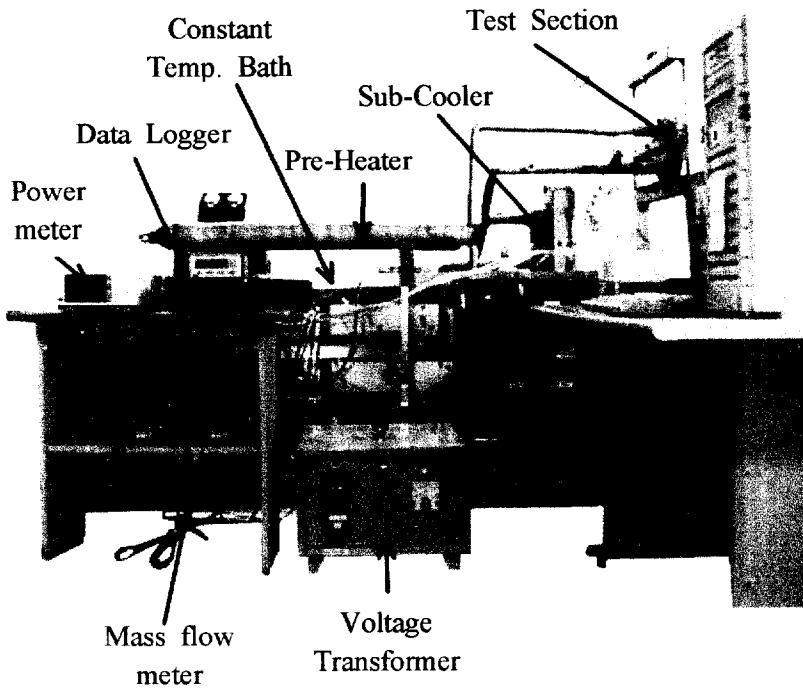
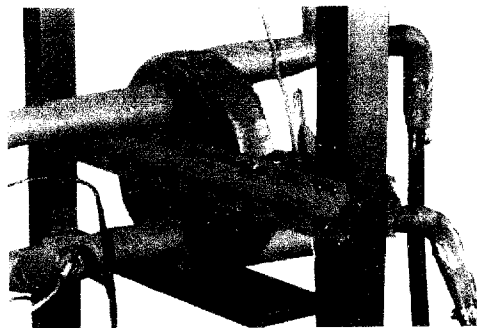


Fig. 4.1 Schematic diagram of the two-phase flow experimental system



**Photo. 4.1** Two-phase flow heat transfer and pressure drop experimental system



**Photo. 4.2** Test section

calibrated with an accuracy of  $\pm 0.25\%$ . Pressure drop across the test section was measured with a differential pressure transducer(DRUK, Model : PMP4170) that was calibrated with an accuracy of  $\pm 0.2\%$ .

The test section water loop in the condensation experimental test system designed for circulation cold water through the test section contain a 200 ℓ constant temperature water bath with a 5 kW heater and an air cooled refrigerant unit of 1 RT cooling capacity intending to accurately control the water temperature. The water loop in the evaporation experimental system for circulation the hot water through the test section contains an 200 ℓ water thermostat with a 5 kW heater and an air-cooled refrigeration system of 1 RT cooling capacity, intending to control the water temperature. A 0.5 hp water pump is used to drive the cold water to the plate heat exchanger with a specified water flow rate. Another by-pass water valve can also be used to adjust the water flow rate.

The sub-cooler water loop designed for the two-phase flow the R-134a vapor contains 200 ℓ constant temperature bath with a water both with a 5 kW heater and an air cooled refrigeration unit of 3 RT cooling capacity intending to accurately control the water temperature. Then, a 0.5 hp water pump with an inverter is also used to drive the cool water at a specified water flow rate to the sub-cooler.

#### **4.1.2 Experimental procedures**

In each test the saturation temperature of the refrigerant is maintained at a specified level by adjusting the sub-cooler water loop temperature and its flow rate. The vapor quality of R-134a at the test section inlet can

be kept at the desired value by adjusting the voltage of the voltage transformer for the pre-heater. Finally, the heat transfer rate between the counter flow channels in the test section can be varied by changing the temperature in the water loop for the test section. Any change of the system variables will lead to fluctuations in the temperature and pressure of the flow. It takes about 60 ~ 120 min to reach a statistically steady state at which variations of the time-average inlet and outlet temperatures are less than 0.1°C and the variations of the pressure and heat flux are within 1% and 5%, respectively. Then the data acquisition unit is initiated to scan all the data channels for 30 times in 5 min. The mean values of the data for each channel are obtained to calculate the heat transfer coefficient and pressure drop.

Before examining the condensation and evaporation heat transfer characteristics, a preliminary experiment for single phase water convection in the plate and shell heat exchanger was performed. The modified Wilson's method was adopted to calculate the relation between single phase heat transfer coefficient and flow rate from these data.

This single phase heat transfer coefficient can then be used to analyze the data acquired from the two-phase heat transfer experiments.

The data acquisition unit includes a 20 channel Fluke NetDAQ 2645A recorder combined with a personal computer. The recorder was used to record the temperature and voltage data.

The water pressure and differential pressure transducer need a power supply as a driver to output an electric voltage of 0 ~ 10 V. The NetDAQ 2645A recorder allows the measured data to transmit to personal computer and then to be analyzed by the computer immediately.

Table 4.1 summarizes the two-phase flow test conditions.

**Table 4.1** Summary of two-phase flow test conditions

		Type A	Type B
Refrigerant mass flux [ $\text{kg/m}^2\text{s}$ ]		45, 55, 65	65, 100, 120
Heat flux [ $\text{kW/m}^2$ ]		6.0, 8.0	
Refrigerant saturation temperature [ $^{\circ}\text{C}$ ]	condensation	30, 40	
	evaporation	20,30	



## 4.2 DATA REDUCTION

An analysis is needed in the present measurement to deduce the heat transfer rate from the water flow to the refrigerant flow in the test section.

Convection heat transfer coefficient and friction factor were calculated from reducing the measured raw data in a computer program. The reduction procedures are given in the following.

### 4.2.1 Two phase heat transfer

The procedures to calculate the two-phase flow heat transfer coefficient of the refrigerant flow are described in the following. Firstly, the total heat transferred in the test section is determined from an energy balance on the water flow in the shell side.

$$\begin{aligned} Q_w &= \dot{m}_{w,c} c_{p,w} (T_{w,c,o} - T_{w,c,i}) && \text{condensation} \\ Q_w &= \dot{m}_{w,h} c_{p,w} (T_{w,h,i} - T_{w,h,o}) && \text{evaporation} \end{aligned} \quad (4.1)$$

Then, the refrigerant vapor quality entering the test section is evaluated from the energy balance for the pre-heater. The heat input to the refrigerant from the pre-heater ( $Q_p$ ) is the summation of the sensible heat transfer and latent heat transfer.

$$Q_p = Q_{sens} + Q_{lat} \quad (4.2)$$

where

$$Q_{sens} = \dot{m}_r c_{p,r} (T_{r,sat} - T_{r,p,i}) \quad (4.3)$$

$$Q_{lat} = \dot{m}_r i_{fg} x_{p,o} \quad (4.4)$$

The above equations can be combined to evaluate the refrigerant quality at the exit of the pre-heater, that is considered to be the same as the vapor quality of the refrigerant entering the test section. Specifically,

$$x_i = x_{p,o} = \frac{1}{i_{fg}} \left[ \frac{Q_p}{\dot{m}_r} - c_{p,r} (T_{r,sat} - T_{r,p,i}) \right] \quad (4.5)$$

The change in the refrigerant vapor quality in the test section is then deduced from the heat transfer from the refrigerant to the water flow in the test section  $Q_w$  :

$$\Delta x = \frac{Q_{w,c}}{i_{fg} \dot{m}_r} \quad (4.6)$$

and the average quality in the test section is

$$\begin{aligned} x_m &= x_{in} - \frac{\Delta x}{2} && \text{condensation} \\ x_m &= x_{in} + \frac{\Delta x}{2} && \text{evaporation} \end{aligned} \quad (4.7)$$

The refrigerant side heat transfer coefficient is determined from the

overall heat transfer coefficient and the shell side heat transfer coefficient as follows. The overall heat transfer coefficient based on real area is

$$U = \frac{Q_w}{A \text{ LMTD}} \quad (4.8)$$

where

$$\begin{aligned} \Delta T_1 &= T_{r,o} - T_{w,c,i} , & \Delta T_2 &= T_{r,i} - T_{w,c,o} & \text{condensation} \\ \Delta T_1 &= T_{w,h,i} - T_{r,o} , & \Delta T_2 &= T_{w,h,o} - T_{r,i} & \text{evaporation} \end{aligned} \quad (4.9)$$

with  $T_{r,i}$  and  $T_{r,o}$  being the saturation temperatures of R-134a corresponding respectively to the inlet and outlet pressures in the refrigerant flow in the P&SHE. Finally, the condensation and evaporation heat transfer coefficient in the flow of R-134a is evaluated from the equation

$$\frac{1}{h_r} = \frac{1}{U} - \frac{1}{h_w} - R_{wall} A \quad (4.10)$$

where  $h_w$  is determined from the empirical correlation for the single phase water to water heat transfer.

#### 4.2.2 Two-phase friction pressure drop

To evaluate the friction factor associated with the R-134a two-phase flow in the refrigerant channel, the frictional pressure drop  $\Delta p_f$  was first calculated by subtracting the pressure losses at the test section inlet and

exit manifolds and ports  $(\Delta p)_{mam}$ , then adding the deceleration pressure rise during the R-134a condensation  $\Delta p_{de}$ , (in case evaporation, subtracting acceleration pressure drop during the R-134a evaporation  $\Delta p_a$ ) and the elevation pressure rise  $\Delta p_{ele}$  from the measured total pressure drop  $\Delta p_{exp}$  for the refrigerant channel. Note that for the vertically downward refrigerant flow studied here the elevation pressure rise should be added in evaluating  $\Delta p_f$ . Thus

$$\begin{aligned}\Delta p_f &= \Delta p_{exp} - (\Delta p)_{mam} + \Delta p_{de} + \Delta p_{ele} && \text{condensation} \\ \Delta p_f &= \Delta p_{exp} - (\Delta p)_{mam} - \Delta p_a - \Delta p_{ele} && \text{evaporation}\end{aligned}\quad (4.11)$$

The deceleration and elevation pressure rises were estimated by the homogeneous model for the two phase gas-liquid flow<sup>(45)</sup>,

$$\Delta p_{de} \text{ (or } \Delta p_a) = G^2 v_{fg} \Delta x \quad (4.12)$$

$$\Delta p_{ele} = \frac{g \cdot L}{v_m} \quad (4.13)$$

where  $v_m$  is the mean specific volume of the vapor-liquid mixture in the refrigerant channel when they are homogeneously mixed and is given as

$$v_m = [x_m v_g + (1 - x_m) v_l] = (v_l + x_m v_{fg}) \quad (4.14)$$

The pressure drop in the inlet and outlet manifolds and ports was

empirically suggested by Shah and Focke<sup>(6)</sup>. It is approximately 1.5 times the head due to the flow expansion at the channel inlet

$$(\Delta p)_{man} \approx 1.5 \left( \frac{u_m^2}{2v_m} \right)_i \quad (4.15)$$

where  $u_m$  is the mean flow velocity. With the homogeneous model the mean velocity is

$$u_m = G v_m \quad (4.16)$$

Based on the above estimation the deceleration pressure rise(or, acceleration pressure rise), the pressure losses at the test section inlet and exit manifolds and ports, and the elevation pressure rise were found to be rather small. The frictional pressure drop ranges from 93% to 99% of the total pressure drop measured. According to the definition

$$f_{tp} \equiv - \frac{\Delta p_f D_h}{2G^2 v_m L} \quad (4.17)$$

the friction factor for the two-phase flow of R-134a in the P&SHE is obtained.

To estimate the uncertainties of the experimental results, an uncertainty analysis was carried out. Kline and McClintock<sup>(46)</sup> proposed a formula for evaluating the uncertainty. The detailed results of the uncertainty analysis are summarized in Table 4.2

**Table 4.2** Parameters and estimated uncertainties

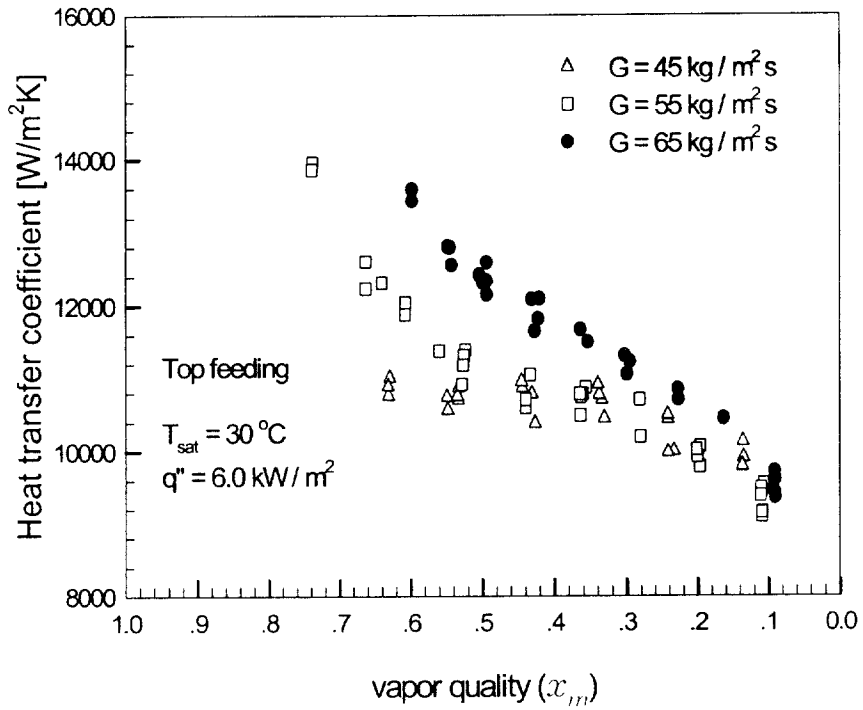
Parameter	Uncertainty
Temperature, $T(^{\circ}\text{C})$	$\pm 0.1$
Temperature difference $\Delta T(^{\circ}\text{C})$	$\pm 0.2$
Pressure, $p(\text{MPa})$	$\pm 0.002$
Pressure drop, $\Delta p \text{ (Pa)}$	$\pm 200$
Water flow rate, $\dot{m}(\%)$	$\pm 1.5$
Mass flux of refrigerant, $G(\%)$	$\pm 2$
Single phase heat transfer coefficient(%)	$\pm 10$
two phase flow heat transfer coefficient(%)	$\pm 18.6$

### 4.3 CONDENSATION HEAT TRANSFER CHARACTERISTICS

In the present investigation of the R-134a condensation in the P&SHE the R-134a mass flux was varied from 45 to 120  $kg/m^2s$ , average imposed heat flux from 6.0 to 8.0  $kW/m^2$  and saturation temperature from 30 to 40°C. The measured heat transfer coefficient are to be presented in terms of their variations with their average vapor quality in the test section, since the P&SHE is small and has only three plates, the vapor quality change in the test section is small,  $\Delta x < 0.06$ .

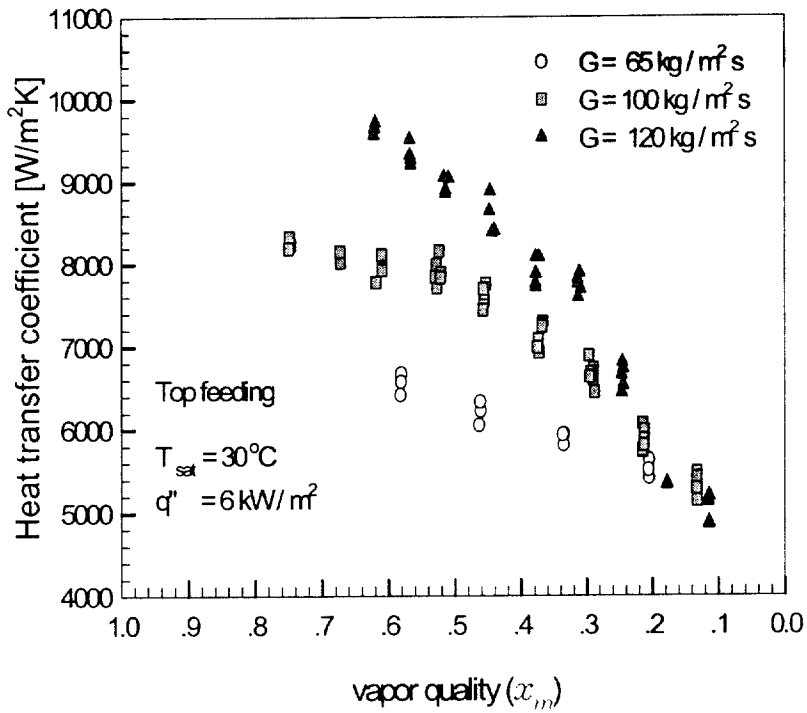
#### 4.3.1 The effects of mass flux, heat flux, saturation temperature and feeding method.

Figure 4.2 and 4.3 show the effect of the refrigerant mass flux on the measured R-134a condensation heat transfer coefficient at saturation temperature of 30°C and an average imposed heat flux of 6.0  $kW/m^2$  for the mass flux ranging from 45 to 65  $kg/m^2s$  in type A, 65 to 120  $kg/m^2s$  in type B and the mean vapor quality varying from 0.1 to 0.75. The mean vapor quality  $x_m$  is the average vapor quality in the P&SHE estimated from  $x_i$  and  $\Delta x$ . These data indicate that at a given mass flux the condensation heat transfer coefficient increases with the mean vapor quality of the refrigerant in the P&SHE. This increase is rather significant. For instance at 55  $kg/m^2s$  in the type A plate the condensation heat transfer coefficient at the quality  $x_m$  of 0.75 is about



**Fig. 4.2** Variations of condensation heat transfer coefficient with mean vapor quality for various mass fluxes, Type A.





**Fig. 4.3** Variations of condensation heat transfer coefficient with mean vapor quality for various mass fluxes, Type B.

55% larger than that at 0.13.(at 100 kg/m<sup>2</sup>s in the type B plate the condensation heat transfer coefficient at the same quality is about 50% larger) This obviously results from the simple fact that at a higher  $x_m$  the liquid film on the surface was thinner and the condensation rate is thus higher. But at a low quality with  $x_m < 0.25$  the heat transfer coefficient is only slightly affected by the mass flux. Note that at a low quality the vapor flow is slow. Thus, the differences in the condensation rates for different mass fluxes are limited<sup>(47)</sup>. The condensation heat transfer coefficient of the type A in high vapor quality is increased sharply compare than that of type B. This results from the fact that partitioning rib in the P&SHE suppresses vapor velocity in the higher vapor quality regime.

The effect of the average imposed heat flux on the condensation heat transfer is shown in Fig. 4.4 and Fig. 4.5 by presenting the heat transfer data for two heat fluxes of 6.0 kW/m<sup>2</sup> and 8.0 kW/m<sup>2</sup> at  $G = 55$  kg/m<sup>2</sup>s in type A,  $G = 100$  kg/m<sup>2</sup>s in the B and  $T_{sat} = 30^\circ\text{C}$ . It is well known that the condensation rate would be proportional to the heat flux. The results indicate that at a given vapor quality the heat transfer coefficient is higher for a higher heat flux except at a higher vapor quality with  $x_m > 0.65$  in type A and  $x_m > 0.52$  in type B. Note that the R-134a quality-averaged condensation heat transfer coefficients at 8.0 kW/m<sup>2</sup> in type A and B are respectively about 9% and 6% larger than that at 6.0 kW/m<sup>2</sup>. However, Compared with the mass flux effects shown in Fig. 4.2 and Fig. 4.3, the heat flux has a smaller effect on the condensation heat transfer coefficient in the higher vapor quality regime.

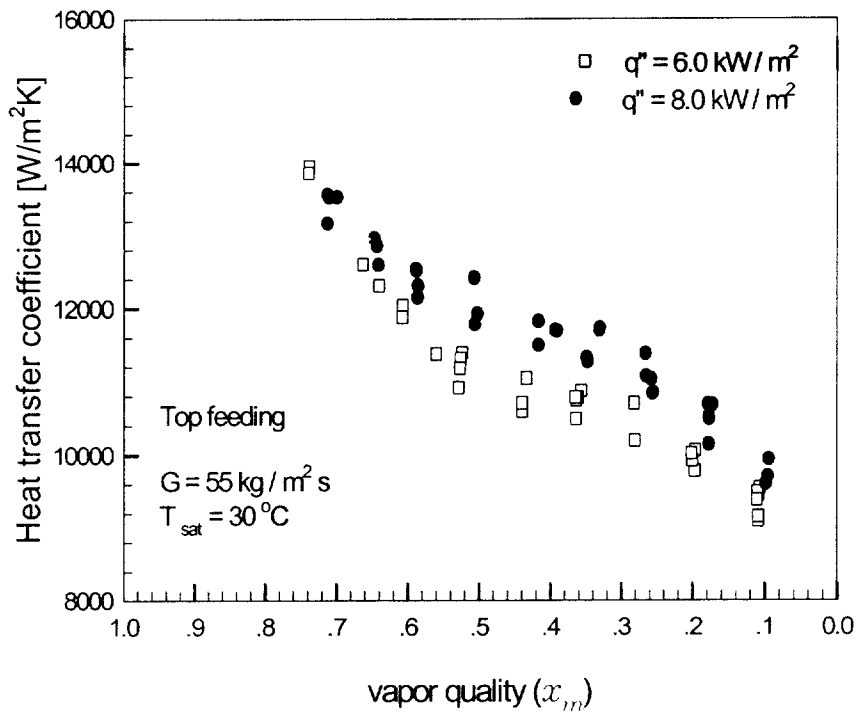


**Fig. 4.4** Variations of condensation heat transfer coefficient with mean vapor quality for two heat fluxes, Type A.

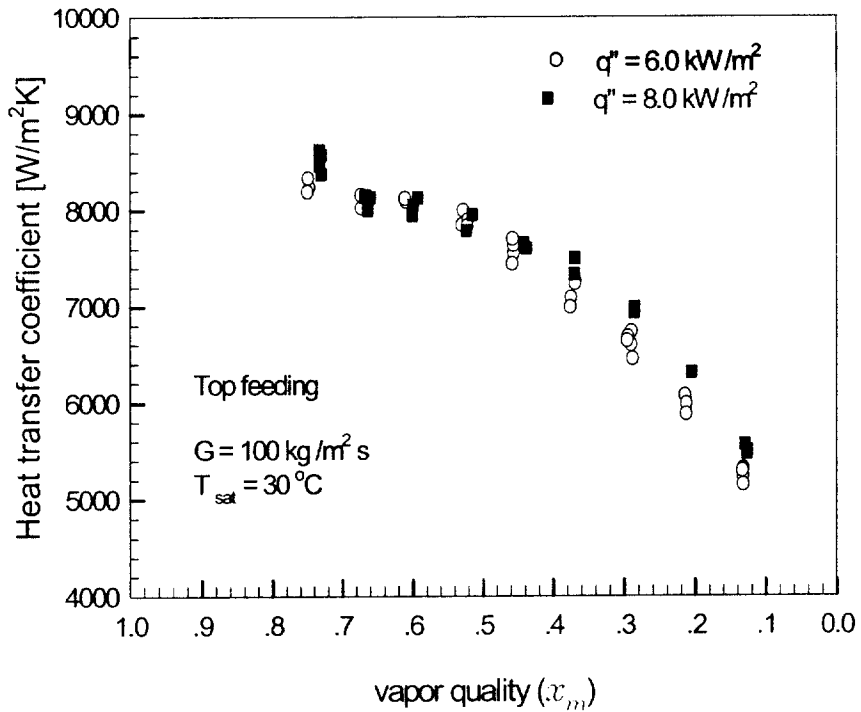


**Fig. 4.5** Variations of condensation heat transfer coefficient with mean vapor quality for two heat fluxes, Type B.

The effects of the refrigerant saturation temperature on the condensation heat transfer coefficient is illustrated in Fig. 4.6 and 4.7 by presenting the data for two typical cases at  $G = 55 \text{ kg/m}^2\text{s}$  in type A,  $G = 100 \text{ kg/m}^2\text{s}$  in type B and  $q_w'' = 6.0 \text{ kW/m}^2$  at different mean vapor qualities for  $T_{\text{sat}}$  ranging from 30 to 40°C. The temperature difference of refrigerant saturation temperature and cooling water was maintained 3°C ( $\pm 0.2^\circ\text{C}$ ) at the both cases. The results suggest that at a given saturation temperature the condensation heat transfer coefficient rises significantly with the mean vapor quality. While at a fixed  $x_m$ , the condensation heat transfer coefficient is poorer at a higher  $T_{\text{sat}}$  in the total quality region. Specifically, the mean heat transfer coefficient at 30°C is about 30 to 40% bigger than that at 40°C. There are two primary reasons for the decrease in condensation heat transfer coefficient as saturation temperature increases. A decrease in the density ratio, which results in lower slip velocities between the vapor and liquid phase, and a decrease in the thermal conductivity. Compared with the heat flux shown in Fig. 4.4 and Fig. 4.5, the saturation temperature has an effect on the condensation heat transfer coefficient in the total vapor quality regime.

The effect of the refrigerant feeding method on the condensation heat transfer is shown Fig. 4.8 by presenting the heat transfer data for bottom feeding and top feeding at  $G = 100 \text{ kg/m}^2\text{s}$  and  $T_{\text{sat}} = 30^\circ\text{C}$  in type B. The condensation heat transfer coefficient at top feeding is about 1.5 ~ 2.8 higher than that at bottom feeding. In the case of bottom feeding, the refrigerant exit port is located the top of the channel. Consequently, refrigerant must be accumulated in the channel before exiting. Due to the hold up of liquid in the test section, the velocity of the vapor was

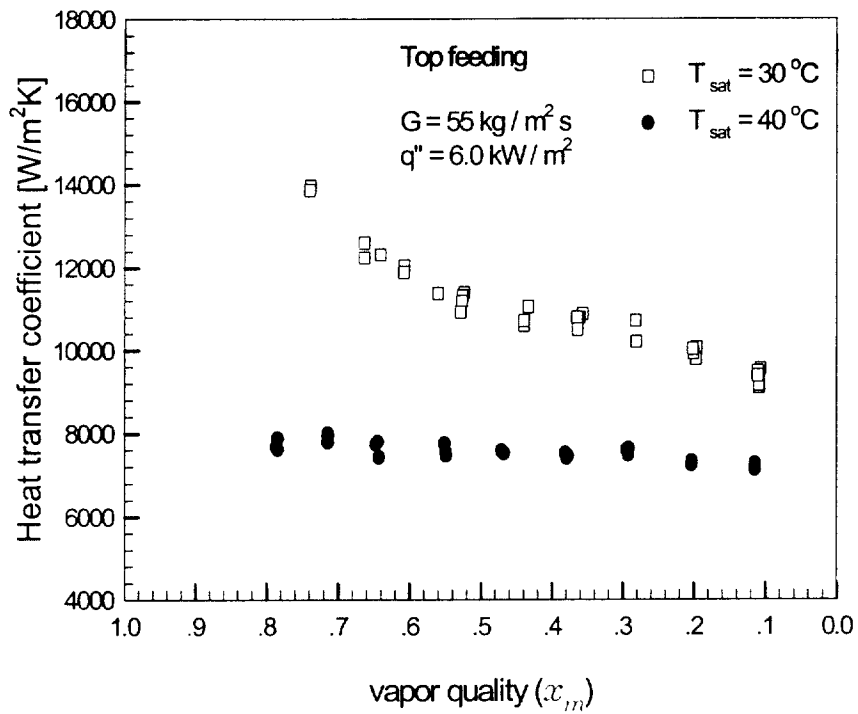


**Fig. 4.6** Variations of condensation heat transfer coefficient with mean vapor quality for two saturation temperature, Type A.

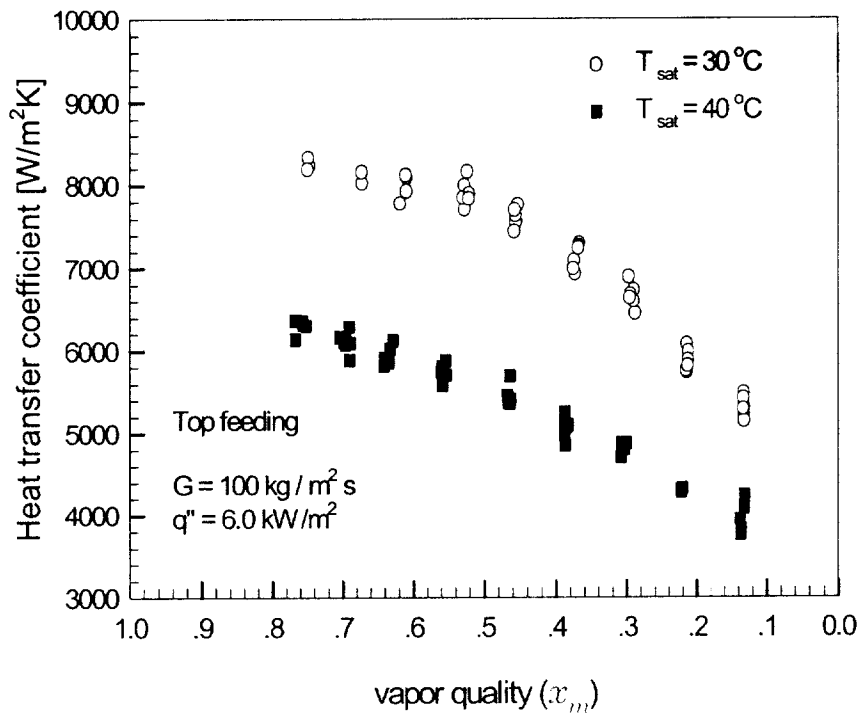


**Fig. 4.7** Variations of condensation heat transfer coefficient with mean vapor quality for two saturation temperature, Type B.

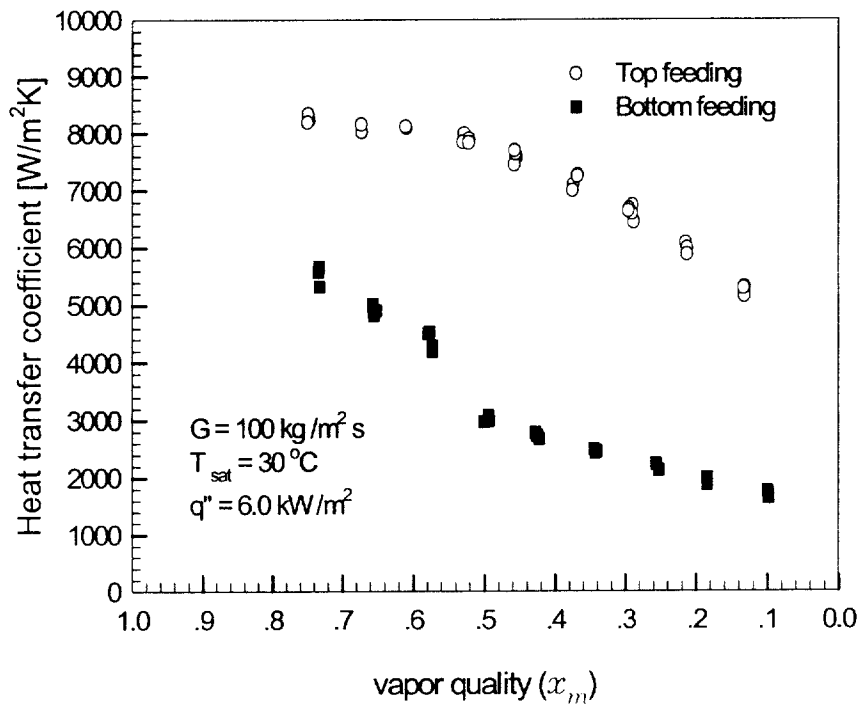


Fig. 4.8 Effects of the refrigerant feeding method on the condensation heat transfer, Type B.



restrained and it caused poor heat transfer.

### 4.3.2 Comparison with Plate heat exchanger

It is necessary to compare the present data for the R-134a condensation heat transfer coefficient in the P&SHE to those in plate heat exchanger reported in the literature. Due to the limited availability of the data for plate heat exchanger with the same ranges of the parameters covered in the present study. The comparison is only possible for a few cases. This is illustrated in Fig. 4.9, in which our data are compared with correlation of Yan et al.<sup>(36)</sup>. Note that the data from Yan et al. are average condensation heat transfer coefficient measured in a plate heat exchanger with the vapor quality from 0.08 to 0.86. Yan et al proposed condensation heat transfer correlation equation such as

$$Nu = \frac{h_r D_h}{k_l} = 4.118 Re_{eq}^{0.4} Pr_l^{1/3} \quad (4.18)$$

$Re_{eq}$  is the equivalent Reynolds number.  $Re_{eq}$  is defined as

$$Re_{eq} = \frac{G_{eq} D_h}{\mu_l} \quad (4.19)$$

in which

$$G_{eq} = G \left[ 1 - x_m + x_m \left( \frac{\rho_l}{\rho_v} \right)^{1/2} \right] \quad (4.20)$$

Here  $G_{eq}$  was proposed by Akers et al<sup>(34)</sup>. and is an equivalent mass flux which is a function of the R-134a mass flux, mean quality and densities at the saturated condition.

The comparison clearly shows that the R-134a condensation heat transfer coefficient for P&SHE is about 5 times (Type A) and 2.5 times (Type B) in average higher than that for the plate heat exchanger.

### 4.3.3 Correlation of condensation heat transfer

To facilitate the use of the plate and shell heat exchanger as a condenser, correlating equations for the dimensionless condensation heat transfer coefficient on the present data are provided. They are modified Yan et al's correlation

Type A :

$$Nu = \frac{h_r D_h}{k_l} = 50.8 Re_{eq}^{0.27} Pr_l^{1/3} \quad 1800 < Re_{eq} < 6500 \quad (4.21)$$

Type B :

$$Nu = \frac{h_r D_h}{k_l} = 4.94 Re_{eq}^{0.45} Pr_l^{1/3} \quad 3000 < Re_{eq} < 11000 \quad (4.22)$$

Fig. 4.11 and 4.12 show the comparison of the proposed condensation heat transfer correlation to the present data, indicating that most of the experimental values are within  $\pm 10\%$ (Type A) and  $\pm 20\%$ (Type B).

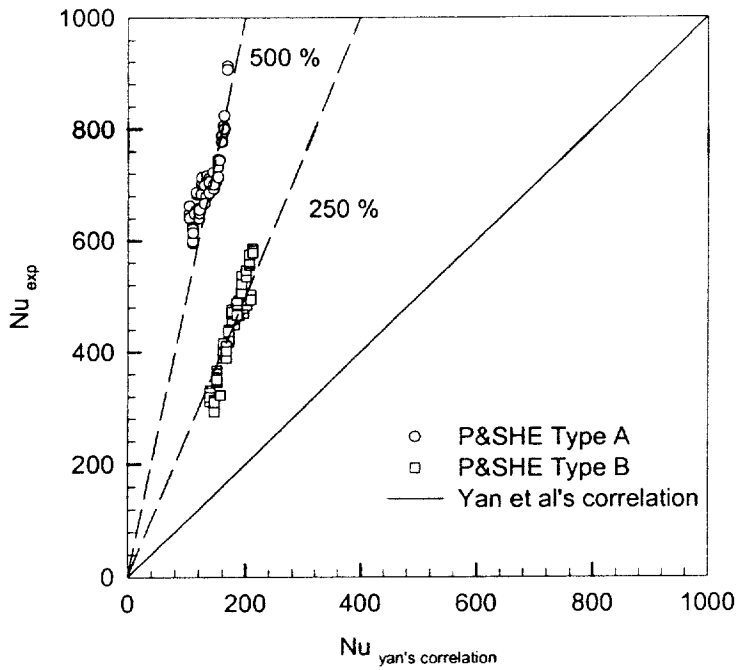


**Fig. 4.9** Comparison of the present heat transfer data with those for plate heat exchanger from Yan et al.

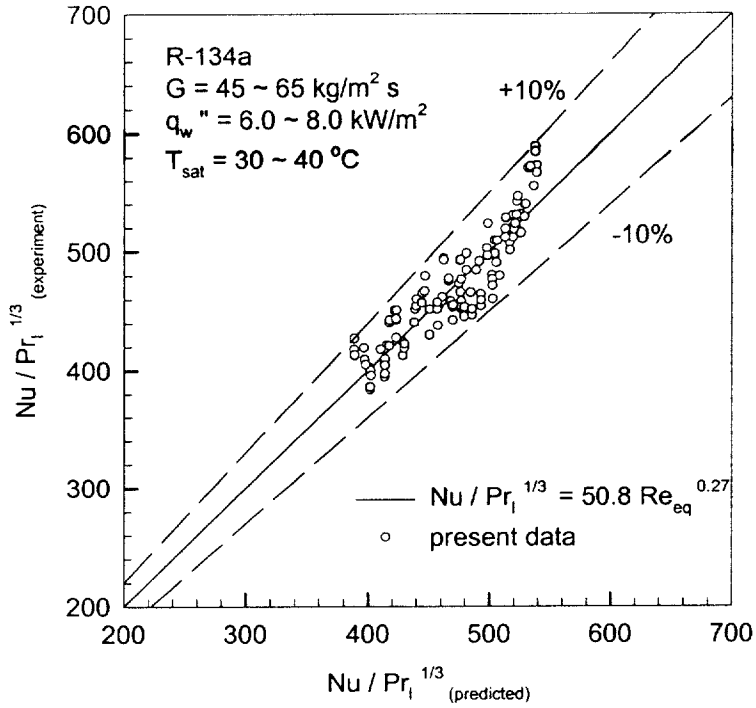


**Fig. 4.10** Comparison of the proposed correlation for Nusselt number with the present data, Type A.

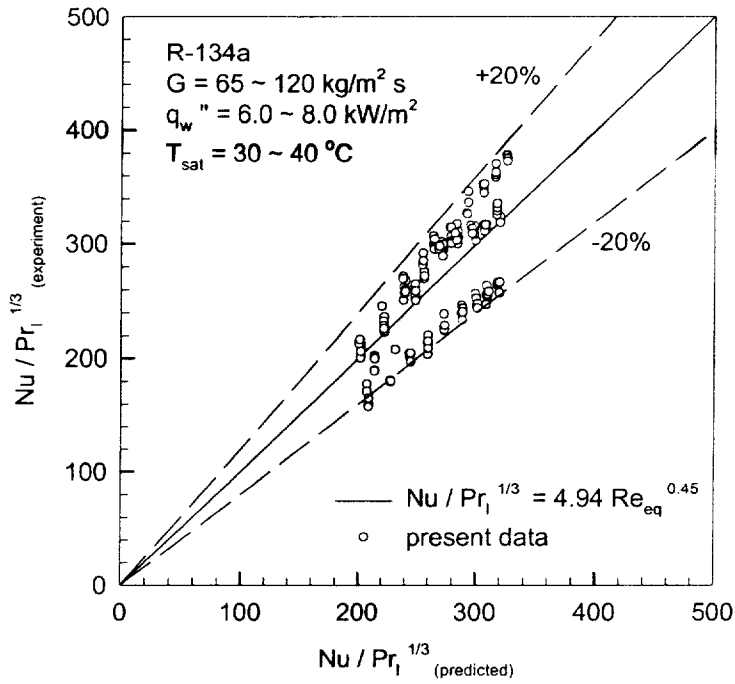


Fig. 4.11 Comparison of the proposed correlation for Nusselt number with the present data, Type B.

## **4.4 EVAPORATION HEAT TRANSFER CHARACTERISTICS**

Effects of the mass flux, heat flux saturation temperature and feeding method on the evaporation heat transfer of refrigerant R-134a in the plate and shell heat exchanger were examined in the following.

Selected measured data are presented in Figs. 4.12 ~ 4.19 to illustrate the changes of the heat transfer coefficient with the vapor quality for various mass fluxes, heat fluxes, saturation temperature and feeding method. In the plots  $x_m$  denotes the average vapor quality in the P&SHE.

### **4.4.1 The effects of mass flux, heat flux, saturation temperature and feeding method.**

Figure 4.12 and 4.13 shows the effects of the mass flux on the heat transfer coefficient.

In traditional test facilities, the refrigerant is heated by an electrical resistance wire wound around the tube or by direct electrical heating of the tube itself and the heat flux is fixed by the electrical power dissipated. Instead, in the present test facility, the refrigerant inside the plate is heated by hot water flowing counter-currently in the shell side (which corresponds more closely to the real situation in a water chiller evaporator). In this case the heat flux is not an independent variable imposed by the experimenter, it comes from controlling the hot water inlet temperature and it also depends on the overall  $U_o$  and the

logarithmic mean temperature difference (LMTD). Thus, the resulting heat flux is dependent on the unknown boiling heat transfer coefficient to be measured. Therefore, the influence of using electrical heating as opposed to a hot fluid stream, as in a real heat exchanger, is a controversial issue that needs to be addressed in tests using electrical heating<sup>(48)</sup>.

In Fig. 4.12, the data for three different mass fluxes of 45, 55, 65  $\text{kg/m}^2\text{s}$  are compared at the same heat flux and saturation temperature in type A plate. Note that at a low-vapor quality ( $x_m < 0.35$ ) the mass flux exhibits an insignificant influence on the heat transfer in the flow. At this low-vapor quality, boiling in the refrigerant appears to be suppressed at this heat flux level for these three mass fluxes. As the vapor quality is above 0.35, the difference in the heat transfer coefficient for the three mass fluxes begins to grow. The heat transfer coefficient for the higher mass flux rises more quickly than that for the lower mass flux. This is attributed to the fact that at 30°C the liquid density of R-134a is about 35 times of the corresponding vapor density. Thus, a great increase in the vapor volume during the evaporation process causes the vapor flow to move in a high speed, which in turn breaks the adjacent liquid film into a large number of tiny liquid droplets in the channel. This highly turbulent mist flow results in a substantial rise in the heat transfer coefficient. The high-speed turbulent mist flow continuously wets the heat transfer wall and significantly reduces the resistance of heat transfer from the channel wall to the flow. At a higher mass flux the mist flow is at a higher velocity and the heat transfer is better. A distinct maximum in heat transfer coefficient after the peak was observed to be caused by the partial plate wall dryout as shown in Fig. 12.

A similar trend is noted in Fig. 4.13 for three different mass fluxes of 65, 100, 120  $\text{kg/m}^2\text{s}$  are compared at the same heat flux and saturation temperature in type B plate. There exists a sudden drop in the heat transfer coefficient at  $x_m = 0.45$  for  $G = 100 \text{ kg/m}^2\text{s}$  in type B plate. The existence of this drop is conjectured to be due to the significant suppression of the boiling process when the vapor quality rises to 0.45 with the vapor velocity being high enough to rupture the thin liquid film on the channel wall.

The effect of the average imposed heat flux on the evaporation heat transfer is shown Fig. 4.14 and Fig. 4.15 by presenting the heat transfer data for two heat fluxes of 6.0  $\text{kW/m}^2$  and 8.0  $\text{kW/m}^2$  at  $G = 55 \text{ kg/m}^2\text{s}$  in type A plate ( $G = 100 \text{ kg/m}^2\text{s}$  in type B plate ) and  $T_{\text{sat}} = 30^\circ\text{C}$ .

Two different heat flux are generated by modifying the inlet water temperature of the test section, which affects the LMTD of the test section. Before the maximum value of the heat transfer coefficient the plate wall is completely wet and the heat flux depends on the LMTD fixed by the inlet water temperature of the test section. After the maximum value of the heat transfer coefficient, with the beginning of partial plate wall dryout, the measured heat flux values decrease even though the inlet water temperature is kept the same for each heat flux. In this region the heat flux depends on the flow pattern configuration inside the plate, i.e., how much of the plate wall is dry. Using an electrically heated tube the heat flux is kept artificially constant before and after the maximum value of the heat transfer coefficient so that the



heat flux becomes an independent variable imposed by the experimenter. This means that in an annular flow with partial dryout the heat transfer coefficient at the top of the tube decreases while the electrical resistance tends to keep a constant heat flux, inducing a temperature increase of the tube wall. For a given mass flux  $G=55 \text{ kg/m}^2\text{s}$  in type A plate ( $G=100 \text{ kg/m}^2\text{s}$  in type B plate) the heat transfer coefficients at two heat fluxes are distinctly different at low qualities, merging into a single line beyond certain transition qualities. The above mentioned results indicate that there are two distinct heat transfer regions in flow boiling of refrigerants. The first is a 'partial boiling' region occurring at low qualities in which heat transfer coefficients are a strong function of heat flux. Both the forced convective evaporation and nucleate boiling mechanisms were found to be responsible for the heat transfer in this region. The rapid suppression of the latter even leads to a temporary reduction of the heat transfer coefficients with increasing quality as shown in Fig. 4.14 and Fig. 4.15, which was observed also with smooth tube. The second is a 'convective evaporation' region beyond the transition quality where heat transfer coefficients are independent of heat flux. Instead, the present results advocate a conventional concept of the suppression of nucleate boiling with increasing quality in annular flow. As quality is increased in annular flow, the effective wall superheat decreases due to a thinner liquid film (less thermal resistance) and an enhanced convection caused by high vapor velocity. Thus, the number of active nucleation sites decreases till a transition quality is reached. Beyond the transition quality, the effective wall superheat is below the threshold value required for bubble nucleation on the wall.

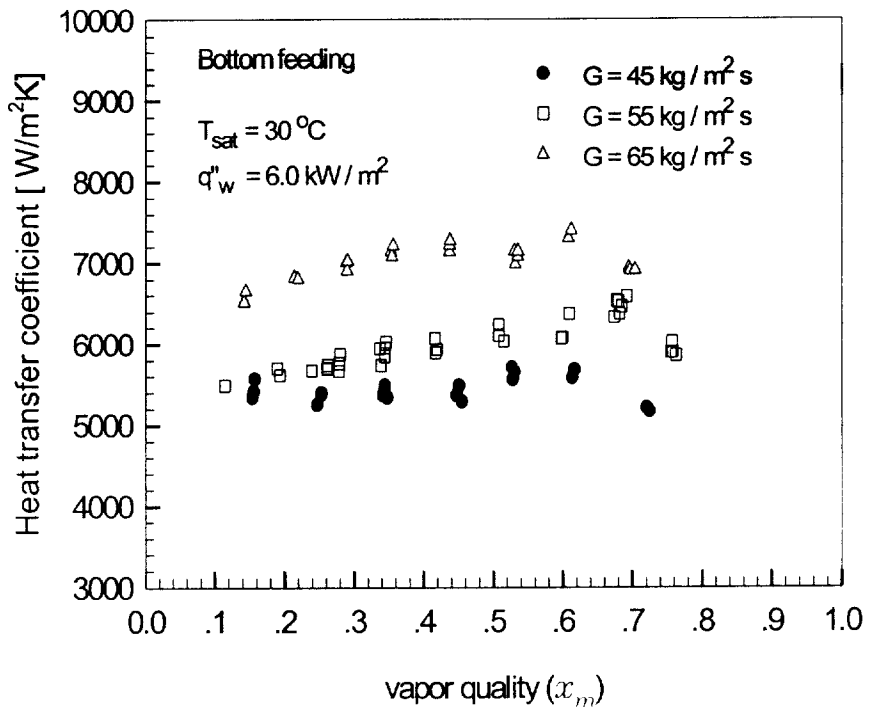


**Fig. 4.12** Variations of evaporation heat transfer coefficient with mean vapor quality for various mass fluxes, Type A.

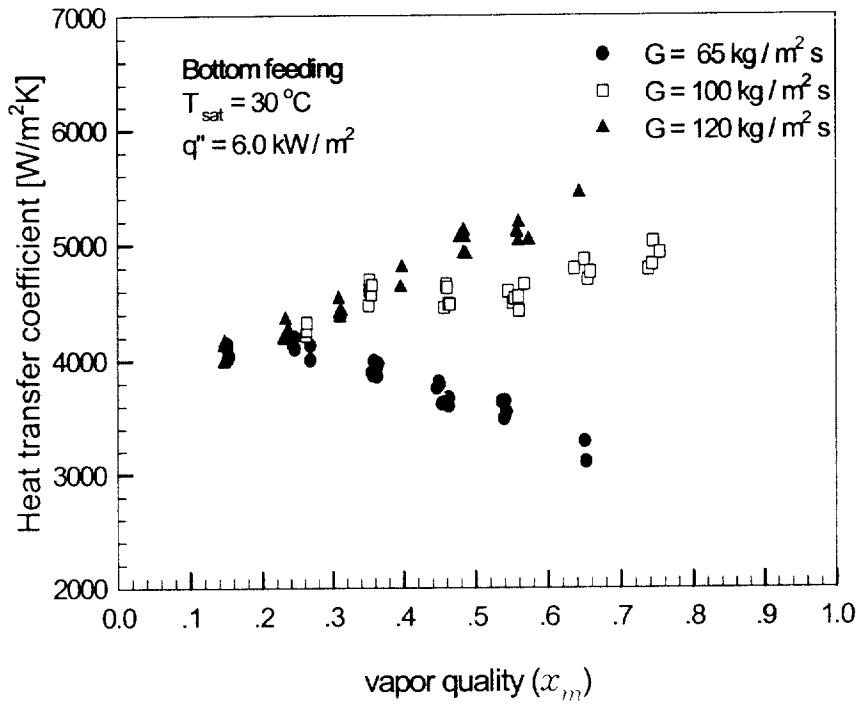


**Fig. 4.13** Variations of evaporation heat transfer coefficient with mean vapor quality for various mass fluxes, Type B.

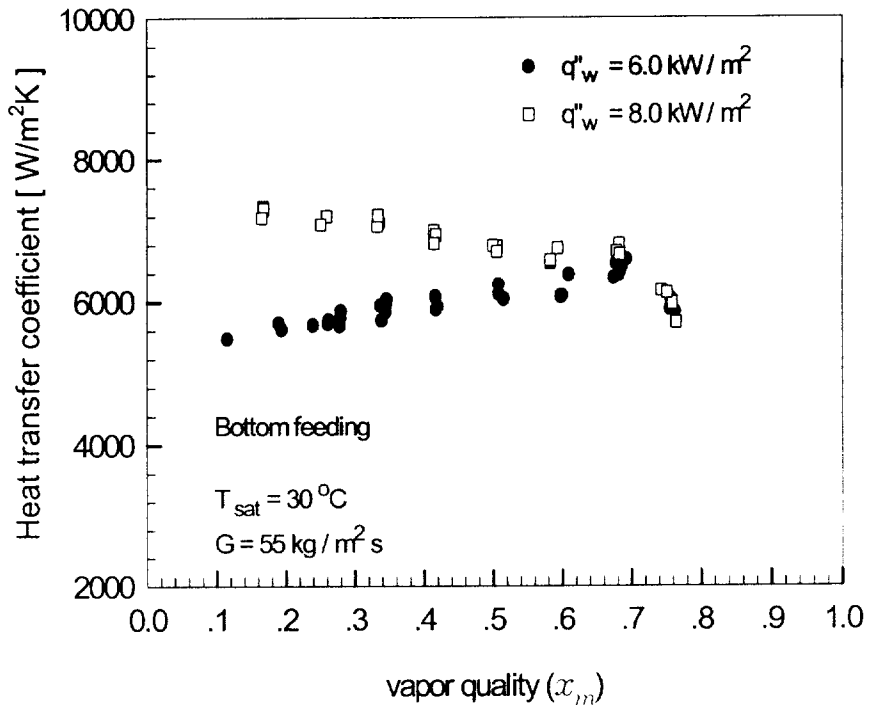


**Fig. 4.14** Variations of evaporation heat transfer coefficient with mean vapor quality for two heat fluxes, Type A.

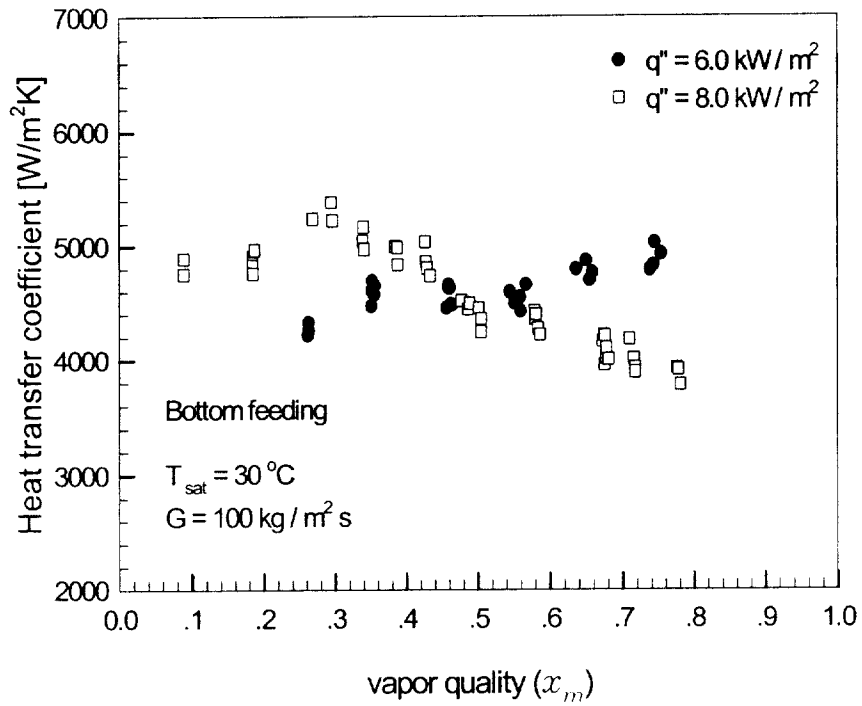
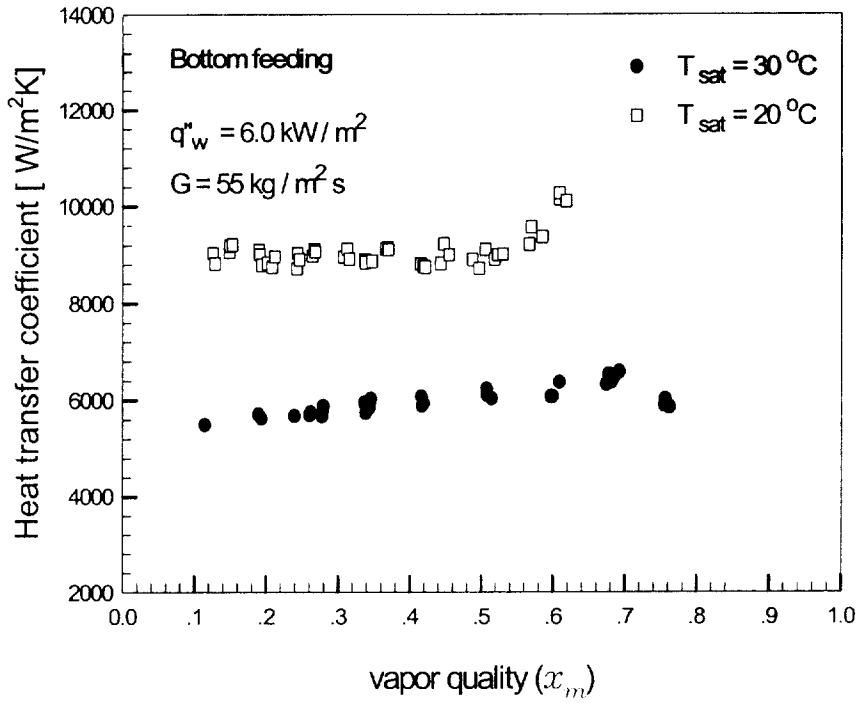


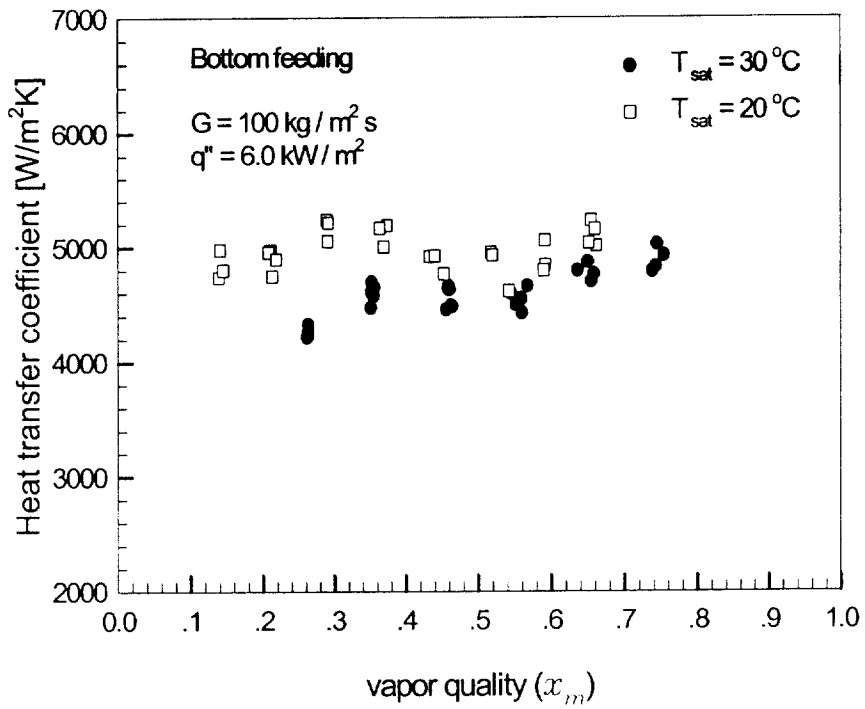
Fig. 4.15 Variations of evaporation heat transfer coefficient with mean vapor quality for two heat fluxes, Type B.

Figure 4.17 and Figure 4.18 illustrates the effects of the saturation temperature on the evaporation heat transfer. Two cases with the saturation temperature of 30°C and 20°C, which are, respectively, equivalent to the saturated pressure of 0.77 MPa and 0.57 MPa for R-134a, are examined. The results show that evaporation heat transfer coefficient is poorer at a higher saturation temperature in the total quality region. Specifically, the mean heat transfer coefficient at 30°C is about 10~30% lower than that at 20°C. This is attributed to the lower specific volume of R-134a vapor at a higher saturation temperature, which, in turn, causes lower vapor flow rate and hence lower shear force to the liquid film on the heat transfer surface. Moreover, the latent heat of vaporization is smaller for a higher R-134a pressure and the channel wall may be partially dried when the vapor quality is high.

The effect of the refrigerant feeding method on the evaporation heat transfer is shown Fig. 4.18 and Fig. 4.19 by presenting the heat transfer data for top feeding and bottom feeding at  $G = 55 \text{ kg/m}^2\text{s}$  and  $T_{\text{sat}} = 30 \text{ }^\circ\text{C}$  in type A plate and  $G = 100 \text{ kg/m}^2\text{s}$  in type B plate. The evaporation heat transfer coefficient at bottom feeding is about 1.3 ~ 1.7 times higher than that at top feeding. Gravity and flow regime changes both acted to reduce the heat transfer as the feeding method was changed from bottom feeding to top feeding.



**Fig. 4.16** Variations of evaporation heat transfer coefficient with mean vapor quality for two saturation temperature, Type A.



**Fig. 4.17** Variations of evaporation heat transfer coefficient with mean vapor quality for two saturation temperature, Type B.



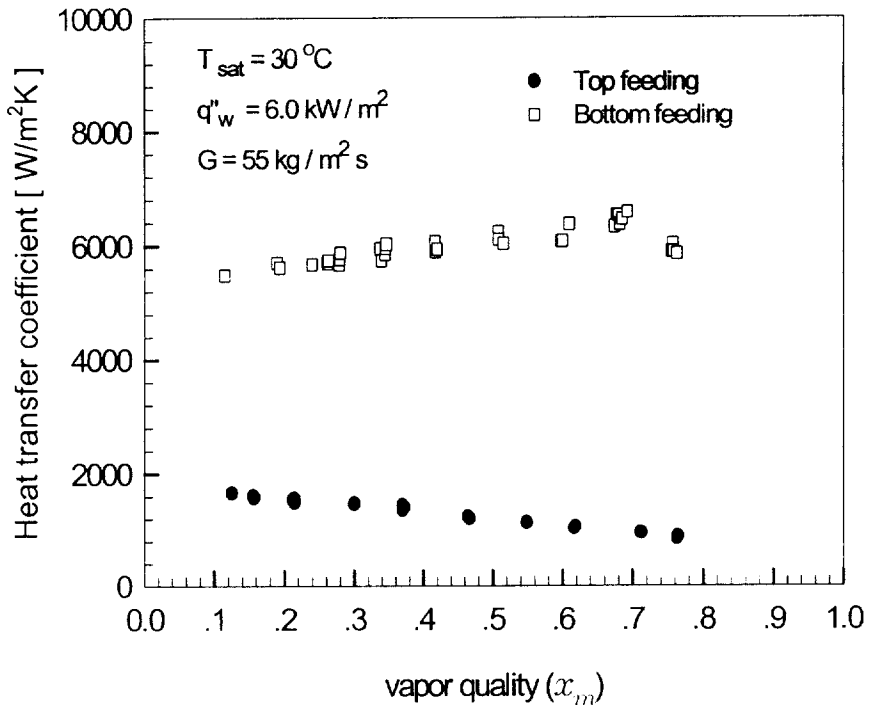


**Fig. 4.18** Effects of the refrigerant feeding method on the evaporation heat transfer, Type A.

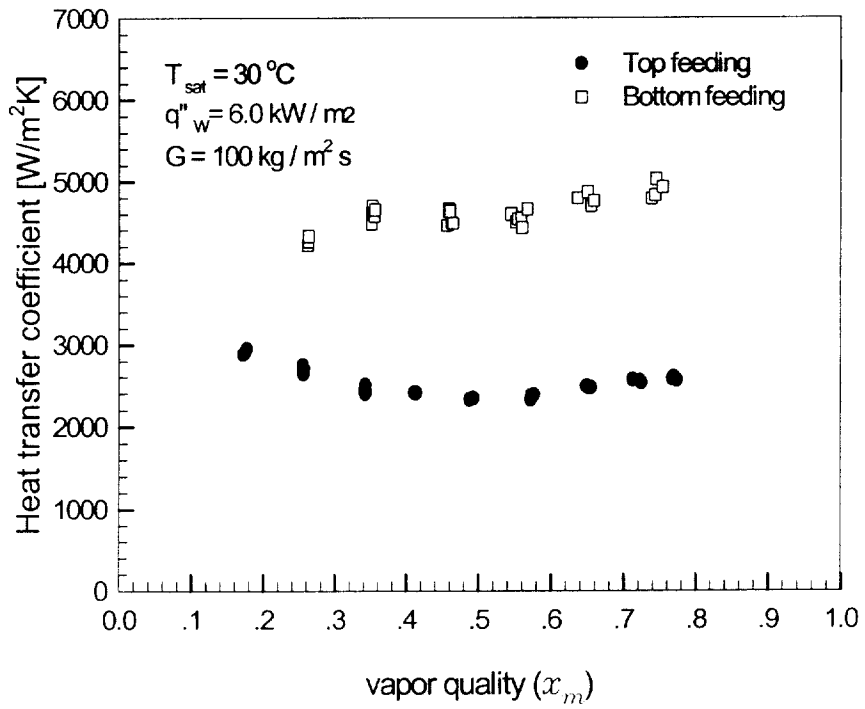


**Fig. 4.19** Effects of the refrigerant feeding method on the evaporation heat transfer, Type B.

#### 4.4.2 Comparison with Plate heat exchanger

It is necessary to compare the present data for the R-134a evaporation heat transfer coefficient in the P&SHE to those in plate heat exchanger reported in the literature. Due to the limited availability of the data for plate heat exchanger with the same ranges of the parameters covered in the present study. The comparison is only possible for a few cases. This is illustrated in Fig. 4.20, in which our data are compared with correlation of Yan et al.<sup>(37)</sup>. Note that the data from Yan et al. are average condensation heat transfer coefficient measured in a plate heat exchanger with the vapor quality from 0.08 to 0.86. Yan et al proposed condensation heat transfer correlation equation such as

$$\frac{h_c D_h}{k_l} \text{Pr}_l^{-1/3} Re^{0.5} Bo_{eq}^{-0.3} = 1.926 Re_{eq} \quad (4.23)$$

$$Bo_{eq} = \frac{q_w''}{G_{gq} \cdot i_{fg}} \quad (4.24)$$

The comparison clearly shows that the R-134a condensation heat transfer coefficient for P&SHE is about 2 times (Type A) and 1.3 times (Type B) in average higher than that for the plate heat exchanger.

#### 4.4.3 Correlation of evaporation heat transfer

To facilitate the use of the plate and shell heat exchanger as a evaporator, correlating equations for the dimensionless evaporation heat transfer coefficient on the present data are provided. They are modified

Yan et al's correlation

Type A :

$$\frac{h_r D_h}{k_l} \text{Pr}_l^{-1/3} Re^{0.5} Bo_{eq}^{-0.3} = 2623 Re_{eq}^{0.23} \quad 2000 < Re_{eq} < 7000 \quad (4.25)$$

Type B :

$$\frac{h_r D_h}{k_l} \text{Pr}_l^{-1/3} Re^{0.5} Bo_{eq}^{-0.3} = 94.59 Re_{eq}^{0.58} \quad 2500 < Re_{eq} < 11000 \quad (4.26)$$

Fig. 4.21 and 4.22 show the comparison of the proposed evaporation heat transfer correlation to the present data, indicating that most of the experimental values are within  $\pm 20\%$ (Type A) and  $\pm 15\%$ (Type B).

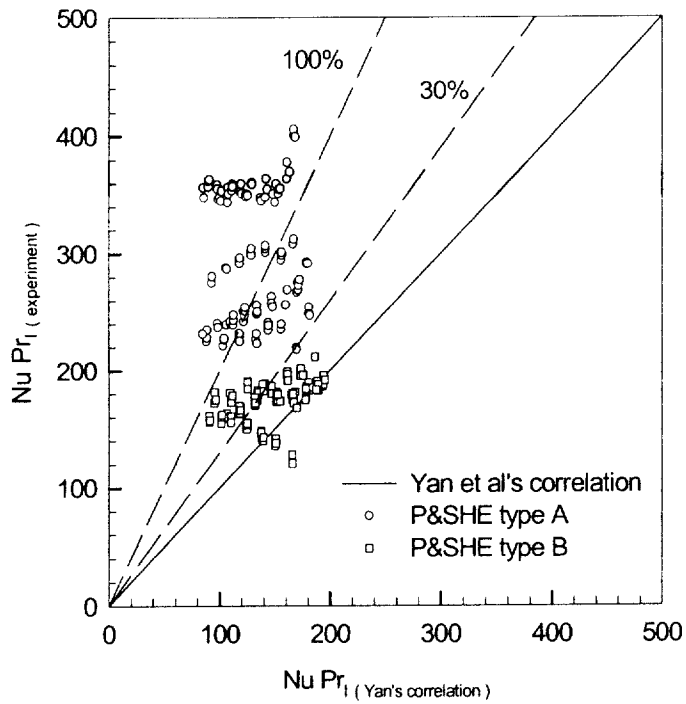


**Fig. 4.20** Comparison of the present heat transfer data with those for plate heat exchanger from Yan et al.

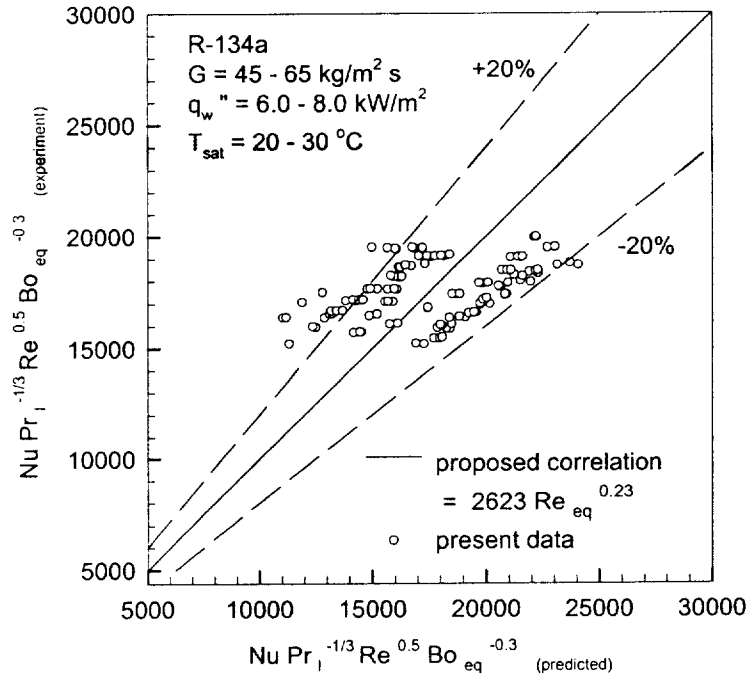


**Fig. 4.21** Comparison of the proposed correlation for Nusselt number with the present data, Type A.

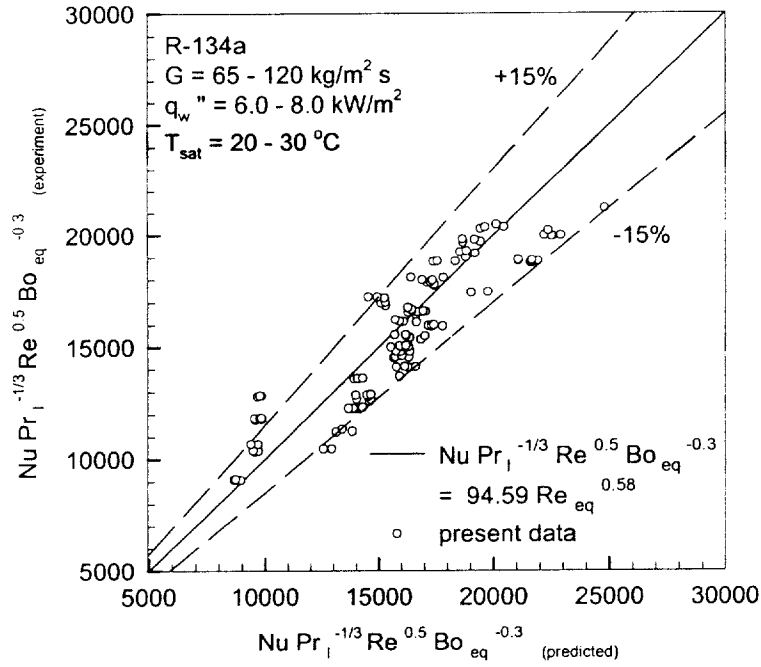


**Fig. 4.22** Comparison of the proposed correlation for Nusselt number with the present data, Type B.

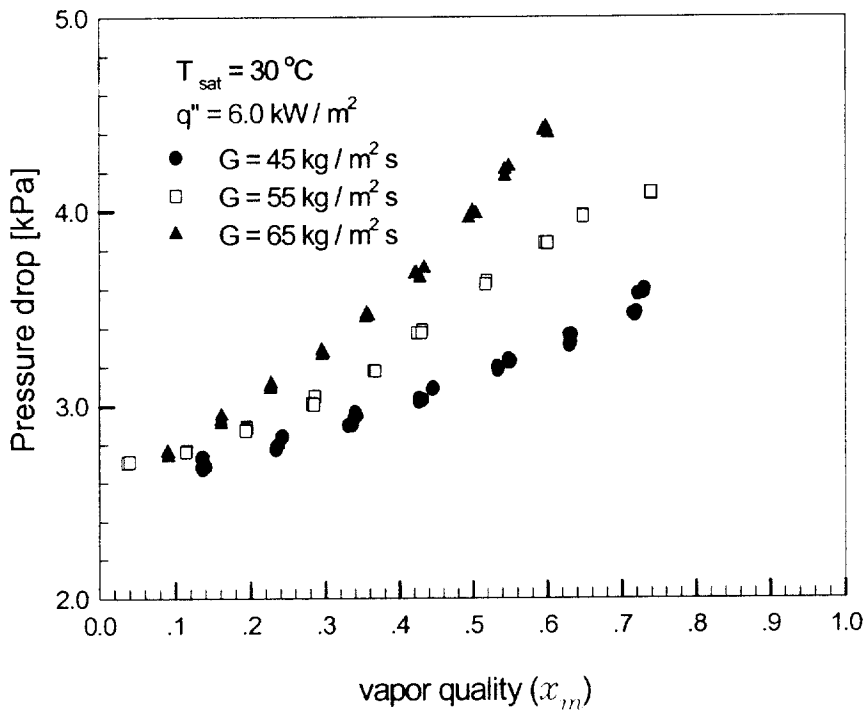
## 4.5 TWO-PHASE FLOW PRESSURE DROP CHARACTERISTICS

The variations of the frictional pressure drops in the P&SHE with the vapor quality are shown in Figs. 4.23 ~ 4.28 for different mass fluxes, heat fluxes and saturation temperature.

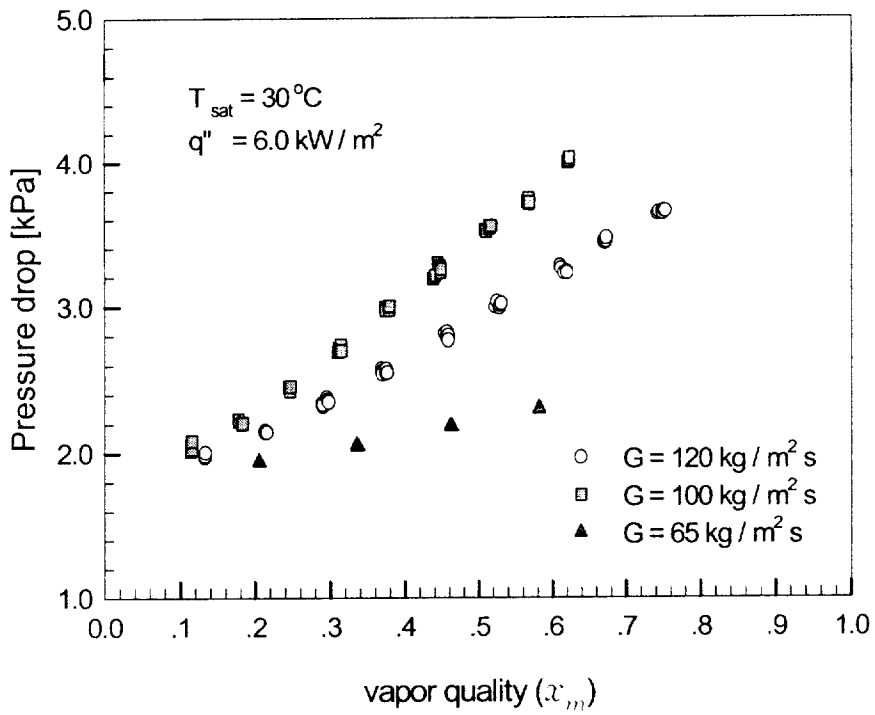
### 4.5.1 The effects of mass flux, heat flux and saturation temperature.

Figure 4.23 and 4.24 show the effects of the mass flux on the friction pressure drop. In Fig. 4.23, the data for three different mass fluxes of 45, 55, 65  $\text{kg/m}^2\text{s}$  are compared at the same heat flux and saturation temperature in type A plate. And in Fig. 4.24, the data for three different mass fluxes of 65, 100, 120  $\text{kg/m}^2\text{s}$  are compared at the same heat flux and saturation temperature in type B plate. The changes of the frictional pressure drop with the vapor quality and mass flux, as shown in Fig. 4.23 and Fig. 4.24, are similar to trend in the evaporation heat transfer coefficient change with mass flux shown in Fig. 4.2 and 4.3, respectively. The results in Fig. 4.24 indicated that at a given mass flux the pressure drop is larger for a higher vapor quality. In addition, the pressure drop increases with the quality is more pronounced for a higher mass flux. Note that the variation of  $\Delta p_f$  with vapor quality is much larger than the heat transfer coefficient. At  $G = 55 \text{ kg/m}^2\text{s}$  in type A plate, the frictional pressure drop can be approximately increased by 40% for  $x_m$  raised from 0.13 to 0.75. and at  $G = 100 \text{ kg/m}^2\text{s}$  in type B





**Fig. 4.23** Variations of pressure drop with mean vapor quality for various mass fluxes, Type A.



**Fig. 4.24** Variations of pressure drop with mean vapor quality for various mass fluxes, Type B.

plate, the frictional pressure drop can be approximately increased by 85% for the same range. This obviously results from the simple fact that at a higher  $x_m$  the velocity of vapor was larger and the pressure drop was thus higher.

Fig. 4.25 and 4.26 shows the effects of the average imposed heat flux on the frictional pressure drop for  $T_{\text{sat}} = 30^\circ\text{C}$  at  $G = 100 \text{ kg/m}^2\text{s}$  in type A plate and  $G = 55 \text{ kg/m}^2\text{s}$  in type B plate. The data indicate that at a given heat flux the frictional pressure drop increases linearly with the mean vapor quality of the refrigerant in the P&SHE. An increase in the heat flux dose not show significantly effect on the frictional pressure drop in the P&SHE.

The results in Fig. 4.27 and 4.28 for different saturation temperatures of R-134a indicated that at a given  $T_{\text{sat}}$  the pressure drop is larger for a higher vapor quality. This pressure drop increase with the quality is more pronounced for a lower saturation temperature. Note that in the total vapor quality range the pressure drop gets smaller at a higher  $T_{\text{sat}}$ . This is conjectured to be mainly resulting from a reduction in the velocity of vapor for the R-134a saturation temperature raised from 20 to 40°C. This trend is similar to the effect of  $T_{\text{sat}}$  on the heat transfer coefficient.

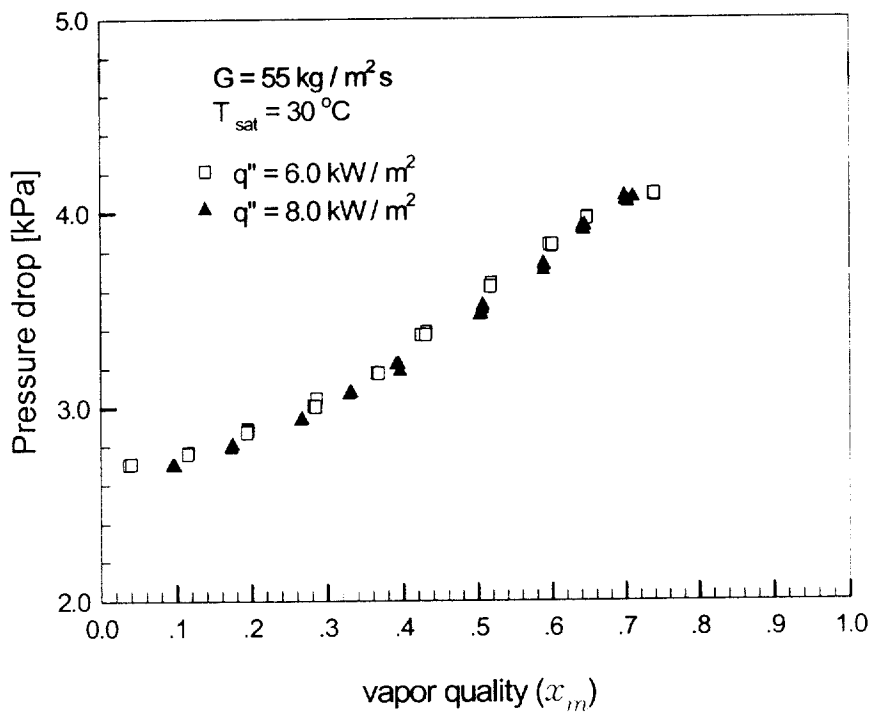
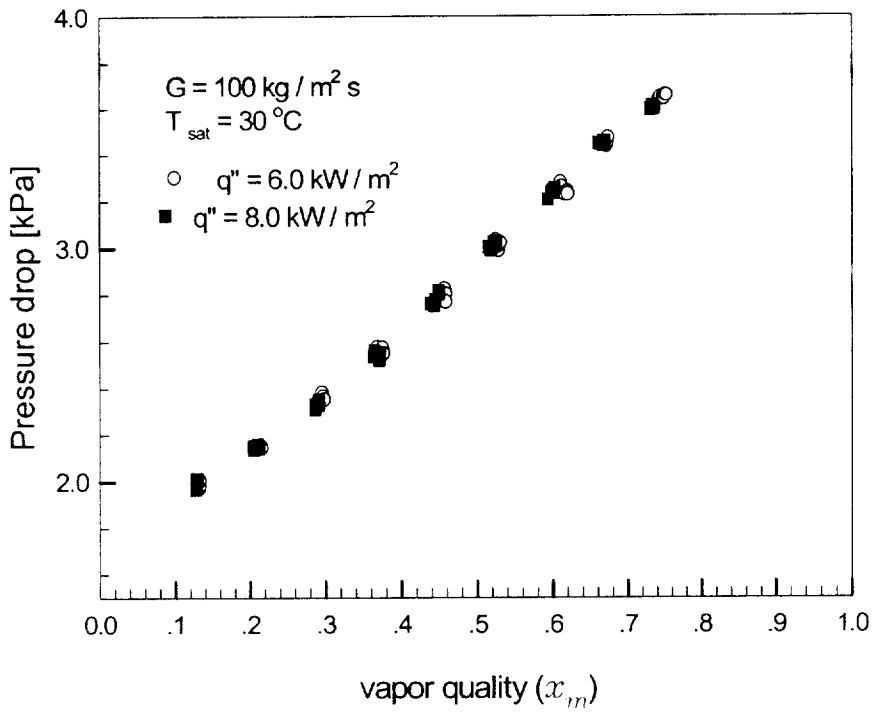
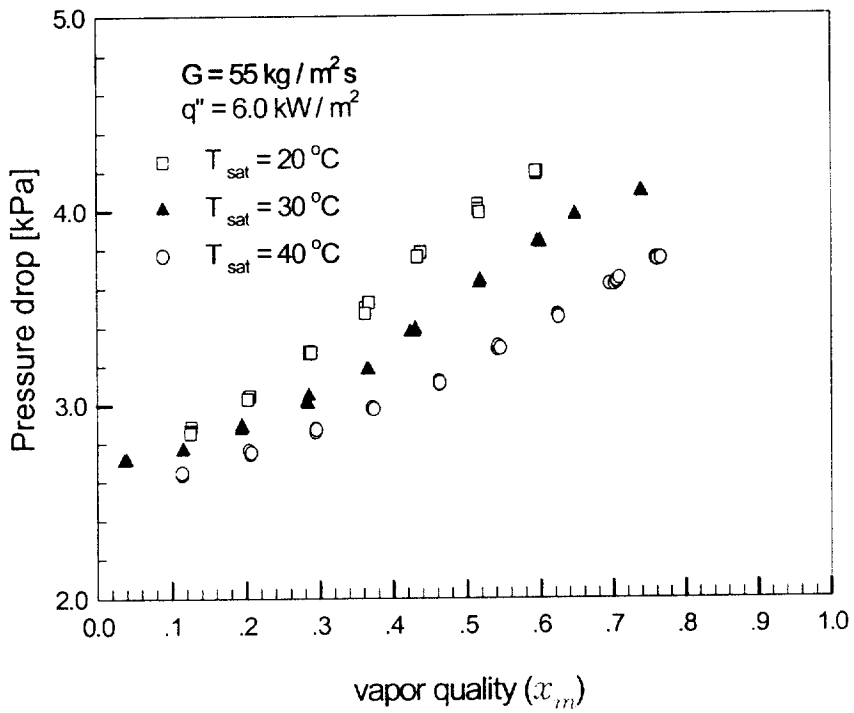


Fig. 4.25 Variations of pressure drop with mean vapor quality for two heat fluxes, Type A.



**Fig. 4.26** Variations of pressure drop with mean vapor quality for two heat fluxes, Type B.



**Fig. 4.27** Variations of pressure drop with mean vapor quality for various saturation temperature, Type A.

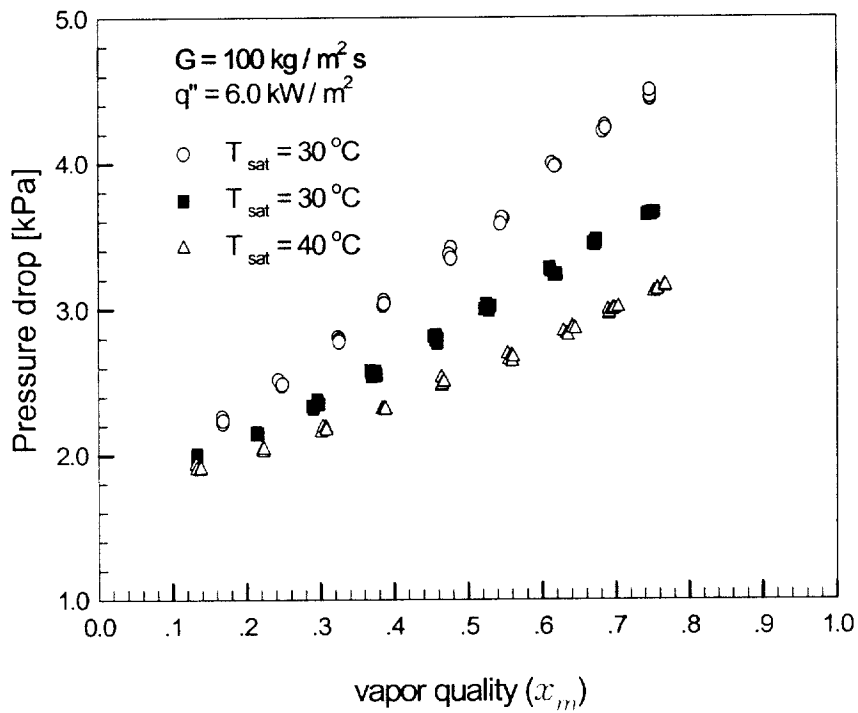


**Fig. 4.28** Variations of pressure drop with mean vapor quality for various saturation temperature, Type B.

### 4.5.2 Comparison with Plate heat exchanger

It is necessary to compare the present data for the R-134a friction factor in the P&SHE to those in plate heat exchanger reported in the literature. Due to the limited availability of the data for plate heat exchanger with the same ranges of the parameters covered in the present study. The comparison is only possible for a few cases. This is illustrated in Fig. 4-25, in which our data are compared with correlation of Yan et al.<sup>(36)</sup>. Note that the data from Yan et al. are friction factor in a plate heat exchanger with the vapor quality from 0.08 to 0.86. Yan et al proposed friction factor correlation equation such as

$$f_{tp} Re^{0.5} = 31.21 Re_{eq}^{-0.04557} \quad (4.27)$$

The comparison clearly shows that the R-134a friction factor for P&SHE is about 75% (Type A) and 45% (Type B) in average less than that for the plate heat exchanger.

### 4.5.3 Correlation of pressure drop

To facilitate the use of the plate and shell heat exchanger as a condenser and evaporator, correlation equations for the dimensionless two-phase flow friction factor based on the present data are provided. They are

Type A :

$$f_{tp} Re^{0.5} = 8.92 \times 10^5 Re_{eq}^{-1.179} \quad 2000 < Re_{eq} < 7000 \quad (4.28)$$



Type B :

$$f_{tp} Re^{0.5} = 8.312 \times 10^4 Re_{eq}^{-0.938} \quad 2500 < Re_{eq} < 11000 \quad (4.29)$$

Figure 4.30 and 4.31 illustrates the comparison of the proposed correlation for the friction factor to the present data. It is found that the average deviation is about 15%(Type A) and 20%(Type B) between the  $f_{tp}$  correlation and the data.

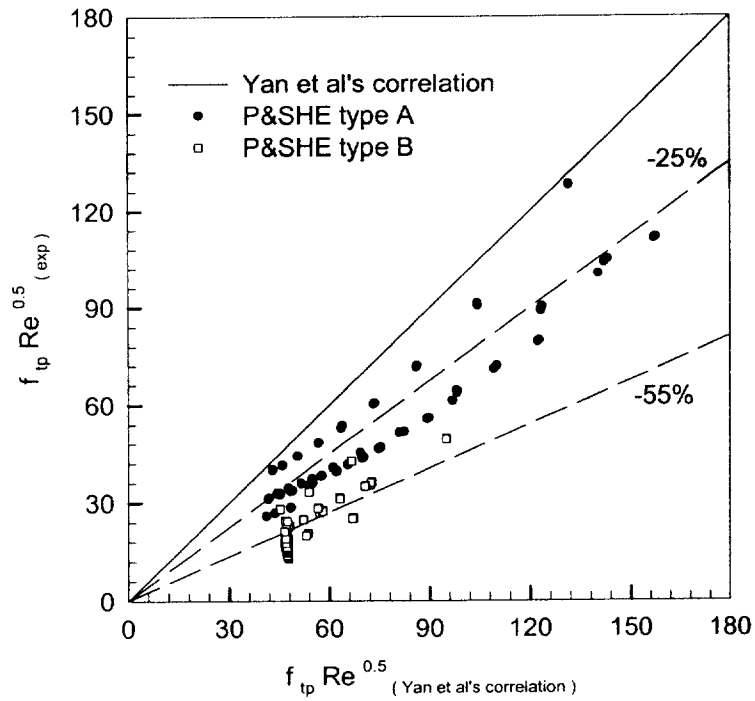


**Fig. 4.29** Comparison of the present friction factor with those for plate heat exchanger from Yan et al.

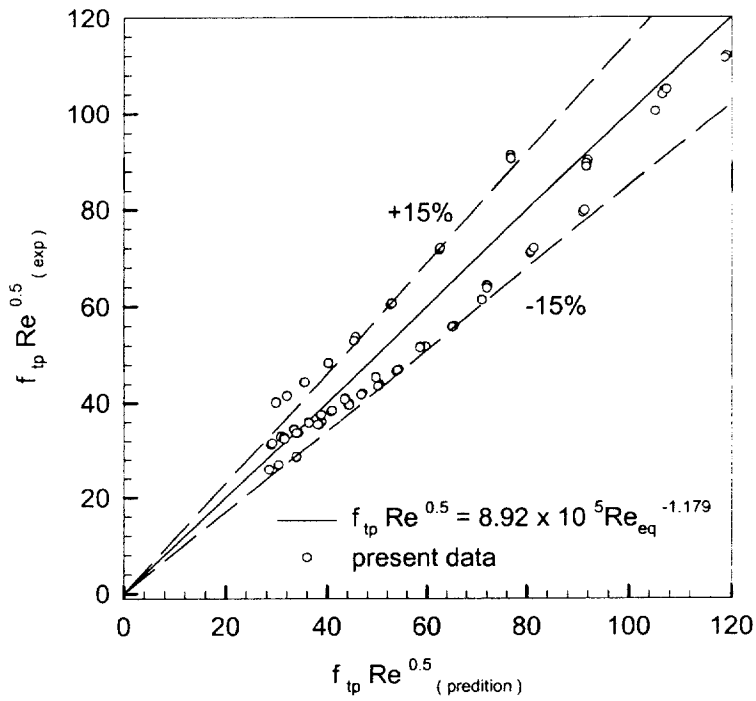


**Fig. 4.30** Comparison of the proposed correlation for friction factor with the present data, Type A.

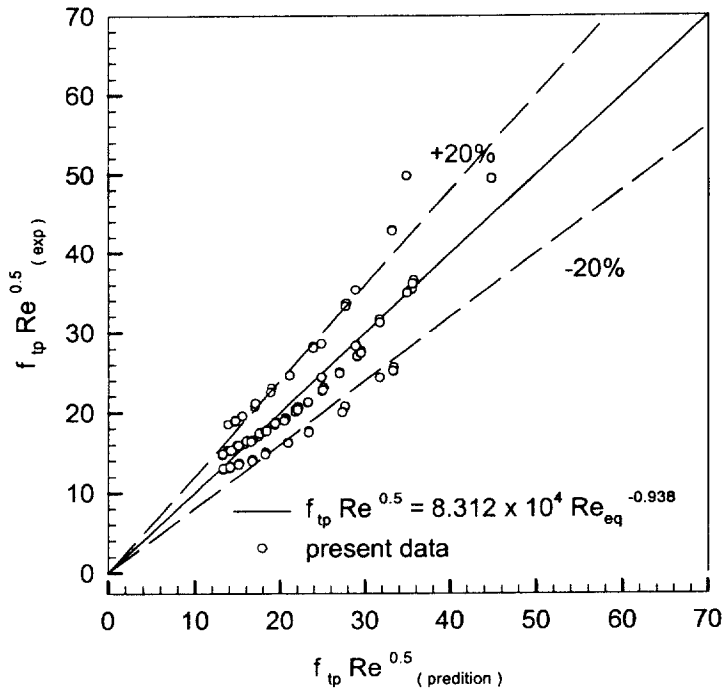


**Fig. 4.31** Comparison of the proposed correlation for friction factor with the present data, Type B.

## CHAPTER 5

### CONCLUSIONS

In order to set up the database for the design of the P&SHE, heat transfer and pressure drop characteristics for single phase flow of water were experimentally and numerically investigated in this study. Single phase heat transfer coefficients were measured for turbulent water flow in a plate and shell heat exchangers by Wilson plot method. Numerical work was conducted to find the optimum design parameters by using the FLUENT code.

And, the characteristics of condensation and evaporation heat transfer and pressure drop for refrigerant R-134a flowing in a plate and shell heat exchanger were explored experimentally.

The following conclusions were obtain from the results of this research on the heat transfer and pressure drop characteristics for the plate and shell heat exchanger.

1. Single-phase heat transfer and pressure drop characteristics for 2 types of plate and shell heat exchanger are investigated in the present study. Experiments were conducted in a P&SHE with water as the test fluid. The heat transfer coefficients for the test were obtained from the modified Wilson plot technique. In the range of  $800 < Re < 5000$  (type A),  $1000 < Re < 8000$  (type B), the proposed heat transfer correlation can predict of the experimental data within 10%, and the friction factors within 3.6%.

2. Numerical predictions were obtained for the flow and thermal fields

in plate and shell heat exchanger geometries under transitional and weakly turbulent conditions, and were compared with the authors' own experimental measurements. The CFD predictions by using the standard  $k-\varepsilon$  model for the plate channel were found to be in reasonable agreement with the experimental results. The influence of Reynolds number, partitioning rib, Chevron angle, pitch and height was investigated. Correlations were proposed for heat transfer coefficients and pressure drops, including the effects of  $\theta$  based on the CFD analysis data. Determination of minimum cost analysis method was investigated.

3. An experimental investigation has been conducted in the present study to measure the condensation and evaporation heat transfer coefficient and pressure drop of R-134a in a plate and shell heat exchanger. The effects of the mass flux, average imposed heat flux, saturation temperature, feeding method and vapor quality of R-134a on the measured data were examined in detail.

In traditional test, the refrigerant is heated by an electric, but in this study the refrigerant inside of the plate is heated by hot water flowing counter-currently in the shell side (Which corresponds more closely to the real situation in a water chiller evaporator).

The results show that the condensation and evaporation heat transfer coefficient and pressure drop normally increase with the refrigerant mass flux. Contrary to the mass flux effects, the heat flux does not have significant effects on the heat transfer at high quality, but at a high wall heat flux it shows some influences at low quality. A distinct maximum in evaporation heat transfer coefficient after the peak was observed to be caused by the partial plate wall dryout.

In the higher vapor quality regime, relatively a lower heat transfer coefficient was obtained by increasing the saturation temperature. Gravity and flow regime changes both acted to the heat transfer as the feeding method. Both the mass flux and saturation temperature have some effects on the pressure drop for the entire quality range. A higher mass flux results in a higher pressure drop but a higher saturation temperature results in a lower pressure drop. Moreover, the increasement of the heat transfer coefficient according to the vapor quality is larger than that of the pressure drop. Correlations were also proposed for the measured heat transfer coefficients and pressure drops in terms of Nusselt number and friction factor for the P&SHE.

## REFERENCES

- (1) Kays W. M. and London A. L., 1984, Compact Heat Exchanger, 3rd ed., McGraw-Hill.
- (2) Marriott J, 1971, "Where and How to use plate heat exchangers," Chemical engineering, Vol. 78, No. 8, pp. 127~134.
- (3) Kandlikar S. G. and Shah R. K., 1989, "Multipass Plate Heat Exchangers Effectiveness NTU Results and Guidelines for Selecting Pass Arrangements," ASME J. of Heat Transfer, Vol. III, pp. 300-313.
- (4) Gerd Gaiser and Volker Kottke, 1989, "Flow Phenomena and Local Heat Transfer and Mass Transfer in Corrugated Passages," Chem. Eng. Techol. No. 12, pp. 400~405.
- (5) Stasiek J., Collins M. W., Colfalo M. and Chew P. E, 1996, "Investigation of flow a and heat transfer in corrugated passages-I Experimental results," Int. J. Heat Mass Transfer, Vol. 39, No. 1, pp. 149~164.
- (6) Shah, R. K. and Focke, W. W., 1988, "Plate Heat Exchangers and Their Design Theory," in : Shah, R. K., Subbarao, E. C., Mashelkar, R. A. (Eds.), "Heat Transfer Equipment Design," Hemisphere, Washington, DC, pp. 227~254.
- (7) Manglik, R. M., 1996, "Plate Heat Exchangers for Process Industry Applications: Enhanced Thermal-Hydraulic Characteristic of Chevron Plates," Process Enhanced and Multiphase Heat Transfer, R. m. Manglik and A. D. Kraus, ed., Begell House, New York, pp. 267~276.
- (8) Buonopane R. A., Troupe. R. A. and Morgan J. C., 1963, "Heat transfer design method for plate heat exchangers," Chemical engineering progress, Vol. 59, No. 7, pp. 57~61.



- 
- (9) Raju K. S. N. and Bansal J. C, 1983a, "Plate Heat Exchangers and Their Performance", in: Low Reynolds Number Flow Heat Exchangers, S. Kakac R. K. Shah and A. E. Bergles, eds, pp. 899~912.
- (10) Edwards M. F., 1974, "Heat transfer and Pressure Drop Characteristics of a Plate Heat Exchanger Using Newtonian and Non-Newtonian Liquids," The Chemical Engineer, Vol. 259, No. 1, pp. 286-288.
- (11) A. Cooper, 1974, "Recover more heat with plate heat exchangers," The Chemical Engineer, Vol. 259, No. 1, pp. 280-285.
- (12) Gerd Gaiser and Volker Kottke, 1989, "Flow Phenomena and Local Heat Transfer and Mass Transfer in Corrugated Passages," Chem. Eng. Technol. No. 12, pp. 400~405.
- (13) Bogaert, R. and Bolcs, A., 1995, "Global Performance of a Prototype Brazed Plate Heat Exchanger in a Large Reynolds Number Range," Experimental Heat Transfer, Taylor & Francis, No. 8, pp. 293~311.
- (14) Stasiek, J., Colliins, M. W. and Chew, P. E., 1996, "Investigation of Flow and Heat Transfer in Corrugated Passages-1 Experimental Results," Int. J. Heat and Mass Transfer, Vol. 39, No. 1, pp. 149~164.
- (15) Manglik, R. M. and Muley, A., 1993, "Heat Transfer and Pressure Drop Characteristics of Plate-and-Frame Heat Exchangers," : A Literature Review, Report No. TFL-Int-1. Thermal-Fluids Laboratory, University of Cincinnati, Cincinnati, OH, Sept.
- (16) Okada, K., Ono, M., Tominura, T., Okuma, T., Konno, H. and Ohtani, S., 1972, "Design and Heat Transfer Characteristics of a New Plate Heat Exchanger," Heat Transfer-Japanese Research, Vol. 1. No. 1. pp. 90~95.
- (17) Marriott, J., 1977, "Performance of an Alfaflex Plate Heat

Exchanger," Chemical Engineering Progress, Vol. 73, No. 2, pp. 73~78.

(18) Focke, W. W., Zachariades, J. and Oliver, I., 1985, "The Effect of the Corrugation Inclination Angle on the Thermohydraulic Performance of Plate Heat Exchangers," Int. J. Heat Mass Transfer, Vol. 28, No. 8, pp. 1469~1479.

(19) Talik, A. C., Fletcher, L. S., Anand, N. K. and Swanson, L. W., 1995a, "Heat Transfer and Pressure Drop Characteristics of a Plate Heat Exchanger," Proc. ASME/JSME Thermal Engineering Conference, Vol. 4, ASME, New York, pp. 321~329.

(20) Talik, A. C., Fletcher, L. S., Anand, N. K. and Swanson, L. W., 1995b, "Heat Transfer and Pressure Drop Characteristics of a Plate Heat Exchanger Using a Propylene-Glycol/Water Mixture as the Working Fluid," Proc. 1995 National Heat Transfer Conference, Vol. 12. HTD-Vol. 314, ASME, New York, pp. 83~88.

(21) Muley, A. and Manglik, R. M., 1995, "Experimental Investigation of Heat Transfer Enhancement in a PHE with  $\beta=60^\circ$  Chevron Plates," Heat and Mass Transfer 95, Tata McGraw-Hill, New Delhi. pp. 737~744.

(22) Muley, A. and Manglik, R. M., 1997, "Enhanced Heat Transfer Characteristics of Single-Phase Flows in a Plate Heat Exchangers with Mixed Chevron Plates," Journal of Enhanced Heat Transfer, Vol. 4, pp. 187~201.

(23) Muley, A. and Manglik, R. M., 1998, "Heat Transfer and Pressure Drop in Plate Heat Exchangers," Thermal-Fluids Laboratory Report No. TFL-2, Department of Mechanical, Industrial and Nuclear Engineering, University of Cincinnati, Cincinnati, OH.

(24) Thonon, B., Vidil, R. and Marvillet, C., 1995, "Recent Research

and Developments in Plate Heat Exchangers," Journal of Enhanced Heat Transfer, Vol. 2, Nos. 1-2, pp. 149~155.

(25) Savostion, A. F. and Tikhonov, A. M., 1970, "Investigation of the Characteristics of the Plate Heating Surfaces," Thermal Engineering, Vol. 17, No. 9, pp. 75~78.

(26) Tovazhnyanski, L. L., and Kapustenko, P. A. and Tsibulnik, V., 1980, "Heat Transfer and Hydraulic Resistance in Channel of Plate Heat Exchangers," Energetika, Vol. 9, pp. 123~125.

(27) Wanniarachchi, A. S., Ratnam. U., Tilton, B. E. and Dutta-Roy, K., 1995, "Approximate Correlations for Chevron-Type Plate Heat Exchangers," Proc. 1995 National Heat Transfer Conference, Vol. 12. HTD-Vol. 314, ASME, New York, pp. 145~151.

(28) Schlager, L. M., Pate, M. B. and Bergies, A. E., 1990, "Evaporation and Condensation Heat Transfer and Pressure Drop in Horizontal, 12.7 mm Micro-fin Tubes with Refrigerant 22," J. Heat Transfer 112, pp. 1041~1047.

(29) Schlager, L. M. and Pate, M. B., 1989, "Heat Transfer and Pressure Drop during Evaporation and Condensation of R22 in Horizontal Micro-fin Tubes," Int. J. Refrig. 12, pp. 6~14.

(30) Eckels, S. J. and Pate, M. B., 1991, "An Experimental Comparison of Evaporation and Condensation Heat Transfer Coefficients for HFC-134a and CFC-12," Int. J. Refrig. 14, pp. 70~77.

(31) Torikoshi, K. and Ebisu, T., 1993, "Evaporation and Condensation Heat Transfer Characteristics of R-134a, R-32 and a Mixture of R-32/R-134a Inside a Tube," ASHRAE Trans. 99 (I), pp. 90~96.

(32) Liu X., 1997, "Condensing and Evaporating Heat Transfer and Pressure Drop Characteristic of HFC-134a and HCFC-22," Transaction of

the ASME, vol. 119, FEBRUARY, pp. 158-163.

(33) Chamra, L. M. and Webb, R. L., 1996, "Advanced Micro-fin Tubes for Condensation," *Int. J. Heat Mass Transfer* 39, pp. 1839~1846.

(34) Akers, W. W., Dean, H. A. and Crosser, O., 1958, "Condensation Heat Transfer within Horizontal Tubes," *Chem. Eng. Prog.* 54 (10), pp. 89~90.

(35) Shah, M. M., 1979, "A General Correlation for Heat Transfer during Film Condensation Inside Pipes," *Int. J. Heat Mass Transfer* 22, pp. 547~556.

(36) Yi-Yie Yan, Hsiang-Chao Lio and Tsing-Fa Lin, 1999, "Condensation Heat Transfer and Pressure Drop of Refrigerant R-134a in a Plate Heat Exchanger," *Int. J. Heat Mass Transfer* 42, pp. 993~1006.

(37) Yi-Yie Yan, Hsiang-Chao Lio and Tsing-Fa Lin, 1999, "Evaporation Heat Transfer and Pressure Drop of Refrigerant R-134a in a Plate Heat Exchanger," *Transactions of the ASME*, Vol. 121, pp. 118~127.

(38) Shah, R. K. and Wanniarachchi, A. S., 1992, *Plate Heat Exchanger Design Theory*, Industrial Heat Exchangers, J.M. Buchlin, ed., Von Karman Institute for Fluid Dynamics, Belgium.

(39) Farrell, P., Wert, K. and Webb, R., 1991, "Heat Transfer and Friction Characteristics of Turbulent Radiator Tubes," *SAE Technical Paper Series*, No. 910197

(40) Kays, W. M., 1950, "Loss Coefficients for Abrupt Changes in Flow Cross Section with Low Reynolds Number Flow in single and Multiple Tube Systems," *Transactions of ASME*, Vol. 72, pp. 1067~1074.

- 
- (41) Hinze. J. O., 1975, "Turbulence," mcGraw-Hill Publishing Co., New York
- (42) Launder. B. E., and Spalding. D. B., 1972, "Lectures in Mathematical Models of Turbulence," Academic Press, London, England
- (43) Yakhot, V., and Orszag, S. A., 1986, "Renormalization Group Analysis of Turbulence: I. Basic Theory", Journal of Scientific Computing, pp. 1 ~ 51
- (44) Ciofalo, M., Collins, M. W., and Stasiek, J. A., 1988, "Flow and Heat transfer predictions in flow passages of air preheaters: assessment of alternative modeling approaches", Comutational mechanics Publications, pp. 169 ~ 225
- (45) Collier, J. G., 1982, "Convective Boiling and Condensation," 2nd ed., McGraw-Hill International Book Company, pp. 32, 90 ~ 93.
- (46) Kline, S. J. and McClintock, F. A., 1953, "Describing Uncertainties in Single Sample Experiments," Mechanical Engineering, Vol. 75, No. 1, pp. 3 ~ 12.
- (47) Davis E. J. and David M. M., 1964, "Two-phase gas-liquid convective heat transfer," I & EC Fund., 3(1964) 111
- (48) Kattan, N., Thome, J. R. and Favrat, D., 1998, "Flow Boiling in Horizontal Tubes : Part 2-New Heat Transfer Data for Five Refrigerants," trans. ASME, Vol. 120, pp. 148 ~ 155
- (49) Wilson, E. E., 1915, "A basis for rational design of heat transfer apparatus," Trans. ASME 37 pp. 47 ~ 70.
- (50) Sieder, E. N. and Tate, G. E., 1936, Ind. eng. chem., Vol 28, 1429.
- (51) Hufschmidt, W. and burck, E., 1968, "Der Dinfluss Temperatureabhängiger stoffwerte aur den warmeubergang bei turbulenter stromung von flussigkeiten in rohren bei gogen warmestromdichten und

prandtlzahlen," Int. J. Heat Mass Transfer, Vol. 41, pp. 1041~1048.

(52) Young, E. H. and Wall, J. R. et al., 1957, "Engineering Research Institute," Univ. Mich., Rept. No. 48.

(53) briggs, D. E. and Young, E. H. 1969, "Modified Wilson plot techniques for obtaining heat transfer correlations for shell and tube heat exchangers," Chem. eng. Prog. Symp. Seri. 65(92), pp. 35~45.

(54) Mayhew, Y. R., 1981, "Additional observations on vapour shear and condensate inundation," Power Condenser Heat Transfer Technology, pp.243~247.

(55) Khartabil, H. F., Christensen, R. N. and Richards, D. E. 1988, "A modified Wilson plot technique for determining heat transfer correlations. 2nd U. K. National Conf. on Heat Transter, September.

(56) Webb, R. L. and Yang, C. Y., 1996, "Condensation of R-12 in Small Hydraulic Diameter Extruded Aluminum Tubes with and without Micro-fins," International J. of Heat & Mass Transfer, Vol. 39, No. 4, pp. 791~800.

(57) Kim, N. H. and Cho, J. P., 1999, "Experimental Investigation of R-22 Condensation in Tubes with Small Inner Diameter," Journal of Air-Conditioning and Refrigeration, Vol. 7, pp. 45~54.

(58) Yi-Yie Yan and Tsing-Fa Lin, 1999, "Condensation Heat Transfer and Pressure Drop of Refrigerant R-134a in a Small Pipe," Int. J. Heat Mass Transfer 42, pp. 697~708.

(59) Yi-Yie Yan and Tsing-Fa Lin, 1999, "Evaporation Heat Transfer and Pressure Drop of Refrigerant R-134a in a Small pipe", Int. J. Heat Mass Transfer 41, pp. 4183~4194.

(60) Incropera and Dewitt, 1981, Fundamenals of Heat Transfer, John Wiley and Sons, New York, pp. 399~407.

(61) Dutt T. K. and Chanda B. G., 1971, "Studies on heat transfer in a plate-type paraflow heat exchanger with a Liquid-Liquid System," Indian Chemical Engineer, vol VIII No. 4 pp. 41~45.

(62) Flack P. H., 1964, "The Feasibility of Plate Heat Exchangers," Chemical and Process Engineering, 1964, pp. 469~472.

(63) Clark D. F, 1974, "Plate heat exchanger design and recent development," The Chemical Engineering, No. 285, pp. 275~279.

(64) Ashley C. M., 1941, "The Heat Transfer of Evaporating Freon," Journal of The A.S.R.E. pp. 89~96.

(65) Brayan W. L. and Quaint G. W., 1951, "Heat Transfer Coefficients in Horizontal Tube Evaporators," Journal of the ASRE, January, pp. 67~73.

(66) Schrock V. E. and Grossman L. M., 1962, "Forced Convection Boiling in Tubes," NUCLEAR SCIENCE AND ENGINEERING: 12, pp. 474~481.

(67) BO PIERRE, 1964 "Flow resistance with Boiling refrigerants-part1," ASHRAE JOURNAL, september.

(68) Chaddock J. B. and Noerager J. A., 1966 "Evaporation of Refrigerant 12 in a Horizontal Tube with Constant Wall Heat Flux," The project described in this paper was supported by ASHRAE Research Project RP. 45, pp. 90~103.

(69) Stephan K. and Abdelsalam M., 1980, "Heat Transfer Correlations for Natural Convection Boiling," Int. J. Heat Transfer, Vol. 23, pp. 73~87.

(70) Gungor K. E. and Winterton R. H. S., 1986, A general correlation for flow boiling in tubes and annuli," Int. J. Heat Mass Transfer, Vol. 29, No. 3, pp. 351~358.

(71) Sami S. M. and Duong T. N., 1992, "Two phase Boiling Characteristics of R-134a and R-12 in Annuli of Enhanced Surface Tubing," Int. Comm. Heat Mass Transfer Vol. 19, pp. 203~214.

(72) Oh, Myung-Do and Kim, Seon-Chang, 1995, "An Experiment on

Evaporating Heat Transfer of HCFC-22 for a Transport Refrigerant System," Journal of Air-Conditioning and Refrigeration, Vol. 3, August, pp. 21~30.

(73) Hewitt G. F. and Roberts D. N., 1969, "Studies of two-phase flow patterns by simultaneous flash and x-ray photography," AERE-M2159.

(74) Dengler C.E.Sc..D Thesis, Mass. Inst 1952.

(75). Guerrieri S. A. and Talty R. D. 1956, "A study of heat transfer to organic liquids in single tube boilers," Chemical engineering Progress Symposium Series, Vol. 52, No.18 pp.69~77.

(76) Dengler C. E and Abboms J.N 1956, "Heat transfer mechanism for vaporization of water in a vertical tube," Vol.52 No 18, pp. 95~103.

(77) pierre bo. 1995, "The coefficient of heat transfer for boiling Freon-12 in horizon tubes." S. F. Review, Vol. 2, No. 1, Published by Svenska Flaktabriken Ab, Stockholm, Sweden.

(78) Shans P. and Long R A. K 1961, "A correlation for heat transfer in saturated two-phase flow with vaporization," International Journal of Heat and Mass Transfer, Vol. 2, No. 3, April, pp. 222~230.

(79) Schrock V. E. and Grossman 1962, "Fluid convection boiling in tubes," Nuclear Science and Engineering, Vol. 12, no 4, pp. 474~481.

(80) Chen J.C 1963, "A correlation for boiling heat transfer to saturated fluids in convective flow, "ASME paper, 63-HT-34.

(81) Private discussion with M. G. Cooper at Oxford university.

(82) Lavin J. G. and Young E.H., 1964, "Heat transfer to evaporating refrigerants in two-phase flow," AIChE Preprint 21e, Symposium on Two-Phase Flow and Heat Transfer, February.

(83) Seo, M. K. and Kim, Y. S., 1999, "Experimental Study on Heat Transfer and Pressure Drop Characteristics for Single-Phase Flow in Plat and Shell Heat Exchangers," Korean Journal of Air-Conditioning and Refrigeration Engineering, Vol. 12, No. 4. pp. 422~429.



(84) Seo, M. G., Park, J. H., and Kim, Y. S., 2001, "Experimental Study on R-22 Condensation Heat Transfer and Pressure Drop Characteristic in Plat and Shell Heat Exchangers," Trans. KSME, Vol. 25, No. 6. pp. 860~867.

(85) Seo, M. G., Park, J. H., and Kim, Y. S., 2001, "Experimental Study on R-22 Evaporation Pressure Drop Characteristic in Plat and Shell Heat Exchangers," Korean Journal of Air-Conditioning and Refrigeration Engineering, Vol. 13, No. 10. pp. 930~938.

(86) Seo, M. G., Park, J. H., and Kim, Y. S., 2001, "Evaporation Heat Transfer and Pressure Drop Characteristic of refrigerant R-22 in Plat and Shell Heat Exchangers," Trans. KSME, Vol. 25, No. 10. pp. 1318~1326.

## APPENDIX

### WILSON PLOT TECHNIQUE

In order to obtain the heat transfer coefficients from the experimental, the single phase heat transfer correlation for the plate and shell side used in this study was requisite. Experiments were conducted systematically for Wilson plot technique.

Wilson plot technique is a method for determining the individual heat transfer resistance from the overall resistance of heat exchangers. Since Wilson<sup>(49)</sup> developed the method, many modified forms have been developed

#### A.1 Original Wilson plot technique

The total resistance to heat transfer for a shell-and-tube heat exchanger is expressed as follows;

$$\frac{1}{UA} = \frac{1}{h_t A_t} + \frac{1}{h_s A_s} + R_w \quad (\text{A.1})$$

Where the subscripts t and s mean the tube- and shell-side, respectively.

Wilson supposed the tube-side single phase heat transfer coefficient would be function of reduced velocity, which is Reynolds number. So he

considered Equation (A.1) as the following form:

$$\frac{1}{UA} = C_t \frac{1}{Re_D^a} + R \quad (A.2)$$

Where R is as follows:

$$R = R_s + R_w = \frac{1}{h_s A_s} + R_w \quad (A.3)$$

If the shell-side resistance is kept constant, though it is practically difficult, Equation (A.2) has a straight line as

$$y = mx + b \quad (A.4)$$

$$\text{where } y = \frac{1}{UA}, \quad m = C_t, \quad x = \frac{1}{Re_D^a}, \quad b = R$$

Wilson chose the Reynolds number exponent  $a$  such that the experimental data were fitted best. Finally he obtained the constant  $C_t$  and the tube-side heat transfer coefficient from the overall heat transfer data.

Wilson originally intended to investigate the effects of water temperature on tube-side single phase heat transfer. If the resistances of shell-side and tube wall are maintained constant, the tube-side resistance can be determined precisely. But in the case of Wilson, the shell-side condition was condensing steam and not constant heat flux, the accuracy

of derived tube-side heat transfer coefficient was not in good agreements.

## A.2 Modified Wilson plot Technique by Farrell et al.<sup>(39)</sup>

To determine the heat transfer coefficient within the tube, it was necessary to split the overall thermal resistance of the counterflow heat exchanger. The overall thermal resistance was given by

$$\frac{1}{UA} = \frac{1}{h_a A_a} + \frac{1}{h_t A_t} + R_w \quad (\text{A.5})$$

It was desired to develop an expression for the tube side Nusselt number having the form

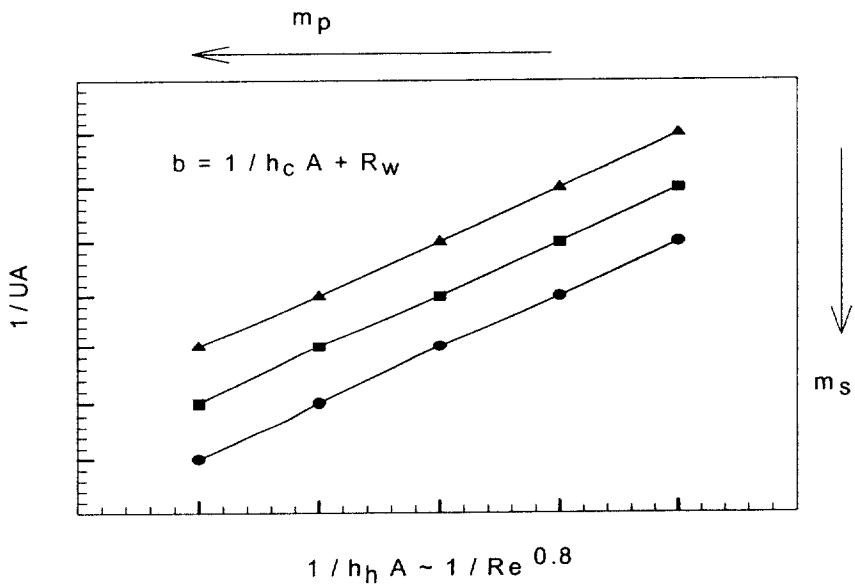


Fig. A.1 Concept of Wilson Plot Method.

$$Nu_{D,t} = C Re_D^m Pr^{\frac{1}{3}} \left( \frac{\mu}{\mu_w} \right)_t^{0.11} \quad (A.6)$$

The form of equation(A.6) is similar to the Sieder and Tate equation<sup>(50)</sup> although the viscosity ratio exponent of 0.11 was suggested by Hufschmidt and Burck<sup>(51)</sup>.

The average Nusselt number for the annulus was assumed to behave according to an expression of the form

$$Nu_{D,a} = g(Re_D, Pr) \left( \frac{\mu}{\mu} \right)_a^{0.11} \quad (A.7)$$

Solving equation (A.6) and (A.7) for the heat transfer coefficients and substituting into equation (A.5) yielded

$$\begin{aligned} \frac{1}{UA} = & \frac{1}{A_a \left( \frac{k_f}{D_h} \right)_a g(Re_D, Pr) \left( \frac{\mu}{\mu_w} \right)_a^{0.11}} \\ & + \frac{1}{A_t \left( \frac{k_f}{D_h} \right)_t [C Re_D^m Pr^{\frac{1}{3}} \left( \frac{\mu}{\mu_w} \right)_t^{0.11}]} + R_w \end{aligned} \quad (A.8)$$

Knowing the geometries, flow rates and fluid temperatures, only three terms in equation (A.8) were unknown: the coefficient C, the Reynolds number exponent m and the value of the unknown function g (Re<sub>D</sub>, Pr).

The modified Wilson plot is a graphical technique which made it possible to determine these unknowns. To do so, it was necessary to

hold the flow rate and average temperature constant within the annulus. If this was accomplished, the function  $g(Re_D, Pr)$ , though unknown, remained constant while testing each tube. Subsequent sections describe the necessary equations and data.

### Development of Equation

To determine the overall thermal resistance of the counterflow heat exchanger, the LMTD method of heat exchanger analysis was used.

$$\frac{1}{UA} = \frac{\Delta T_{lm}}{Q_{ave}} \quad (A.9)$$

where

$$\Delta T_{lm} = \frac{(T_{t,o} - T_{a,i}) - (T_{t,i} - T_{a,o})}{\ln \left( \frac{T_{t,o} - T_{a,i}}{T_{t,i} - T_{a,o}} \right)} \quad (A.10)$$

and

$$Q_{ave} = \frac{Q_t + Q_a}{2} \quad (A.11)$$

The heat transfer rates in the tube and annulus were calculated from

$$Q_t = (mc_p) (T_{t,i} - T_{t,o}) \quad (A.12)$$

$$Q_a = (mc_p)_a (T_{a,o} - T_{a,i}) \quad (\text{A.13})$$

The modified Wilson plot is graphical technique which allowed the unknowns  $C$ ,  $m$  and  $g(Re_D, Pr)$  to be determined by manipulating equation (A.8) into two linear forms. Rearranging equation (A.8) gave

$$\begin{aligned} \left[ \frac{1}{UA} - R_w \right] A_a \left( \frac{\mu}{\mu_w} \right)_a^{0.11} &= \frac{1}{\left( \frac{k_f}{D_h} \right) g(Re_D, Pr)} \\ &+ \frac{A_a \left( \frac{\mu}{\mu_w} \right)_a^{0.11}}{A_i \left( \frac{k_f}{D_h} \right)_i \left[ C Re_D^m Pr^{\frac{1}{3}} \left( \frac{\mu}{\mu_w} \right)_i^{0.11} \right]} \end{aligned} \quad (\text{A.14})$$

If  $C$  and  $g(Re_D, Pr)$  are constant, the above equation is in the linear form

$$Y_1 = AX_1 + B \quad (\text{A.15})$$

where

$$Y_1 \equiv \left[ \frac{1}{UA} - R_w \right] A_a \left( \frac{\mu}{\mu_w} \right)_a^{0.11} \quad (\text{A.16})$$

$$A \equiv \frac{1}{C} \quad (\text{A.17})$$

$$X_1 = \frac{A_a \left( \frac{\mu}{\mu_w} \right)_a^{0.11}}{A_t \left( \frac{k_f}{D_h} \right)_t \left[ Re_D^m Pr \right]^{\frac{1}{3}} \left( \frac{\mu}{\mu_w} \right)_t^{0.11}} \quad (\text{A.18})$$

$$B \equiv \frac{1}{\left( \frac{k_f}{D_h} \right)_a g(Re_D, Pr)} \quad (\text{A.19})$$

Equation (A.15) is the first equation needed for the modified Wilson plot.

The second necessary equation results from further manipulation of equation (A.14). Rearranging gives

$$\begin{aligned} \frac{1}{CRe_D^m} &= \left[ \frac{1}{UA} - R_w \right] A_t \left( \frac{\mu}{\mu_w} \right)_t^{0.11} \left( \frac{k_f}{D_h} \right)_t Pr_t^{\frac{1}{3}} \\ &\quad - \frac{\frac{A_t}{A_a} \left( \frac{\mu}{\mu_w} \right)_t^{0.11} \left( \frac{\mu}{\mu_w} \right)_a^{-0.11} \left( \frac{k_f}{D_h} \right)_t Pr_t^{\frac{1}{3}}}{\left( \frac{k_f}{D_h} \right)_a g(Re_D, Pr)} \end{aligned} \quad (\text{A.20})$$

Taking logarithms of both sides produces an equation in the linear form

$$Y_2 = DX_2 + E \quad (\text{A.21})$$

where



$$\text{Exp } Y_2 = \left[ \frac{1}{UA} - R_w \right] A_t \left( \frac{\mu}{\mu_w} \right)_t^{0.11} \left( \frac{k_f}{D_h} \right)_t \text{Pr}_t^{\frac{1}{3}} - \frac{\frac{A_t}{A_a} \left( \frac{\mu}{\mu_w} \right)_t^{0.11} \left( \frac{\mu}{\mu_w} \right)_a^{-0.11} \left( \frac{k_f}{D_h} \right)_t \text{Pr}_t^{\frac{1}{3}}}{\left( \frac{k_f}{D_h} \right)_a g(Re_D, \text{Pr})} \quad (\text{A.22})$$

$$D \equiv -m \quad (\text{A.23})$$

$$X_2 = \log Re_d \quad (\text{A.24})$$

and

$$E \equiv -\log C \quad (\text{A.25})$$

This completes the development of the necessary equations. The algorithm for determining C, m and  $g(Re_D, \text{Pr})$  will now be discussed.

### Solution Algorithm

Test data taken for each tube consisted of flow rates and fluid temperatures for a range of tube side flow rates. This data was input to a program which used the modified Wilson plot.

The program first uses equations (A.9)~(A.13) to determine the overall thermal resistance for each data point. Next, equations (A.15) and (2.16) are used to calculate  $Y_1$  and  $X_1$  for each data point. Note that to calculate  $X_1$  it is first necessary to estimate the value of the Reynolds number exponent, m. Using a subroutine to calculate a best fit straight line, the constants A and B are calculated for equation (2.15).

Next it is necessary to check the estimate of  $m$ .  $Y_2$  and  $X_2$  are calculated from equations (A.22) and (A.24). To calculate  $Y_2$ ,  $g(Re_D, Pr)$  is obtained from  $B$ , the intercept of the best fit line previously calculated. Again, a subroutine is used to determine a best fit straight line. The constants  $D$  and  $E$ , the slope and intercept, of equation (A.21) are then known. From  $D$ , the value of  $m$  is calculated as the negative of  $D$ , equation (A.23).

The reduction program iterates over a range of estimates for  $m$  beginning with 0.5 and ending with 1.5, jumping by steps of 0.01. For each estimate, the best fit straight lines are calculated as described above. The correct values for  $C$ ,  $m$  and  $g(Re_D, Pr)$  are those resulting from the guess of  $m$  which results in the smallest difference between the initial estimate and the value calculated from the slope of equation (A.21).

## ACKNOWLEDGEMENTS

This dissertation would not have been completed without the help of many people. Especially, I wish to extend thanks to Professor Young-Soo Kim for his support and encouragement of this study. Without his full confidence in me and timely advice, this study could not have been completed. I also thank Professor Hoo-Kyu Oh, Professor Jong-Soo Kim, Professor Jong-Soo Kum, Professor Kwang-Hwang Choi, Professor Suk-Kwon Jung, Professor Eun-Pil Kim of Department of Refrigeration and Air-conditioning Engineering, Professor Oh-Boong Kwon of School of Mechanical Engineering of Pukyong National University and Professor Hyung-Ho Jung of Korea Maritime University for their many valuable suggestions and discussions for this research.

Many thanks are also due to all research members of System Design Lab., including Professor Ki-Baik Lee, Jae-Hong Park, Byoung-Tae Kim, Soo-Jin Kim, Byoung-Jo Min, Yong-Ha Kwon, Jong-Hwan Jung, Do-Wan Gong, Jae-Won Heo and Ho-Hyun Jung.

I deeply appreciate my mother, brothers and in particular my wife Ji-Yeon Lee and my daughter Ji-Hae for their great support and patience and love during the course of this study. I also thank to parents-in-law and brothers-in-law for their patience and encouragement.